1-1-2014

Altered Morphology And Composition Of Zymogen Granules In Acute Pancreatitis

Amanda Flack
Wayne State University,

ALTERED MORPHOLOGY AND COMPOSITION OF ZYMOGEN GRANULES IN ACUTE PANCREATITIS

by

AMANDA FLACK

DISSERTATION

Submitted to the Graduate School

of Wayne State University,

Detroit, Michigan

in partial fulfillment of the requirements

for the degree of

DOCTOR OF PHILOSOPHY

2014

MAJOR: PHYSIOLOGY

Approved by:

_____

Advisor Date

_____

_____

_____

_____

_____

DEDICATION

I dedicate my work to all of my family and friends:

To my future husband, William. I would have never been able to accomplish the things that I have in the past years without you and your support. You have encouraged me above all others to achieve my goals and to take the steps necessary to succeed. I will forever be grateful for all of the patience you have had for me during these years. I love you William, and I look forward to the rest of our lives together.

To my family, for their unconditional love and unwavering support. To my dad for his strength, support, and love. I have looked to you in the face of despair and known that I can and I must succeed. Knowing you and all you have overcome has shown me by example how to lead a responsible, mature, loving, and motivated life. To my mom, because you have been a huge supporter of my education and has always encouraged me to do my best. You have encouraged me to lead and to march forward in the face of adversity with my head held high. I have learned many life lessons from both of you and I hope to continue to make you both proud. I could not ask for better parents. I truly love and appreciate all the sacrifices you made so that Kyle and I could have all of the opportunities that we have had.

I also dedicate this work to my valuable friends. To Sara Denton, for her friendship, advice, and understanding. I value our friendship above others and consider you my best friend. You and I both know I would be lost without you. To my other friends, Eboni and Monica. I have valued and looked forward to our lunches and long conversations together over the years. I look forward to keeping in touch and keeping our friendships strong. To my future sister-in-law, Hannah, I have always known you were someone to count on. I appreciate the love and welcoming arms you have had for my entering of your family.

ACKNOWLEDGMENTS

I would like to acknowledge and express my sincerest gratitude to my advisor, Dr. Bhanu Jena. He has provided guidance and support to my research as well as myself during my graduate schooling. I have been very fortunate to be able to call him my mentor. I would also like to acknowledge my graduate committee, Dr. Dunbar, Dr. Walz, Dr. Manke, Dr. Mao, and Dr. Chen. They have all guided my research and my development as a scientist. I have learned to think critically and analytically about research concepts from your guidance. I have greatly valued all of your input in directing the course of my research to achieve my goals.

I would like to acknowledge Ms. Christine Cupps for her advice, support, and assistance during the past years. I, as well as all of the other Department of Physiology graduate students, would be lost without you. Thank you for all that you do.

I would also like to acknowledge the Department of Physiology and Wayne State University School of Medicine. I would also like to acknowledge the Interdisciplinary Biomedical Science program for their financial support.

TABLE OF CONTENTS

LIST OF TABLES

LIST OF FIGURES

CHAPTER 1

SUPRAMAXIMAL PANCREATIC STIMULATION WITH CAERULEIN LEADS TO ACUTE PANCREATITIS IN RATS

Abstract

Pancreatic digestive enzymes secreted following a meal are stored as inactive zymogens within membrane-bound secretory vesicles called Zymogen Granules (ZG), and activated extracellularly. In acute pancreatitis however, the digestive enzymes are prematurely activated within the cell, resulting in autodigestion of the tissue. A rat model of acute pancreatitis has previously been established to study the etiology of the disease. In the current study, acute pancreatitis was induced using an established published procedure by supramaximal stimulation of the exocrine pancreas using caerulein. Elevated amylase activity as well as increased immunoreactivity in the blood along with an increase in organ weight confirmed the establishment of acute pancreatitis.

Introduction

The pancreas is a compound organ where only 5% of pancreatic mass comprises endocrine function, and the remaining 95% constitute the exocrine pancreas (Brannon 1990). Here enzymes are stored and released into the duodenum of the small intestine for breakdown of ingested nutrients following a meal. A majority of the digestive enzymes are synthesized in proenzyme form and not activated until their release into the duodenum (Halangk & Lerch 2004, Pandol 2010). Acinar cells are the functional units within the pancreas that are responsible for the synthesis, storage and secretion of digestive enzymes. Individual acinar cells exhibit morphology demonstrating a distinct basolateral pole that contains the nucleus and the endoplasmic reticulum, and an apical pole with high density of secretory granules containing digestive enzymes called zymogen granules (ZG) (Figure 1), that, when stimulated, release their

contents into the luminal space (Pandol 2010). ZGs are electron dense subcellular organelles, ranging in size from 200 – 1200 nm in diameter (Figure 2) (Jena et al. 1997). The integrity of the ZG is essential to proper pancreas health and function. Inappropriate release of ZG contents leads to acinar cell death and is a hallmark in diseases like pancreatitis (VanAcker et al. 2002).

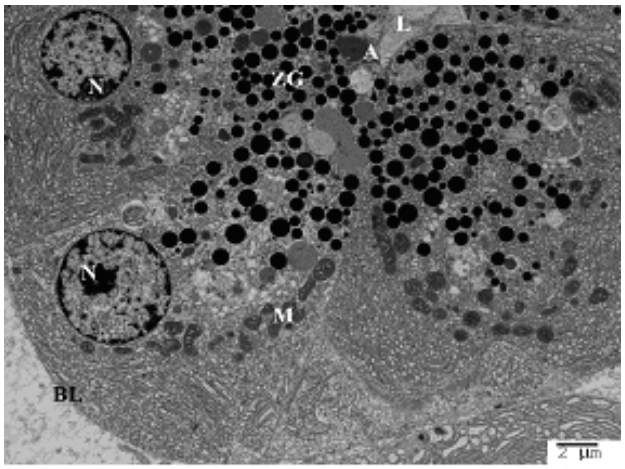

Figure 1. Rat Pancreatic acinar cells imaged with electron microscopy. The nucleus (N) is in the clearly identifiable basolateral (BL) region along with the mitochondria (M) where the ZGs ranging in size from 0.2 to 1.2µm, are concentrated at the apical (A) end of the cells near the lumen (L) (Bar = 2µm) (Flack et al., in preparation).

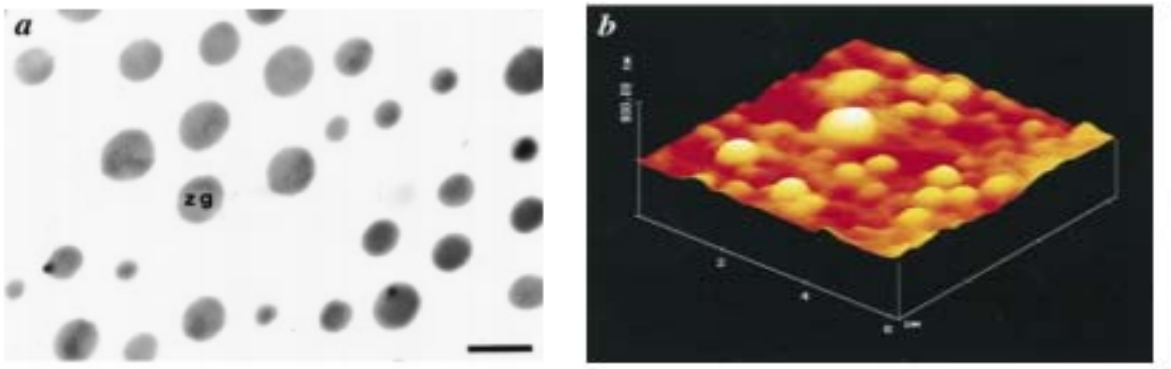

Figure 2. Purified ZGs imaged with electron microscopy (**A**) and atomic force microscopy (**B**) indicate a heterogeneous distribution of vesicles with diameters ranging from 0.2 – 1.2µm (Jena et al. 1997).

Enzymes of the exocrine pancreas are primarily synthesized and stored as inactive proenzymes that are activated upon release (Table 1) (Pandol 2010, Halangk & Lerch). Pancreatic enzymes are essential for the digestion of proteins, carbohydrates, and fat of the chime that enters the duodenum. These enzymes include trypsinogen, chymotrypsinogen, amylase, lipase, and phospholipase (Pandol 2010, Halangk & Lerch 2004, Kim 2008). Released

enzymes travel to the duodenum of the small intestine before they are activated (Figure 3). Trypsinogen is activated to trypsin that activates the other pro-enzymes (Pandol 2010, Halangk & Lerch 2004). The process of storage and release is highly coordinated and regulated. Cholecystokinin, for example, is a potent stimulator of digestive enzyme release, however other regulators include acetylcholine, gastrin releasing peptide, vasoactive intestinal peptide, secretin, and by the presence and contents of the ingested chyme itself in normal and healthy physiology (Brannon 1990, Pandol 2010).

PROENZYMES	ENZYMES
Trypsinogen	α-Amylase
Chymotrypsinogen	Lipase
Procarboxypeptidase A	DNase
Procarboxypeptidase B	RNase
Prophospholipase	
Proelastase	
Mesotrypsin	

Table 1. The exocrine pancreas produces, stores, and secretes enzymes in both an active form and in zymogen precursor to prevent premature activation of the digestive enzymes still housed within the pancreatic acinar cells. (Pandol 2010)

To maintain normal and healthy physiology, the secretory process for digestive enzyme release and other manufactured cellular products occurs in a highly regulated fashion. In disease states such as pancreatitis there appears to be a disregulation of events that is not fully understood (Vanacker et al 2002). The events leading to the proper secretion of vesicle content release have been under investigation in our laboratory as well as and how the secretory cascade is altered in pathological states. This will not only add to our understanding of the secretory process, but will also further the development of treatment modalities in disease states such as pancreatitis.

Pancreatitis is classified as a non-neoplastic gastrointestinal disorder (Foster 2013, Yadav et al. 2013, Ding et al. 2003) of which there is over 200,000 hospitalizations in the United States alone per year with a 5% mortality rate (NIDDK 2012). Of all the gastrointestinal disorders pancreatitis is the most prevalent, with the most unclear understanding of the cause and

progression of the disease (Yadav et al. 2013, Raraty et al. 2000, deDios et al. 2000). Across the United States, pancreatitis afflicts older populations with more frequency than younger populations as well as those populations with higher smoking, obesity, and alcohol consumption rates (Yadav 2013). High fat diets accompanied with diets high in red meat have also been correlated with the incidence of pancreatitis (Pandol et al. 2011).

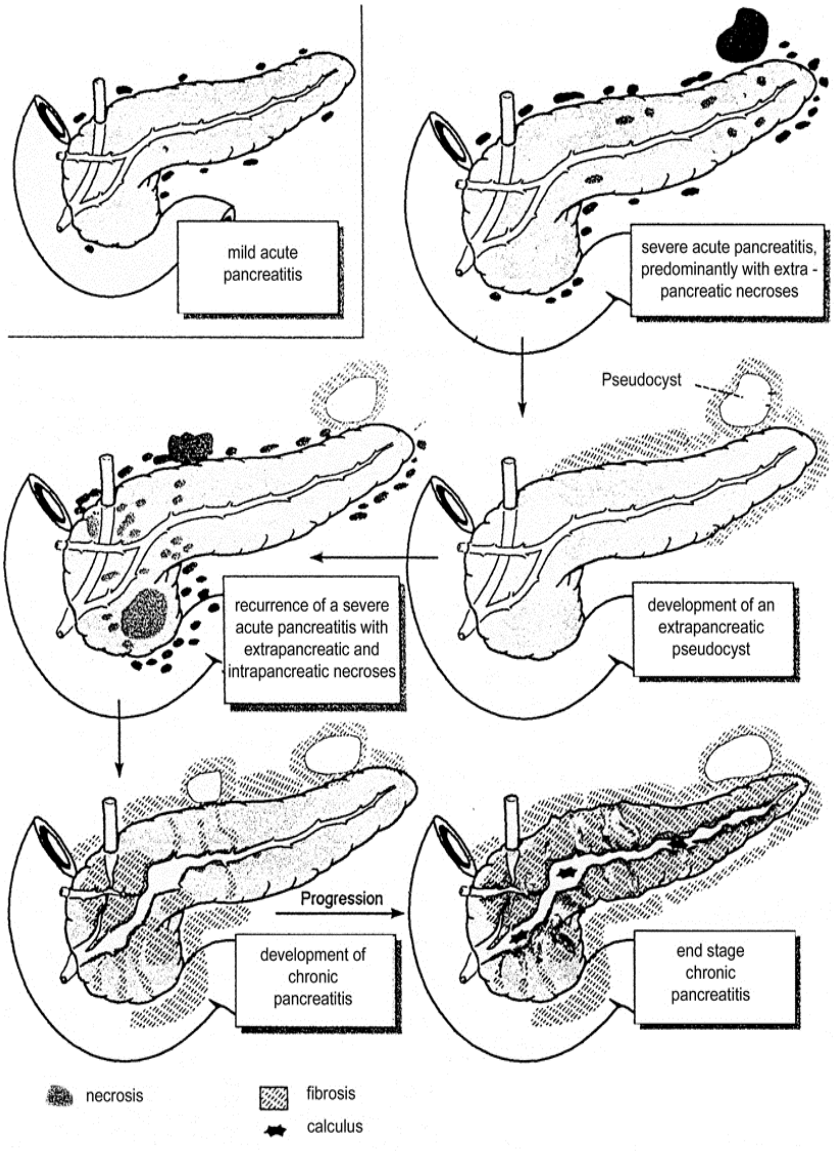

Figure 3. Pancreatitis exists in chronic and acute forms with symptomology that includes inflammation, edema, necrotic damage to the pancreas, and damage to surrounding tissues from inappropriate release of digestive enzymes. The complex causes of pancreatitis are likely cumulative and cyclic in the damage that occurs (Kim 2008).

Gallstones and chronic alcoholism have also been correlated with a predisposition for acquiring pancreatitis (Yadav 2013, National Pancreas Foundation 2013, NIDDK 2012). Acute pancreatitis can be mild or severe and chronic bouts of it can lead to chronic pancreatitis. The

etiology of acute pancreatitis includes rapid onset of pancreatic inflammation that resolves often after a few days, however the disease frequently leads to other complications. Chronic recurrence of acute pancreatitis leads to ductular atrophy and pancreatic damage including fibrosis that may predispose individuals to diabetes due to global glandular destruction (NIDDK 2012, Steer et al. 1995). While acute pancreatitis is characterized by a sudden onset of abdominal pain many of its other features, like edema, hemorrhage, and necrosis often go undetected until hospitalization is necessary (NIDDK 2012, Foster 2013). Pancreatitis as a disease is clinically relevant not only due to the large number of people admitted to the hospital each year with the ailment (NIDDK 2012, National Pancreas Foundation 2013), but because there are few treatment options for it currently. Due to the large number of hospitalizations annually and poor treatment options, institutions such as the National Institute of Diabetes, Digestive, and Kidney disorders have increased research funding 350% between 1999 and 2003 in the area (National Pancreas Foundation 2013).

Pancreatitis is a little understood disease that currently requires focused and rigorous investigation to determine the underlying mechanisms leading to the disease (Magana-Gomez et al. 2006). How the secretory cascade is altered in pancreatitis is critical in the amelioration of the disease. Treatment options remain limited to global anti-inflammatory medication and diet restriction until the pathology resolves (National Pancreas Foundation 2013). Access to the pancreas for diagnosis and/or biopsy is difficult and not often favored as surgical intervention may exacerbate disease progression (Hofbauer et al. 1998). Pancreatitis involves interstitial edema and acinar cellular inflammation (Ding et al 2003). At the level of the acinar cell ZGs do not release contents properly, acidic vacuoles form, other organelles become more fragile, lysosomal hydrolases do not localize to lysosomes properly (Saito et al. 1987), and inflammatory mediators (such as PLA_2 isoforms) are upregulated (Nevalainen et al. 1985). While the final

stage of the disease is characterized by autodigestion of the pancreas, the mechanism regulating this process is little understood (Magana-Gomez et al. 2006). Premature zymogen activation is likely the key to the progression of pancreatitis, and hence the necessity to prevent proenzyme activation within cells.

Caerulein induced pancreatitis mimics pancreatitis that occurs naturally due to inhibition of ZG content release (Saito et al. 1987). The cause of this inhibition of secretion is little understood. Lysosomal hydolase has been found to co-localization to ZGs (Hofbauer et al. 1998, Saluja et al. 1987, VanAcker et al. 2006), and altered v-H^+ATPase function (Waterford et al. 2005) have been previously reported. As early as 15 minutes after stimulation with a supramamimal dose of caerulein, the lysosomal hydrolase, cathepsin B, has been reported to co-localize with the starch digesting enzyme, amylase (Hofbauer et al. 1998). Cathepsin B among other lysosomal hyrolases have an activating capacity for the precursor enzymes housed within the ZGs. Lyosomal hydrolases exist in the lysosome at low pH and are capable of degrading inactivating peptides associated with zymogen precurson enzymes within the ZG (VanAcker et al. 2002). Therefore the first goal of my study was to reliably induce pancreatitis in rats using the established model of caerulein-induced pancreatitis in the rat (Gorelick et al. 1995, Chen et al 2010).

Materials & Methods

Induction of pancreatitis:

Pancreatitis was induced using an established published procedure (Chen et al. 2010). Male Sprague Dawley rats (Harlan, Indianapolis, IN) weighing 100-150 g were used in the study. To induce pancreatitis with caerulein, rats were injected i.p. with either one injection of 50 μg/kg synthetic caerulein (American Peptide Company, Sunnyvale, CA, USA) dissolved in saline for the 1 hour animal studies, or two injections one at zero hour and the other at the 1 hour

for the 2 hour animal studies. Control animals followed the same time regime except they were injected only with the vehicle saline. Blood and pancreas were collected from both control and caerulein-injected rats at one and two hours following the first injection. In each experimental group three to seven animals were used. Both biochemical and morphological approaches were used to determine the establishment of acute pancreatitis.

Estimation of plasma amylase:

Blood was collected from CO_2 euthanized rats by cardiac puncture using heparin-coated needles. The blood was centrifuged at 7,500 x *g* for 15 min at 4°C and the resultant plasma supernatant was collected and stored at −80 °C until assayed both for amylase activity and amylase content. Amylase activity was assayed using the Phadebas Amylase Test Reagent (Magle, Lund, Sweden). Briefly one Phadebas tablet was diluted in 20 mL of amylase buffer (0.05M NaCl, 0.02M NaH_2PO_4, 0.02% sodium azide, pH 7.4). Ten µl of plasma sample was mixed with 1ml of diluted Phadebas reactant and incubated for 10 min at 37°C in a shaking water bath. The reaction was stopped by 0.5N sodium hydroxide and then diluted with 4 ml double distilled H_2O. The optical density of each sample was then measured at 620 nm and amylase activity estimated from the standard curve provided by the company in the data sheet. The relative plasma amylase content between control and experimental animals was estimated using Western blot analysis.

Results

Acute pancreatitis is known to result in increased levels of ZG enzymes in the blood plasma (Chen et al. 2010). Blood plasma levels and activity of the starch digesting ZG enzyme amylase, was therefore assessed following induction of acute pancreatitis in rats using an established procedure (Gorelick et al. 1995, Chen et al 2010). The relative amylase activity (Figure 4D) in blood plasma obtained from both control rats, and from 1h and 2h experimental

animals following caerulein-injection, was estimated. Results from the study demonstrate a near 1.5-fold increase in the activity of plasma amylase in the 1h and over 2-fold increase in the 2h experimental animals (Figure 4D**)**, demonstrating the successful induction of acute pancreatitis as previously reported (Chen et al. 2010), following administration of supramaximal dose of caerulein to rats. Since both control and experimental animals received food at lib; the controls in the study represent physiological levels of pancreatic stimulation.

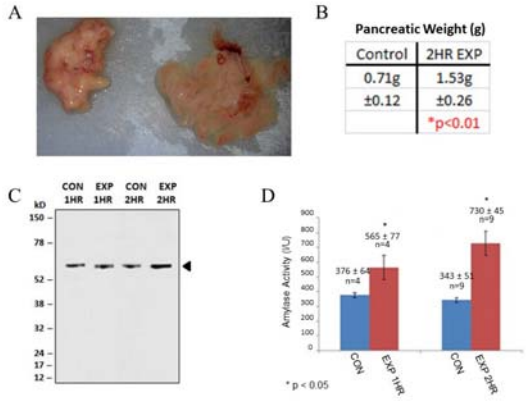

Figure 4. (**A, B**) An increase in pancreas weight is observed in the 2h experimental group. The edematous tissue is more than double the weight of the saline alone (vehicle) treated animals. An increase in both amylase content (**C**) and (**D**) activity in rat blood plasma is demonstrated in both 1h and 2h post intraperitoneal injection of supramaximal caerulein. Note in both the 1h and 2h control animals (CON) intraperitonially injected with vehicle alone, there is less amylase activity (**D**, blue bars), as well as immunoreactivity in the blood plasma compared to experimental animals (**D**, red bars) injected with caerulein.

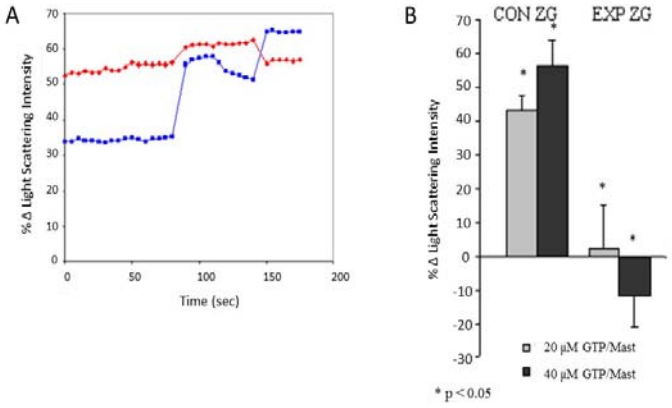

Figure 5. Capability to regulate volume is abrogated in ZG isolated from pancreatitic tissue. Isolated ZGs from rat pancreata were challenged to swell in vitro with GTP and mastoparan. Control ZGs from vehicle injected rats (left) swell vigorously when challenged however, ZGs from rats treated with two injections of 50 μg/kg caerulein (right) failed to swell to the same extent.

The 2h post caerulein injection group of rats experienced a 1.5-fold increase in pancreatic gland weight when compared to the saline injected controls. Edema is visibly noticeable in dissected panreata during the course of pancreatitis and is measured as an increase in gland weight (Figure 4 A & B). Established parameters for induced acute pancreatitis include an

increase in serum amylase, interstitial edema, and the presence of inflammatory mediators (Ding et al. 2003). Results of increase amylase immunoreactivity as well as activity in the blood plasma, and the increase in tissue weight as previously reported, confirm the establishment of acute pancreatitis in my study.

Previous studies have demonstrated that isolated ZGs rapidly swell following exposure to GTP and mastoparan (Jena et al. 1997, Cho et al. 2002, Abu-Hamdah et al. 2004, Kelly et al. 2004a, Kelly et al. 2004b). In acute pancreatitis, this ability of ZG to regulate its volume following exposure to GTP-mastoparan is abrogated as shown in (Figure 5). While isolated ZGs from saline injected animals swell in response to 20 and 40μM GTP and mastoparan, isolated ZGs from pancreata 2h post caerulein injection lose this ability. Other research has shown that secretory vesicles fail to release their contents into the lumenal space after the induction of pancreatitis (Saito et al. 1987). The current results indicate another layer of complexity in the pathophysiology of acute pancreatitis.

Discussion

In our model of pancreatitis, caerulein, a cholecystokinin (CCK) analogue, was used to induce pancreatitis in rats after supramaximal stimulation (50mg/kg, i.p.). Alternative models to caerulein include ductal injections (Aho et al. 1980), closure of the duodenal loop (Foster 2013, Adler et al. 1986), and bile duct ligation (Walker et al. 1987), however these methods often require invasive surgery and have high rates of premature mortality. Other non-invasive approaches also exist such as Charbachol (Chauduri et al. 2005, Sandstrom et al. 2005), anticholinesterase (Ikizceli 2005, Costa et al. 1984), L-argenine administration (Mizunuma et al. 1984, Kishino et al. 1984), or alcohol consumption or infusion (Kono et al. 2001). However caerulein is a CCK analogue, and because CCK serves as a major regulator of secretory events in the exocrine pancreas in rats, it is an optimal tool for the induction of pancreatitis.

While the classification of pancreatitis remains difficult, established parameters for laboratory induced pancreatitis include an increase in serum amylase, interstitial edema leading to increased glandular weight, and the presence of inflammatory mediators (Ding et al. 2003). In both the one and two hour time groups of rats, plasma amylase activity was significantly increased over controls, as was the weight of the pancreatic tissue in the 2h experimental animals, demonstrating the establishment of acute pancreatitis in these animals. As previously reported (Chen et al., 2010), administration of a supramaximal dose of caerulein to rats establishes acute pancreatitis. ZG swelling is required for vesicle content explusion during secretion (Jeremic et al. 2005, Kelly et al. 2004, Cho et al. 2002). Therefore in pancreatitis, the observed loss in the ability of ZG to swell in response to GTP-mastoparan (Figure 5) would compromise cell secretion. Since there is an increase in both amylase activity and content in the blood plasma in acute pancreatitis, this suggests that following supramaximal caerulin stimulation of the pancreas results in the release of intravesicular contents from docked vesicles at the plasma membrane, however the remaining ZGs with compromised volume regulating capability, are incapable of intravesicular release. This hypothesis was tested in my study, using both biochemical, immunochemical, and morphological approaches.

CHAPTER 2

ZG MORPHOLOGY IS ALTERED IN ACUTE PANCREATITIS IN RATS

Abstract

Following a meal, acinar cells of the exocrine pancreas secrete digestive enzymes stored as inactive zymogens within membrane-bound secretory vesicles called zymogen granules (ZG) that become activated extracellularly. In acute pancreatitis however, the digestive enzymes are blocked from being secreted and are activated within the cell leading to the common phenotype in pancreatitis. In the current study ZGs were examined in situ within pancreatic acinar cells as well as in isolated form for morphological changes demonstrated after the induction of pancreatitis. Examination of acinar cells using EM, demonstrate little change in their overall morphology following supramaximal caerulein exposure for up to 2 hours. However these studies demonstrate approximately 14% increase in ZG diameter in acute pancreatitis independently confirmed with EM and AFM analysis.

Introduction

Over one-quarter million patients are diagnosed annually with pancreatitis, with hospital costs of over 2.5 billion dollars (Peery et al. 2012, Fagenholz et al. 2007a, Fagenholz et al. 2007b). Except for limited management of the disease, currently no treatments are available. Furthermore the incidence of acute pancreatitis continues to grow (Peery et al. 2012, Fagenholz et al. 2007a, Fagenholz et al. 2007b), hence understanding pathogenesis of the disease will lead to early diagnosis and treatment. Following a meal, acinar cells of the exocrine pancreas secrete digestive enzymes stored as inactive zymogens within membrane-bound secretory vesicles called zymogen granules (ZG); these enzymes are then activated extracellularly (Neurath 1976). In acute pancreatitis however, the digestive enzymes are blocked from being secreted and are activated within the cell, resulting in autodigestion of the tissue (Chiari 1896). It is well

established that a variety of insults to the exocrine pancreas such as long-term exposure to alcohol, or supramaximal concentrations of cholecystokinin (>10-fold above physiological) or its analogue caerulein, stimulate the activation of zymogen within acinar cells, initiating pancreatitis (Katz et al. 1996, Pandol et al. 1999, Cosen-Binker et al. 2007). Although it is known that the activation of zymogens plays a central role leading to pancreatitis, the molecular underpinnings of the process remain unclear (Fick 2012).

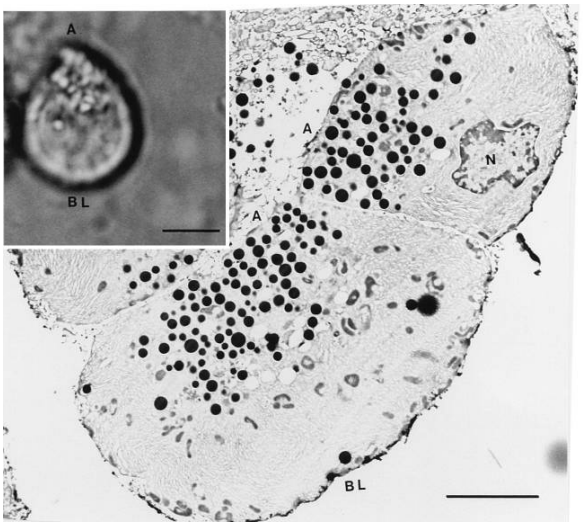

Figure 6. Rat Pancreatic acinar cells seen at the light (inset) and electron microscope level. The polarity of isolated acinar cells with clearly identifiable apical (A) and basolateral (BL) regions is seen in the differential interference contrast image. The nucleus (N) is present toward the basolateral region, and the zymogen granules, ranging in size from 0.1 to 1μm, are concentrated at the apical end of the cells (Schneider et al. 1997). (Bar = 5μm) *Courtesy of BP Jena*

Pancreatic enzymes pose a danger to the gland if activated prematurely due to their digestive capacity. Therefore digestive enzymes produced by the pancreas are often proenzymes that are activated at the site of action (Hofbauer et al. 1998, VanAcker et al. 2002, VanAcker et al. 2007). In the duodenum, the amino terminal trypsin activation peptide (TAP) is cleaved by brush border enzymes thereby converting trypsinogen to its active form trypsin. Trypsin then activates the other zymogen proenzymes into their respective active forms (Hofbauer et al. 1998). In the normal healthy pancreas acinar cells are observed to have a typical morphology that includes basolaterally located nuclei and apically located ZGs (Magana et al. 2006). At the onset of pancreatitis, in rat models, the morphology is altered slightly in that a greater number of ZGs migrate to the apical pole and large vacuoles begin to form (Hofbauer et al. 1998).

The primary function of the exocrine pancreas to produce and secrete digestive enzymes however failure of this biological process does occur in pancreatitis (Halangk & Lerch 2004). This disease is not well understood and has poor treatment options (Saluja et al. 2007). Previous beliefs placed the cause of pancreatitis on leakage of digestive enzymes out of the pancreatic duct, however is has been shown that pancreatitis begins at the level of the acinar cell (Foulis 1980). It is therefore my goal to examine ZGs both isolated from and examined in pancreatic acinar cells for morphological changes demonstrated after the induction of pancreatitis.

Materials & Methods

Isolation of Zymogen granules (ZG):

ZGs were isolated by modification of our published procedure (Jena et al. 1997). Sprague–Dawley rats weighing 150–200 g were euthanatized by CO_2 inhalation for the ZG preparations. Pancreata was dissected and diced into 0.5-mm^3 pieces. The pieces of pancreas were suspended in 15% (wt/vol) ice-cold homogenization buffer (0.3 M sucrose, 25 mM Hepes, pH 6.5, 1 mM benzamidine, 0.01% soybean trypsin inhibitor) and homogenized using a Teflon glass homogenizer. The resultant homogenate was centrifuged for 5 min at 300 x g at 4°C to obtain the supernatant. One volume of this supernatant was mixed with 2 vol of a Percoll–Sucrose–Hepes buffer (0.3 M sucrose, 25 mM Hepes, pH 6.5, 86% Percoll, 0.01% soybean trypsin inhibitor) and centrifuged for 30 minutes at 16,400 x g at 4°C. ZGs as a loose white pellet at the bottom of the tube was isolated for analysis.

Electron Microscopy:

Isolated pancreatic lobules from control, 1 h, and 2 h caerulein-injected rats were fixed in 4% glutaraldehyde/2% paraformaldehyde in ice-cold PBS for 24 hours. Following three rinses in 0.1 M cacodylate buffer (pH 7.2), the samples were embedded in 2% SeaPrep agarose for 15 minutes at 4°C, the agarose was cross-linked by immersion in Karnovsky's fixative (2.5%

glutaraldehyde/1.0% paraformaldehyde in phosphate buffer) for 15 minutes at 4°C, and then rinsed three times (5 minutes each) in 0.1 M cacodylate buffer. Next, minced pieces of the agarose-embedded acinar cell samples were post-fixed in 1% OsO_4 in 0.1 M cacodylate buffer for 1 hour at 4°C, rinsed three times (10 minutes each) in 0.1 M cacodylate buffer, and stored overnight at 4°C in the same buffer. The following day, the samples were dehydrated in a graded series of ethanol, through propylene oxide, and infiltrated with and embedded in Spurr's resin. Ultrathin sections (60-80 nm thick) were cut with a diamond knife and retrieved onto nickel 200 mesh thin-bar grids, and contrasted with 2% alcoholic uranyl acetate and lead citrate. The sections were imaged with a JEOL 1400 transmission electron microscope (JEOL USA, Inc., Peabody, MA) operating at 60 or 80 kV. Digital images were acquired with an AMT-XR611 11 megapixel ccd camera (Advanced Microscopy Techniques, Danvers, MA) at the University of Vermont, and saved in tiff format (12.2 mB/image).

Morphometric Analysis of ZG in Electron Micrographs:

The size (diameter) distribution of ZG in control rat pancreas, and following 1h and 2h post caerulein administration (experimental), was estimated from electron micrographs of the tissue from control and experimental animals. Obtained electron micrographs where enlarged by a factor of 4 and the radii of the ZGs were measured in millimeters. The radii were converted to area via Area = πr^2. The area and diameter in millimeters and square millimeters was compared between ZGs of rats treated with saline and ZGs from rats after 1 or 2 hours of pancreatitis induction by caerulein.

Analysis of Isolated ZG Using Atomic Force Microscopy:

Atomic force microscopy (AFM) was performed on isolated ZGs obtained from both control, 1h, and 2h following caerulein-injection, and fixed using 4% glutaraldehyde and 2% paraformaldehyde in ice-cold PBS for 24 hours. The aldehyde-fixed ZGs were placed on a mica

surface, and imaged by AFM using a minor modification of published procedures (Kelly et al. 2004a, Kelly et al. 2004b). Fixed ZGs in PBS were placed on mica, air-dried for 2 min, washed using distilled water to remove salt crystals, followed by air-drying for 2 min, and imaged using the AFM. ZGs were imaged using a Nanoscope IIIa AFM from Digital Instruments. (Santa Barbara, CA). Images were obtained in the "tapping" mode in air, using aluminum coated silicon tips with a spring constant of 40 $N.m^{-1}$, and an imaging force of <200 pN. Images were obtained at line frequencies of 1-2 Hz, with 256 lines per image, and constant image gains. Topographical dimensions of ZGs were analyzed using the software Nanoscope IIIa4.43r8, supplied by Digital Instruments.

Results

Examination of acinar cells using EM, demonstrate little change in their overall morphology following supramaximal caerulein exposure for up to 2h (Figure 7). However EM and AFM measurements of ZG size demonstrate a significant increase following caerulein exposure. EM and AFM were employed to measure ZG size in control and experimental pancreatic acinar cells using an unbiased randomize approach. ZG size within intact fixed cells were determined from electron micrographs of pancreatic tissue obtained from control rats, and those following 1h and 2h exposure to a supramaximal dose of caerulein. Similarly, AFM measurements of ZG size was assessed using isolated ZG preparations obtained from control and experimental pancreas. Although ZG diameter obtained from EM micrographs would be smaller than its actual size unless the section is taken right through the center of the organelle, the large sample size (>1,000) of ZG used in estimating the average ZG diameter, and the additional information regarding the size distribution of ZGs, provides a near accurate estimate of ZG diameter in different pancreatic tissues. To further test results obtained using EM morphometry,

ZG size was assessed using AFM on the isolated organelle obtained from both control and experimental pancreas.

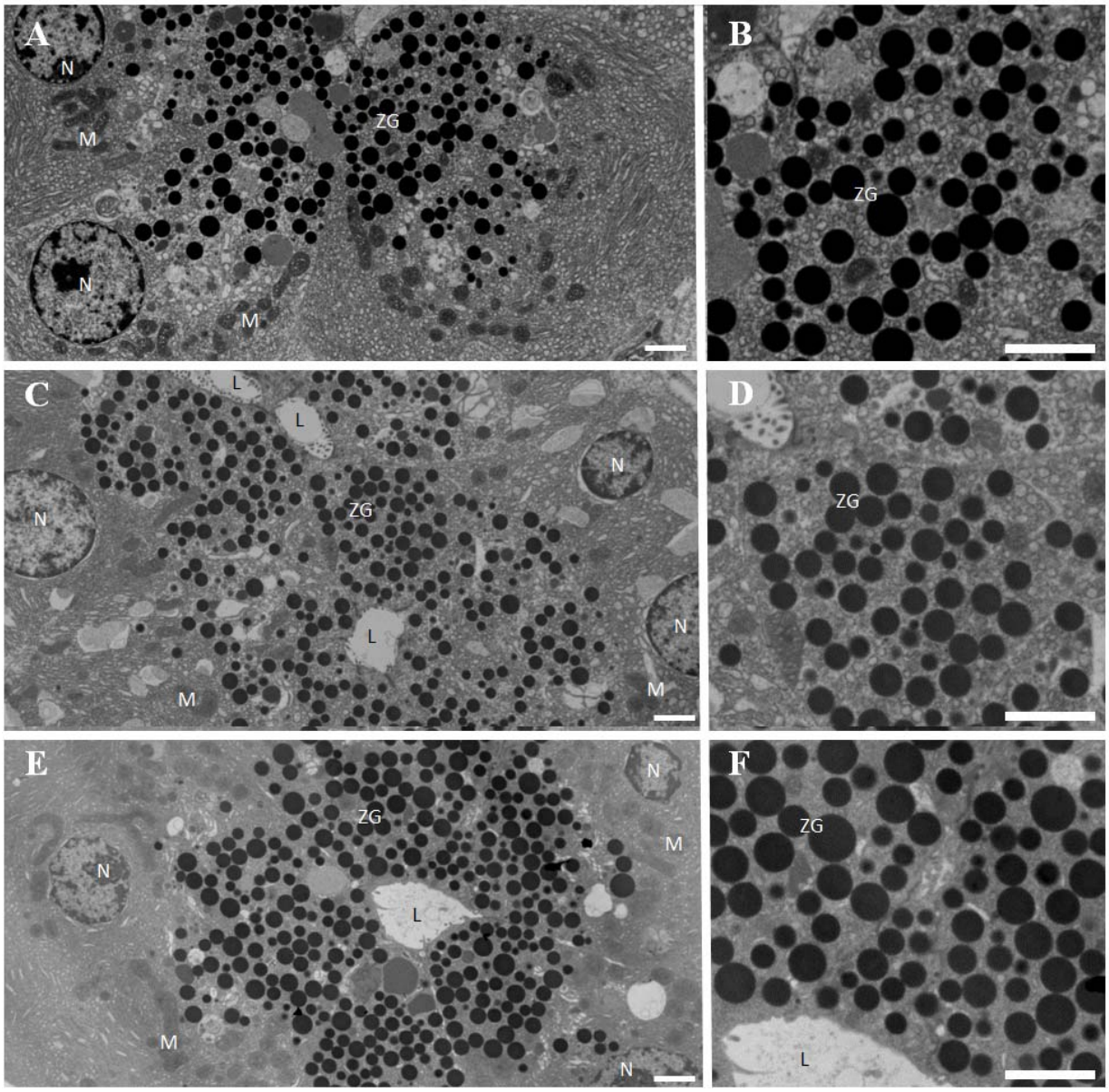

Figure 7. Representative electron micrographs of control rat pancreas (**A**), and 1h (**C**), and (**E**) 2h following caerulein injection with enlargements (**B**, **D**, **F**), respectively. Pancreatic acinar cells demonstrate polarized morphology and the presence of electron dense secretory granules called Zymogen granules (ZG) at the apical compartment of the cell. The acinar lumen (L) at the apical end, and prominent cell nucleus (N) at the basolateral region of the cell is observed. Note little change in the number of ZG in experimental tissue, however vacuolar structures appear in the 2h acinar cells exposed to supramaximal caerulein. *Scale Bar = 2 μm.*

Vesicles from the 1h experimental group did not show a significant size increase however there is a significant increase in vesicle diameter at the 2h time point (N=1155, $p < 0.001$). EM micrograph examination (Figures 7 & 8) reveals vesicle diameter increase from an average of 553nm in control ZGs to 630nm in ZGs from the 2h experimental group. Although amylase activity increased in the one hour group (examined in Chapter 1) and the shift in vesicle distribution (Figure 7 C & D and Figure 8) indicates the beginning of larger vesicle formation no significant change in average vesicle diameter was seen. However, in the two hour group (Figure 7 E & F and Figure 8) the distribution of vesicles is shifted with fewer smaller vesicles present and the number of larger vesicles markedly increased.

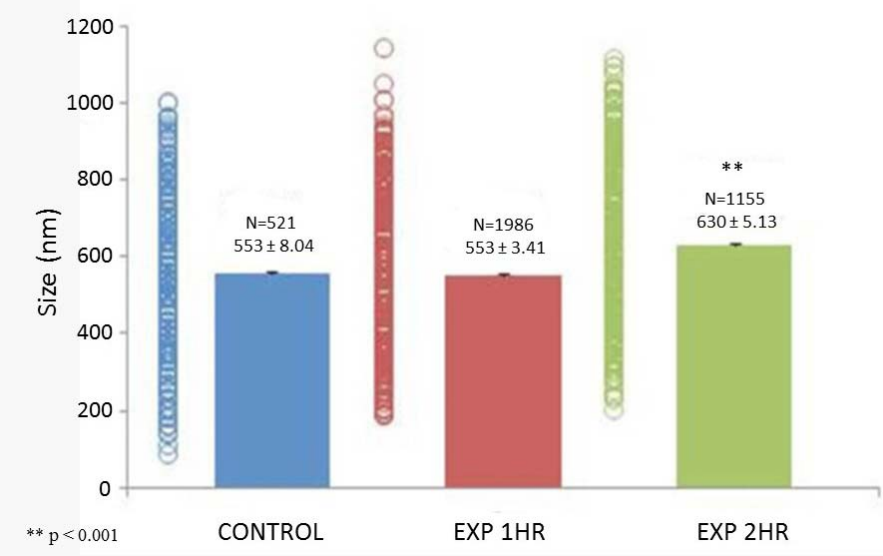

Figure 8. EM morphometry demonstrating ZG swelling in rat pancreatic acinar cells 2h following caerulein administration. Nearly, 13.9% increase in ZG diameter is observed in 2h experimental tissue compared to control or 1h experimental. The numbers of ZG measured for each category are shown as N at the top of the bar, and the distribution range of vesicles plotted are presented to the left of the respective bar graph, blue for control, and red and green for 1h and 2h experimental respectively. Note, although no significant change is noted in the average size of ZGs in the 1h time point, in the 1 and 2h cells there is an upward shift in vesicle size distribution. Data are presented as mean ± SEM ($p < 0.001$).

Independent AFM analysis confirms the EM results. ZGs were isolated from the pancreata of rats injected wither with supramaximal caerulein (50mg/kg, i.p.) or with the volume equivalent of saline for control for AFM analysis. ZGs were isolated and the purity of the

fraction was determined using immunoanalysis. Figure 9 indicates an enrichment in the ZG fraction over the total homogenate fraction of the ZG proteins, VAMP-2, AQP-1, and $G_{\alpha i3}$ verifying purity of the granule population. One hundred fifty vesicles from each the control and 2h group were analyzed and the diameter measured (Figure 10).

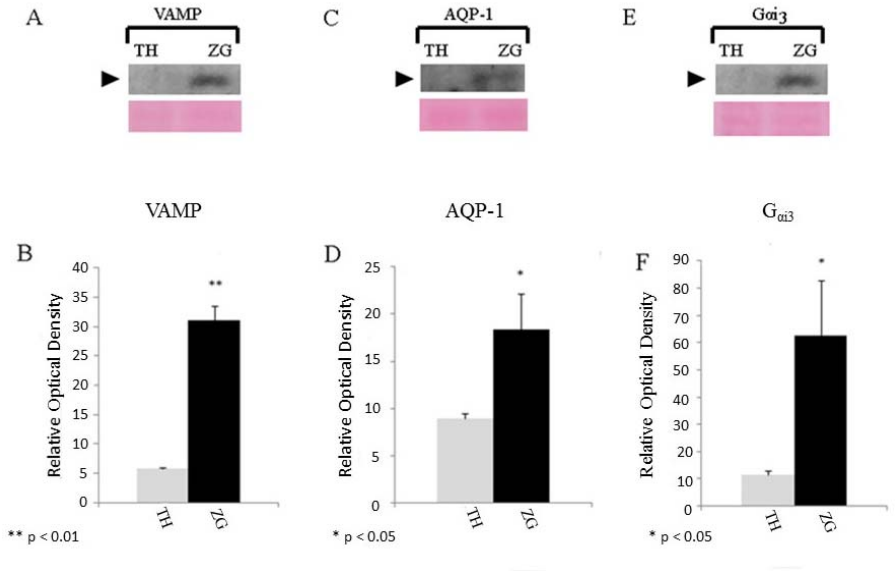

Figure 9. Immunoblot (5µg protein per lane) analysis indicates an enrichment in isolated ZGs over total homogenate fractions indicating the purity of the ZG population. (**A**) Representative western blot of VAMP-2 protein (~15kDa), the v-SNARE present on vesicle membranes is enriched (**B**) in ZG fractions over total pancreatic homogenate (N=6 *p < 0.01). (**C**) Representative blots AQP1 (N=3 *p < 0.05), the water channel (~28 kDa) present on ZGs and (**E**) $G_{\alpha i3}$(N=5 *p < 0.05), the heterotrimeric GTP-binding protein (~42 kDa) found in ZGs also demonstrated to be enriched (**D, F**)in the ZG fractions when compared to their counterpart total homogenate fraction. PonchuS staining confirms total protein sample loaded in each well to be equal in relative content.

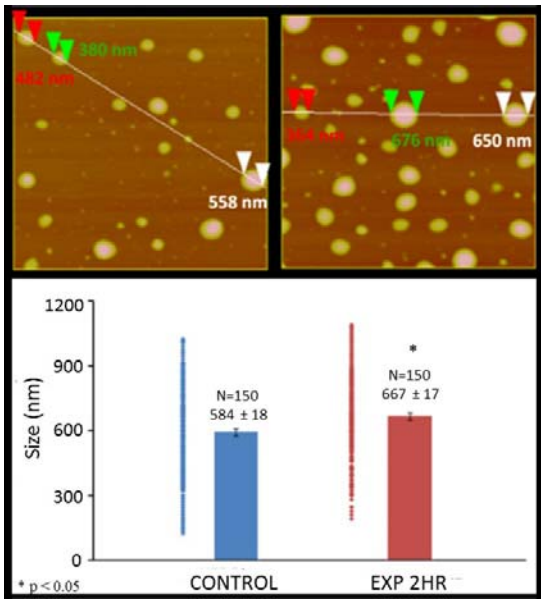

Figure 10. AFM morphometry of isolated pancreatic ZG from 2h post caerulein administered rats demonstrating ZG swelling. A 14.2% increase in ZG diameter is observed in 2h experimental ZG compared to control. The numbers of ZG measured for each category represent N, and the distribution range of ZG plotted are presented to the left of the respective bar graph: blue for control and red for the 2h experimental. Data are presented as mean ± SEM ($p < 0.01$).

Results from the EM study demonstrate a 13.9% increase in ZG mean diameter in the 2h experimental pancreas over those measured in control tissue (Figure 8). AFM measurements of isolated ZG diameter obtained from 2h experimental animals demonstrated a 14.2% increase in ZG size over controls (Figure 10), confirming results obtained using EM morphometry. These studies demonstrate approximately 14% increase in ZG diameter in acute pancreatitis. Due to the significant changes in the morphometry of the two hour group the remainder of the studies will focus on the two hour time point compared to control ZGs from saline treated animals.

Discussion

The EM and AFM micrographs confirm a significant enlargement in the diameter of pancreatic ZGs in the 2h experimental group over saline injected controls. The enlargement is likely due to inappropriate and premature activation of zymogen granule contents as well as biochemical changes taking place at the zymogen granule membrane (ZGM). It has been previously demonstrated that ZGs autoactivate in the early stages of acute pancreatitis (VanAcker et al. 2007, Hofbauer et al. 1998). But the question still remains as to what specifically is causing the granule enlargement. Figures 8 and 10 demonstrate an increase in vesicle diameter indicating a premature enlargement of the vesicle. This may be from premature swelling and therefore disallowing further swelling of the secretory vesicles upon stimulation at the plasma membrane.

A physiological secretory stimulus of pancreatic acinar cells is known to result in approximately a 15% increase in ZG diameter within 2.5 min (Kelly et al. 2004a), followed by a decrease by 5 min. This decrease in ZG size results from a fractional discharge of intravesicular contents (Kelly et al. 2004a). The increased size of ZG even after 2 hours following supramaximal stimulation, suggests the inability of the ZG to fuse at the cell plasma membrane to release its contents. The observed increase in content and activity of plasma amylase (as

examined in Chapter 1) following supramaximal stimulation may be a consequence of ZG swelling and content release from docked vesicles immediately after supramaximal stimulation, prior to a secretion block (Figure 7) resulting from altered ZG chemistry and its compromised ability to fuse at the cell plasma membrane.

As previously reported in humans (Helin et al. 1980), morphometric analysis of ZG using both EM and AFM, demonstrate an increase in vesicle diameter in acute pancreatitis. Results from the study shows that this increase in ZG size in acute pancreatitis results from altered ZGM chemistry, that in-part may be a consequence of the observed overall loss of key ZG volume regulatory proteins at the ZGM including alterations in its lipid profile (Helin et al. 1980). The causes of vesicle enlargement may be multi-factorial but several theories are hypothesized and explored further in Chapter 3. Since the major molecule known to impart volume increase in ZG is water, and the bidirectional water channel AQP1 present at the ZGM is implicated in the process (Cho et al. 2002), ZG swelling in acute pancreatitis may occur prior to the observed loss of AQP1 and other ZG volume regulatory proteins in pancreatitis. Furthermore, the enriched presence of the lysosomal cysteine protease cathepsin B in pancreatitic ZG as well as an increase in co-localization seen in experimental tissue with the LAMP-1 protein supports the likelihood of lysosomal vesicle fusion with ZG. These results suggest that ZG swelling in acute pancreatitis may involve water and ion transport into ZG as well as the fusion of lysosome-derived vesicles.

CHAPTER 3

ALTERED ZG COMPOSITION: IMPLICATION OF THE G-PROTEIN COUPLED RECEPTOR 98 IN GRANULE VOLUME REGULATION

Abstract

Pancreatic digestive enzymes secreted following a meal are stored as inactive zymogens within membrane-bound secretory vesicles called Zymogen Granules (ZG), and activated extracellularly. In acute pancreatitis however, the digestive enzymes are prematurely activated within the cell, resulting in autodigestion of the tissue. Two line of clinical evidence suggest altered ZG morphology and chemistry in causation of the disease. However little is known about the specific mechanism and the proteins and lipids that might participate in this process. Here it is reported that in acute pancreatitis, there are specific changes to both the proteome and lipidome of the ZG, contributing to altered ZG morphology and function. LC-MS-based lipid and protein profiling and immunochemistry, collectively demonstrate altered ZG volume and activity regulating proteins and lipids, in acute pancreatitis. Early events involving alterations in ZG membrane composition lead to zymogen activation within the organelle in thr etiology of the disease. Results from these studies have broader implications in understanding cell signaling.

Introduction

Secretion is a universal process at the cellular level that regulates numerous physiological activities in an organism that includes digestive enzyme release. Cells and their contained membrane-bound vesicles undergo a tightly regulated process for proper release of vesicle contents into the extracellular compartment. Disease states such as pancreatitis inhibit proper secretion. Without correctly functioning secretory machinery the effective release of substances from cells would not be possible as diffusion across the plasma membrane of many cellular products does not occur at a rate that is physiologically beneficial (Jena 1997).

While acute pancreatitis is characterized by a sudden onset of abdominal pain many of its other characterizing symptoms like edema, hemorrhage, and necrosis often go undetected until hospitalization is required (NIDDK 2012, Foster 2013). Due to this there is a lack of clear criteria describing the early stages of this disease. Often, by the time a patient becomes hospitalized the disease symptoms have significantly progressed beyond the initial stages. GI ultrasounds and serum amylase and lipase levels are the only current methods in practice for diagnosis (NIDDK 2012, Carroll et al. 2007). Pancreatic biopsy may prove effective but due to complications and the risk a general surgery poses to the progression of this disease, biopsy is usually avoided (Carroll et al. 2007). A limit on current treatment modalities compounds this problem (Hofbauer et al. 1998).

Two lines of clinical evidence suggest alteration of the ZG and associated lipids in the etiology of the disease. First, ultrastructural studies of the exocrine pancreas in human acute pancreatitic patients demonstrate an increase in ZG size (Helin et al. 2002), and similarly, lipid imbalance and a marked increase in pancreatic PLA_2 activity in patients with acute pancreatitis have been reported (Aufenanger et al. 2002). PLA_2 catalyzes the hydrolysis of phosphatidylcholine (PC) to produce lyso-PC. Calcium-dependent PLA_2 and acyltransferase activity have been demonstrated to be present in ZG membrane (ZGM) in exocrine pancreas (Rubin et al. 1990), and the ZGM-associated $G_{\alpha i3}$ G-protein is implicated in this PLA_2 function (Jena et al. 1997, Cho et al. 2002, Abu-Hamdah et al. 2004, Kelly et al. 2004a, Kelly et al. 2004b, Rubin et al. 1991). Since a sharp rise in intracellular calcium is documented in acute pancreatitis (Fick 2012), and cytosolic PLA_2 ($cPLA_2$) present in the exocrine pancreas is a calcium-dependent PLA_2 requiring Ca^{2+} for both its activity and translocation to a target membrane (Burke and Dennis 2009), its recruitment to the ZGM following induction of acute pancreatitis and the consequent elevation of intracellular Ca^{2+}, was hypothesized. Similarly,

since a drop in intracellular pH has been documented in numerous studies, and the involvement of lysosomes in zymogen activation in acute pancreatitis has previously been reported (Saluja et al. 1985, Saluja et al. 1997a, Saluja et al. 1997b, Saluja et al. 1999, Dawra et al. 2011, Saluja et al. 1987, Saluja et al. 1991, Gorelick and Matovcik 1995), the translocation of the lysosomal cysteine protease cathepsin B to ZG, and the activation of the Ca^{2+}-independent PLA_2 ($iPLA_2$) which requires a low pH optimum (pH 4.5), and its participation in the elevation of lyso-PC in ZG was further hypothesized.

Earlier studies demonstrated the swelling of secretory vesicles during cell secretion (Jena et al. 1997, Cho et al. 2002, Abu-Hamdah et al. 2004, Kelly et al. 2004a), and the requirement of vesicle swelling for the regulated expulsion of intravesicular contents from cells during secretion (Kelly et al. 2004b). This would suggest that since a block in pancreatic acinar cell secretion is observed in acute pancreatitis, the enlarged ZG in acinar cells seen in patients with acute pancreatitis, may reflect the inability of swollen ZGs following supramaximal stimulation to discharge their contents and hence remain larger than normal. Since PLA_2 together with $G_{\alpha i3}$, AQP1, K^+ and Cl^- channels, and vH-ATPase present at the ZGM are involved in ZG volume regulation (Jena et al. 1997, Choss et al. 2002, Abu-Hamdah et al. 2004, Kelly et al. 2004a, Kelly et al. 2004b), alterations in one or more of these ZG volume regulatory proteins in acute pancreatitis was hypothesized.

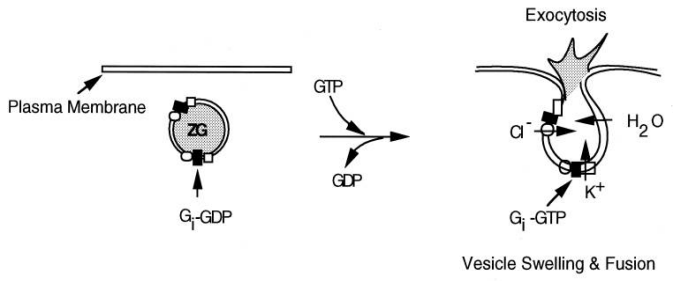

Figure 11. GTP binding proteins regulate a variety of ion channels that are responsible for creating and maintaining the electrochemical gradient necessary for water influx into the secretory vesicle prior to secretion (Jena et al. 1997).

Moreover, since lipid imbalance and an increase in pancreatic PLA_2 activity in patients with acute pancreatitis have been reported (Aufenanger et al. 2002), and PLA_2 catalyzes the

hydrolysis of PC to produce lyso-PC, the involvement of PLA_2 in remodeling of the ZG membrane, thereby influencing lipid protein interaction, was suggested. Membrane function, especially transport and fusogenic properties greatly rely on lipid composition. Specific lipids provide curvature to membranes (vanMeer et al. 2008), they provide interaction with specific membrane proteins to develop platforms for docking and fusion functions in cells (Cho et al. 2007, Lam et al. 2008, Shin et al. 2010), and provide specific mechanical properties (vanMeer et al. 2008) to membrane or vesicle domains, required for optimal function both at the organelle and molecular level. For example, the interaction of syntaxin-1 and N-type calcium channel has been found to be cholesterol dependent (Cho et al. 2007). Syntaxin-1 is known to directly interact with phosphatidic acid and other polyphosphoinositide lipids (Lam et al. 2008). Similarly, lysophosphatidylcholine has been demonstrated to influence both the assembly and disassembly of the t-/v-SNARE complex (Lam et al. 2008, Shin et al. 2011). Therefore, altered ZG lipid composition in acute pancreatitis was hypothesized and investigated using a caerulein-induced rat model of the disease. Employing electron microscopy (EM) and atomic force microscopy (AFM), increase in ZG size in acute pancreatitis was demonstrated. LC-MS-based lipid and protein profiling of ZG, and immunoanalysis, show altered ZG chemistry in acute pancreatitis. Results from the study demonstrate that early events involving alterations in ZG membrane composition likely leads to zymogen activation within the organelle, in acute pancreatitis. These results have now allowed the formulation and will allow for future testing of the hypothesis regarding the specific roles of the identified ZG proteins and lipids altered in acute pancreatitis.

Initiator proteins such as the β_2 adrenergic receptor have been shown to regulate vesicle swelling in synaptic vesicles (Chen et al. 2010). In synaptic vesicles (SVs) co-immunoisolations of $G_{\alpha o}$ and the β_2 adrenergic receptor have been demonstrated. These two proteins have also

been functionally linked. While a β_2 agonist, isoproterenol, did not enhance vesicle swelling beyond control values stimulated by GTP and mastoparan, it did serve the ability to rescue vesicle swelling back to control values after the SV has been previously treated with the β_2 antagonist, alprenolol (Chen et al. 2010), thereby indicating a regulatory function of the β_2 receptor in SV activation.

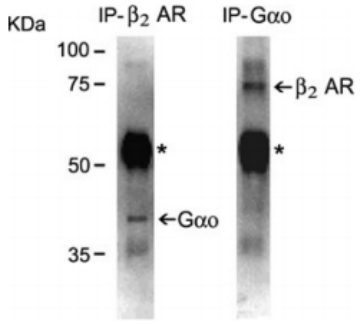

Figure 12. The β-adrenergic receptor was examined for co-immuno isolation with the $G_{\alpha o}$ protein in SVs. Additionally, this physical linkage was confirmed by the ability of $G_{\alpha o}$ to co-immuno isolate with the β-adrenergic receptor (Chen et al. 2011).

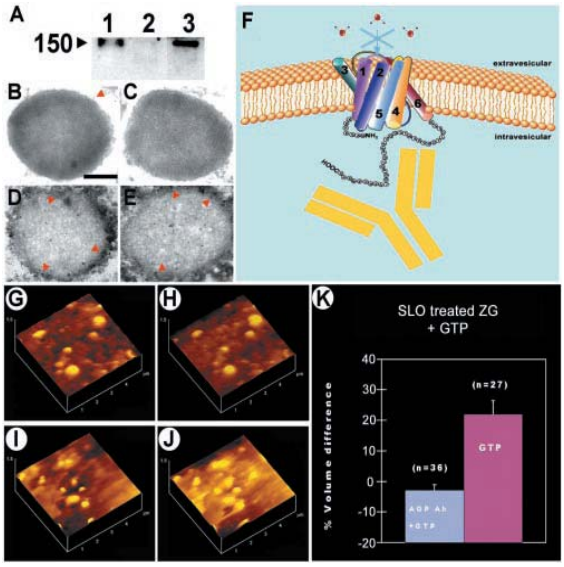

Figure 13. AQP1-specific antibody binds to the ZG membrane and blocks water traffic. (**A**) Immunoblot assay demonstrating the presence of AQP1 antibody in SLO-permeabilized ZG. Lanes: 1, AQP1 antibody alone; 2, nonpermeable ZG exposed to antibody; 3, permeable ZG exposed to AQP1 antibody. Immunoelectron micrographs of intact ZGs exposed to AQP1 antibody demonstrate little labeling (**B** & **C**). (Bar 200 nm.) Contrarily, SLO-treated ZG demonstrate intense gold labeling at the luminal side of the ZG membrane (**D** & **E**). AQP1regulates GTP-induced water entry in ZG. (**F**) Schematic diagram of ZG membrane depicting AQP1-specific antibody binding to the carboxyl domain of AQP1 at the intragranular side to block water gating. (G,H, andK) AQP1antibody introduced into ZG blocks GTP-induced water entry and swelling (from **G** to **H**, after GTP exposure). (**I–K**) However, only vehicle introduced into ZG retains the GTPstimulatable effect (from I to J, after GTP exposure). Courtesy of BP Jena (Cho et al. 2002)

The presence of an activator protein at the SV suggests that other secretory vesicles may contain similar mechanisms. G-protein activation, like in the SV, is a requirement for Cl^- and K^+ gradient formation for water entry into the vesicle (Gilman 1987, Konrad et al. 1995, Weingarten et al. 1990). Limited Mass Spectrometry was undertaken to elucidate any such protein or proteins that may be contributory to secretory activation at the level of the ZG. Previous research has also shown the requirement for vesicular acidification prior to vesicle swelling and content expulsion. In isolated synaptic vesicle preparations, SVs show a significant decrease in swelling when subject to treatment with the v-H^+ATPase inhibitor baflomycin. In normal physiology the v-H^+ATPase pumps protons into the lumen of the vesicle contributing to the gradient created for water movement through the bidirectional water channel AQP1 allowing for the prerequisite swelling (Shin et al. 2010). Since a block in secretion has been previously observed in pancreatitis (Chiari 1896) it would suggest v-H^+ATPase alteration.

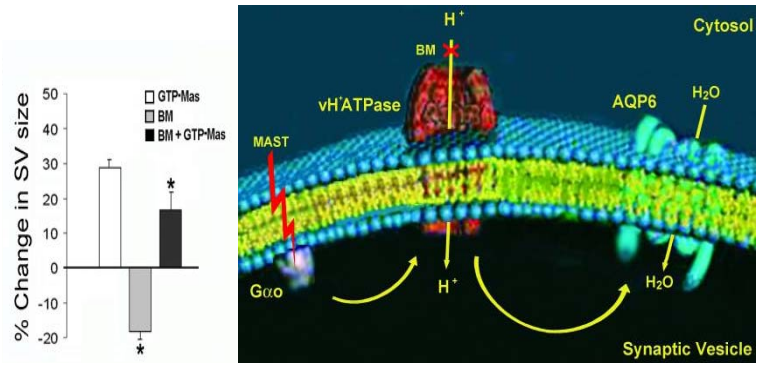

Figure 14. Inhibition of the v-H^+ ATPase proton pump prevents vesicle acidification thereby decreases the gradient along which water enters the vesicle through the AQP disallowing vesicle swelling prior to explulsion of vesicle contents. (Shin et al. 2010).

My research has focused on how volume regulation is altered during this process, and how key lipid players are altered due to pancreatitis. I have assessed many of the integral proteins involved in the secretory cascade and it is evident that changes occur after the induction of this disease. My research has demonstrated a loss in the G-protein ($G_{\alpha i3}$), AQP-1 and the v-H^+ATPase proton pump. In addition to these data I have also confirmed an increase in Cathepsin B in ZGs during pancreatitis as well as a change in the localization of Cathepsin B from the

basolateral pole to more apical regions overlapping with VAMP-2 marked ZGs. An increase in the inflammatory mediators, $cPLA_2$ and $iPLA_2$, were also observed during pancreatitis. Increases in PLA_2 are an indication of inflammation at the cellular level (Nevalainen et al. 1985). In healthy control acinar cells both of the PLA_2 isotypes stained lightly and displayed a diffuse spread throughout the cell. However after the induction of pancreatitis both PLA_2 isoforms increased in quantity migrated apically in a region to colocalize with VAMP-2 marked ZGs. The increase in overall cellular acidity, demonstrated with an increase in BCECF staining, AQP-1 protein, and inflammatory mediators primes the acinar cells and ZGs housed within for digestive enzyme activation. The combination of factors present in the pancreas during pancreatitis predisposes ZGs for early activation and primes the cell for a vicious cycle of pancreatic damage and cellular death. Therefore the third goal of my research has been to focus on the biochemical and lipid changes that occur in pancreatic ZGs after the induction of pancreatitis in rats.

Materials & Methods

Isolation of Zymogen granules (ZG):

Zymogen granules were isolated as previously outlined in Chapter 2.

Western blot analysis:

Five micrograms of isolated ZG or total pancreatic homogenate (TH) preparations in Laemmli buffer (Laemmli 1970) were resolved in a 10% SDS-PAGE, followed by electrotransfer to 0.2 mm nitrocellulose sheets. The nitrocellulose was incubated for 1 h at room temperature in blocking buffer (5% nonfat milk in phosphate buffered saline or PBS containing 0.1% Tween-20 and 0.02% NaN_3) followed by incubation for 1 h at room temperature with primary antibody at a dilution of 1:1,000 in blocking buffer. The immunoblotted nitrocellulose sheets were washed in PBS containing Tween-20, before incubation, for 1 h at room temperature in horseradish peroxidase-conjugated secondary antibody at a dilution of 1:5,000 in blocking

buffer. The immunoblots were washed in PBS containing 0.1% Tween-20 and processed for enhanced chemiluminescence and exposure to X-Omat-AR film. The exposed films then were developed and scanned using a scanner and processed using Adobe Photoshop CS6 (Adobe, SanJose, CA).

Estimation of major lipids in isolated ZG using mass spectrometry

Lipid extraction for mass spectrometry:

ZG were extracted for lipids with methanol and methyl-*tert*-butyl ether (MTBE) according to published methods (Matyash et al. 2008). Briefly, methanol (1.5 mL) containing 100 ng each of internal standards (diheptadecanoyl PC, diheptadecanoyl PE, diheptadecanoyl PS, diheptadecanoyl PA, diheptadecanoyl PG, diheptadecanoyl glycerol-d5, 1,3- diheptadecanoyl -2-(10Z)heptdecenoyl glycerol-d5, 1-palmitoyl(d31)-2-oleoyl-sn-glycero-3-phosphoinositol, and PAF-C16-d4) was added to a suspension of ZG (200 µL) followed by MTBE (5 mL), and mixed well. The mixture was left for 1 h at room temperature with occasional mixing. Water (1.5 mL) was added to the mixture, mixed thoroughly, and centrifuged (1000xg) for 5 min to assist the separation of phases. The upper organic phase was collected to a clean glass tube. The lower aqueous phase was extracted twice (2 mL each time) with MTBE saturated with methanol and water (10:3:2.5 v/v) and the extracts were combined. The MTBE extracts were evaporated to dryness under a gentle stream of nitrogen and the residue was dissolved in LC-MS grade isopropanol-hexane-100 mM aqueous ammonium acetate (58:40:2 v/v). The reconstituted lipid extract was analyzed for lipids by mass spectrometry.

Mass spectrometric quantitation of lipid classes:

Lipid extracts were directly infused into the TurboVion source by a syringe pump at 10 µL/min and analyzed by QTRAP5500 mass spectrometer (ABSCIEX) using Information Dependent Acquisition method. Mass analyzer conditions in the positive ion mode are as

follows: Ionization Potential: 5500 V, Declustering Potential: 120 V, Entrance Potential: 9 V, Collision cell Exit Potential: 9 V. Collision energy for the survey scan was 10 eV and 45 eV for Enhanced Product Ion scans. In each scan, three ions with highest intensity were chosen for dependent product ion acquisition and the detected ions were excluded for the rest of the experiment after three occurrences. Data was analyzed for the identification of lipid species using LipidView software (ABSCIEX). Lipid were quantified against internal standards and normalized against protein values obtained by Bradford assay.

Determination using mass spectrometry ZG proteins resolved using SDS-PAGE

Matrix-assisted laser desorption ionization (MALDI):

Ten micrograms of isolated ZGs each, from control and 2h experimental pancreas, were solubilized in Laemmli buffer (Laemmli 1970) and resolved using a 12.5% SDS-PAGE. The Coomassie-stained protein bands were used for in-gel digest and mass spectrometry. Mass spectrometry was performed using the Applied Biosystems (ABI) 4700 Proteomics Analyzer (TOF/TOF) in positive ion mode. As previously described (Chen et al. 2010), a fraction of the tryptic peptides from each gel band in control ZG and 2h experimental ZG was spotted onto a MALDI target plate for mass spectrometric analysis. Peptide mass fingerprints were collected for each well and the four most intense peaks above S/N of 60 were selected for MS/MS analysis. After the MS and MS/MS, spectra were processed using 4700 Explorer™ software (v2.0, Applied Biosystems). The monoisotopic peak lists generated in ABI's GPS Explorer™ v2.0, was submitted to the GPS Explorer™ v2.0 search tool (based on MASCOT) for protein identities. The Non-redundant Protein Database, NCBInr, was searched using the following parameters for: 0 or 1 missed cleavage by trypsin, carboxyamidomethylation of cysteines as fixed modification, and methionine oxidations, N-terminal protein acetylation, Pyro-glu (N-term E), Pyro-glu (N-term Q) as variable modifications.

LC-MS/MS analysis and database search:

After a detergent removal procedure, tryptic peptides were separated by reverse phase chromatography (Magic C18 column, Michrom), followed by ionization with the ADVANCE ion source (Michrom), and then analyzed in an LTQ-XL mass spectrometer (Thermo Scientific). Abundant species were fragmented with collision-induced dissociation. Data analysis was performed using Proteome Discoverer 1.1 (Thermo), which incorporated the Mascot algorithm (Matrix Science). The NCBI database was used against rat protein sequences and a reverse decoy protein database was run simultaneously for false discovery rate (FDR) determination. Duplicate samples from control and experimental ZG bands were analyzed by nanoLC-MS/MS. In this case, the tryptic peptides were separated on a reversed-phase C18 column with a 90 min gradient using the Dionex Ultimate^{TM} HPLC system. Then the MS and MS/MS spectra were acquired on an Applied Biosystems QSTAR XL mass analyzer using information dependent acquisition mode. A MS scan was performed from m/z 400-1,500 for 1s followed by product ion scans on two most intense multiply charged ions. Peaklists were submitted to Mascot server to search against the NCBInr database for rat sequences with carbamidomethyl (C) used as a fixed modification and oxidation (M), N-acetylation (protein N terminus) as variable modifications. Secondary analysis of both the LTO XL and QSTAR XL were next performed using Scaffold (Proteome Software). A fixed modification of +57 on cysteine (carbamidomethylation) and variable modifications of +16 on methionine (oxidation) and +42 on protein N-terminus (acetylation) were included in the database search. Minimum protein identification probability was set at ≥95% with 2 unique peptides at 95% minimum peptide identification probability.

Immunocytochemistry:

Individual lobules were removed and fixed from pancreata and fixed in 2% paraformaldehyde and 2% gluteraldehyde overnight, washed in and stored at 4°C in PBS until

use. Individual lobules were sliced to 3μm using a cryostat and fixed to glass slides using poly-L-lysine. Lobule slices were incubated in a blocking solution (5% bovine serum albumin in PBS with 0.05% Triton 100-X) for one hour at room temperature. The primary polyclonal antibodies (Santa Cruz Biotechnology, Dallas, TX) were diluted to 1:500-1:1000 in 5% BSA in PBS with 0.05% Triton-100X and incubated at room temperature for one hour. Lobule slices were washed in PBS with 0.05% Triton-100X (3x) for five minutes. The secondary antibodies, Alexa 488 or Alexa 594 fluorescent conjugated donkey anti-goat or anti-rabbit (Santa Cruz Biotechnology, Dallas, TX) were diluted to 1:1000 in 5% BSA in PBS with 0.05% Triton-100X and incubated for one hour at room temperature in dark conditions. Lobule slices were washed in PBS with 0.05% Triton-100X (3x) for five minutes in dark conditions. DAPI (Santa Cruz Biotechnology, Dallas, TX) was diluted 1:1000 in 5% BSA in PBS with 0.05% Triton-100x and exposed to the lobule slices for 10 minutes at room temperature in dark conditions. The sample slices were washed a final time with 0.05% Triton-100X (3x) for five minutes in dark conditions and sterile distilled H_20 (1x) for five minutes before having coverslips placed with Vecta Sheild mounting media. Fluorescent images of acinar cells were obtained using an immunofluorescence FSX100 microscope (Olympus, Center Valley, PA). Images were processed using CellSens and Photoshop CS6 software (Adobe, SanJose, CA).

Immuno Co-Localization Studies:

ZG proteins were solubilized and isolated according to modified procedure (Chen et al. 2010, Jena et al. 2003, Lee et al. 2010). Immunoisolation studies were performed by solubilizing 250μL of isolated ZGs in a solubilization buffer (0.5% Triton-100X, 0.05% Lubrol, 5mM MgATP, 5mM EDTA, 1mM Benzamadine, 10μL/mL protease inhibitor cocktail (Sigma) in PBS, pH 7.5) for two hours with intermittent vortexing. The ZG solution was spun down at 6000 xg. The supernatant was divided in half and exposed to either the GRP-98 or $G_{\alpha i3}$ antibody

(Santa Cruz Biotechnology, Dallas, TX) conjugated to Protein A Plus-Agarose beads (Santa Cruz Biotechnology, Dallas, TX) for one hour on ice followed by washing (3x) with PBS containing 500mM NaCl, 10mM Tris, and 2mM EDTA, pH 7.5. The immunoisolated samples bound to the immune-sepharose beads were eluted using low pH PBS buffer and subsequently brought to neutral pH. SDS-PAGE, electrotransfer to nitrocellulose, followed by immunoblot analysis were then performed on the immunoisolated proteins. GRP-98 immune isolates were probed with $G_{\alpha i3}$ primary antibody and $G_{\alpha ai3}$ isolates were probed with GRP-98 primary antibody to confirm the interaction between the two proteins.

Results

Loss of ZG Volume Regulatory Proteins in Acute Pancreatitis

Proteins from isolated ZGs of rats injected with supramaximal caerulein (50mg/kg, i.p.) or with the volume equivalent of saline for control were resolved using SDS-PAGE for immunoanalysis and demonstrate a loss of $G_{\alpha i3}$, v-H^+ATPase, and AQP1 immunoreactivity, 2h following exposure of rats to a supramaximal dose of caerulein. No change in the membrane fusion protein v-SNARE at the ZG membrane is observed during the period, suggesting that loss from ZG membrane (ZGM) rather than proteolysis is involved in the observed decrease in $G_{\alpha i3}$, v-H^+ATPase, and AQP1 immunoreactivity in pancreatic ZG obtained from rats exposed to a 2h supramaximal dose of caerulein (Figure 15). It is concluded from these results that the loss of ZG volume regulatory proteins must have occurred post ZG swelling, between the 1h and 2h time points following caerulein exposure, since they would be required for the observed ZG swelling at 2h.

Immunoanalysis of resolved ZG proteins from 2h control and experimental pancreas demonstrate the presence of similar amounts of Hsc70 proteins (Figure 15C). AQP1 immunoisolates of solubilized ZG demonstrated greater association of Hsc70 and Hsp70 in

control over experimental (Figure 15 B & D). These results demonstrate that Hsc70 and Hsp70 bind to ZG associated AQP1 and is most likely involved in AQP1 dissociation from ZG in acute pancreatitis. Hsp70 and Hsc70 may similarly regulate association and dissociation of $G_{\alpha i3}$ and vH-ATPase among other proteins at the ZGM. To further confirm results from the study using immunoanalysis, mass spectrometry was performed on resolved ZG proteins from control and experimental animals.

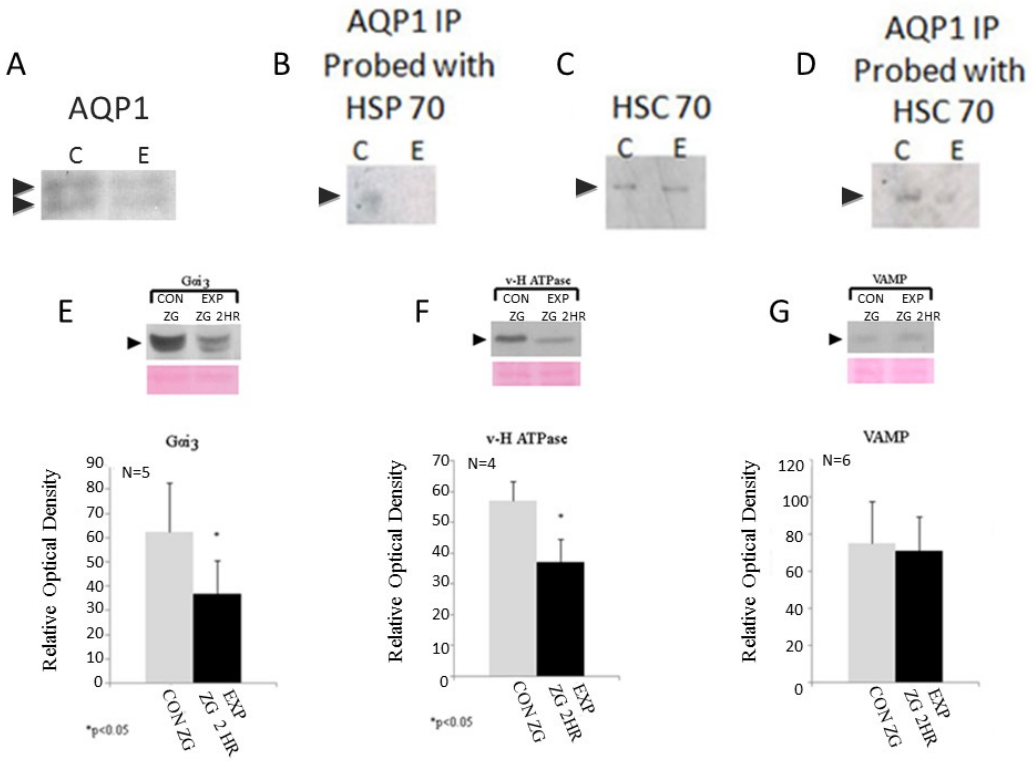

Figure 15. Immunoblot analysis of SDS-PAGE resolved ZG proteins (5µg per lane) from 2h control (**C**) and 2h experimental (**E**) pancreas, demonstrating loss of (**A**) AQP1 (~28kDa, N=6), (**C**) HSC70 (~71kDa), (E) $G_{\alpha i3}$ (~42kDa, N=5) and, (**F**) v-H^+ATPase (~51kDa, N=4), *$p < 0.05$. The SNARE protein VAMP-2 (~15 kDa, N=6) (**G**) does not show any change after caerulein stimulation of the pancreas in isolated ZGs. Immunoprecipitation of solubilized ZG proteins from control and experimental pancreas using AQP1 antibody followed by immunoprobing using HSC70 antibody (**B**) and HSP70 antibody (**B**) implicates the co-localization of AQP1 and both Hsc70 and Hsp70 at the ZGM, and their loss from ZG following supramaximal caerulein exposure of the exocrine pancreas. This study also demonstrates that at the ZGM, AQP1, Hsc70, and Hsp70 are present as a complex, and are potentially dissociated/dislodged following supramaximal caerulein exposure. PonchuS staining of nitrocellulose membranes confirms equal quantities of protein loaded per each lane.

Mass Spectrometry Confirms Loss of ZG Volume Regulatory Proteins in Acute Pancreatitis

To prevent proteolysis, mass spectrometry was performed on ZG proteins first resolved using SDS-PAGE. The separated ZG protein bands were stained using Coomassie Blue, and digested with trypsin following reduction and alkylation. The resultant tryptic peptides were then analyzed by nano LC-MS/MS using an Applied Biosystems QSTAR XL mass analyzer. The separated ZG protein bands from 2h control and 2h experimental appear nearly identical (Figure 16A). Excision of four sets of bands at identical molecular weights from control and experimental ZG, demonstrate loss of the volume regulatory $G_{\alpha i3}$ protein, as demonstrated using immuno analysis (Figure 15). Similarly, mass spectrometry confirms the presence of Hsc70 in both control and experimental ZG as demonstrated using immuno analysis (Figure 15). Interestingly, the G-protein coupled receptor 98 (GRP98), and the guanine nucleotide exchange factor (vav3), were both identified for the first time in control ZGs, and found to be absent in experimental ZGs (Figures 16 and 17), suggesting impaired ZG volume regulation in acute pancreatitis.

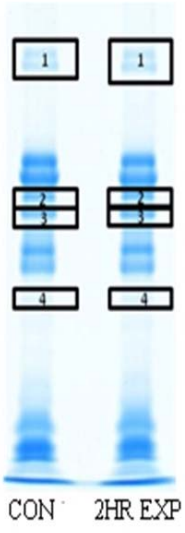

Gel bands	Control	Experiment
1	Hsc70	Hsc70
	GP2	GP2
	Hsp90α, β	Hsp90α, β
2	α-amylase	α-amylase
	Carboxypeptidase A1	Carboxypeptidase A1
	GRP98	-
	Vav3	-
3	Hsc70-interacting protein	Hsc70-interacting protein
	Pancreatic lipase	Pancreatic lipase
4	Chymotrypsinogen B	Chymotrypsinogen B
	Guanine nucleotide-binding protein subunit alpha-13	-

Figure 16. Limited mass spectrometry on ZG from control and 2h post caerulein administered rat pancreas demonstrating loss of $G_{\alpha i3}$, G-protein coupled receptor 98 (GRP98), and the guanine nucleotide exchange factor (vav3). Note: although the SDS-PAGE of resolved bands of proteins appear similar, the mass spectrometry demonstrate otherwise. In each band, multiple protein species were identified. Several representative protein identifications were shown from each band of control and experimental lanes.

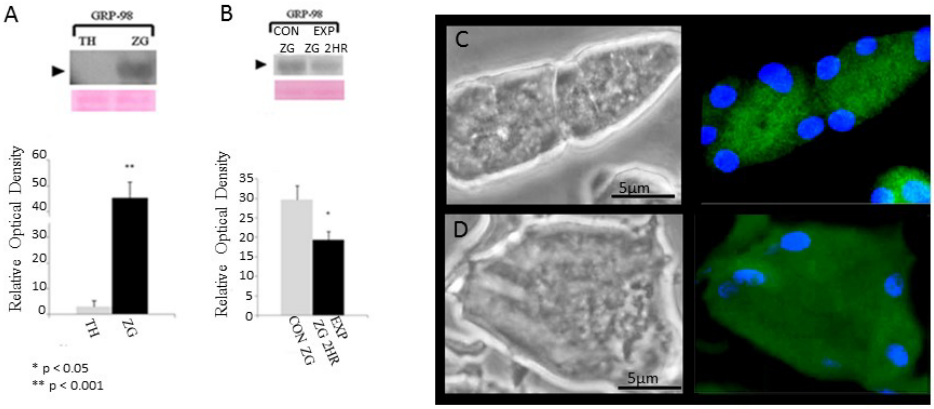

Figure 17. G-protein binding receptor 98 was examined with immunoblot analysis and immunoflourescence. (**A**) Immuno blot analysis of GRP-98 (5µ protein per lane) reveals a significant enrichment in ZGs over total pancreatic homogenate (TH) where it was virtually undetectable (N=6 *p < 0.01). (**B**) Immuno blot analysis (5µ protein per lane) also indicates a significant decrease in GRP-98 presence in ZGs isolated from pancreata of rats injected caerulein (N=5 *p < .05). PonchuS staining of nitrocellulose membranes confirms equal quantities of protein loaded per each lane. (**C**) Phase image of control 3µm thick pancreatic acini immunostained using GRP-98 specific antibody. Note the specific localization of the apical region of the acini where ZGs are located. In contrast, a 3µm thick pancreatic acini (**D**) obtained from the 2h post-caerulein treatment demonstrates diffused staining and enhanced supranuclear GRP-98 staining. A loss of GRP-98 at the acinar lumen is observed. *Scale bar = 5µm*

The wasp venom tetradecapeptide mastoparan, stimulates GTP-induced swelling of ZG (Jena et al. 1997, Cho et al. 2002). Mastoparan potentiates the GTPase activity of G_i/G_o proteins by inserting into the phospholipid membrane, forming a highly structured α-helix that resembles the intracellular loops of G protein-coupled β-adrenergic receptor (Konrad et al. 1995, Higishijima et al. 1998, Vitale et al. 1993). Analogous to receptor activation, mastoparan interacts with the COOH-terminal domain of the G protein α subunit (Weingarten et al. 2011). Hence the presence of a G-protein coupled receptor at the ZG membrane had been hypothesized, and now confirmed from results of the present study (Figures 16 and 17). Similarly, a G protein-coupled β-adrenergic receptor has been reported to be present in the synaptic vesicle membrane of neurons (Chen et al. 2011), and implicated in synaptic vesicle swelling and neurotransmitter release. Collectively, proteomics results from mass spectrometry reveal new players involved in ZG volume regulation, and support the hypothesis that ZG-associated molecules involved in the

regulation of its volume are lost in acute pancreatitis. Results from the study further shows, that the loss of volume regulating proteins such as AQP1 from the ZGM in acute pancreatitis, may in-part be via the Hsp70 and Hsc70 proteins (Figure 18). In recent years, the interaction of Hsp70 with specific membrane lipids such as cholesterol (Zhu et al. 2012) and phosphatidylserine (Arispe et al. 2004), have also been reported. Altered membrane lipids may therefore influence the binding of Hsp70 to its substrate membrane proteins. Since lipid imbalance and a marked increase in pancreatic PLA_2 activity is found in patients with acute pancreatitis (Aufenanger et al.2002), and PLA_2 catalyzes the hydrolysis of phosphatidylcholine (PC) to produce lyso-PC, altered ZG lipid composition in acute pancreatitis was hypothesized and tested.

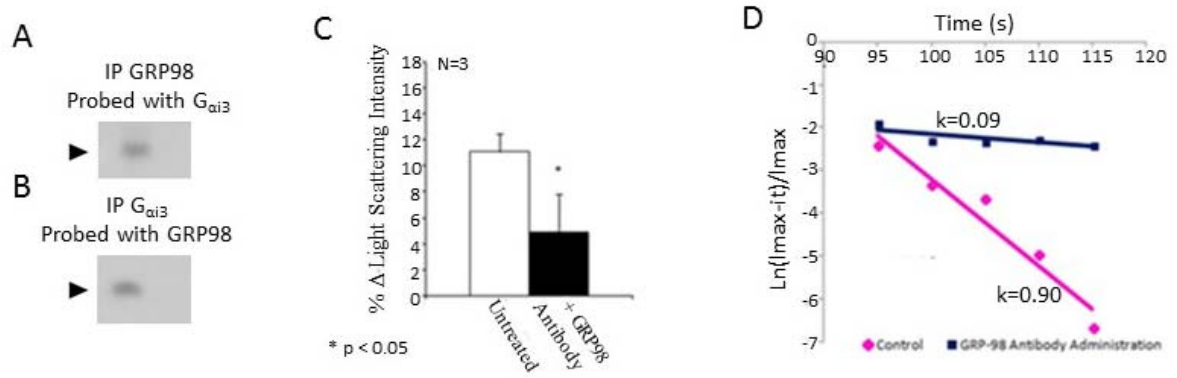

Figure 18. ZG associated GRP98 regulates ZG volume and interacts with $G_{\alpha i3}$. (**A**) ZG immunoisolates using GRP98-specific antibody when probed using $G_{\alpha i3}$-specific antibody, demonstrate colocalization of GRP98 and $G_{\alpha i3}$. (**B**) Similarly, ZG immunoisolates using $G_{\alpha i3}$-specific antibody when probed with GRP98-specific antibody demonstrate co-localization of the two proteins. $G_{\alpha i3}$-mediated ZG volume regulation by GRP98 is demonstrated by the ability of a GRP98 specific antibody to inhibit the potency and efficacy of GTP-Mastoparan induced swelling of isolated ZGs. ZGs pre-incubated with the GRP98 antibody swell much less (**C**) and slower (**D**) when exposed to GTP-Masoparan.

Elevated ZG PLA_2 and Lyso-PC levels in Acute Pancreatitis

Confirming the hypothesis, examination of the lipid profile using mass spectrometry (MS) of isolated ZG from control and 2h post supramaximal caerulein-treated rats, demonstrate elevated lyso-PC levels following caerulein exposure (Figure 19), suggesting elevation of PLA_2

in ZG. While ceramide PE and PE lipids decreased, PC lipids demonstrate a significant increase in ZG following caerulein treatment. Furthermore, several lipid species with high polyunsaturated fatty acid (PUFA) content appeared exclusively in ZG from caerulein-treated animals (Figure 20). Since unsaturated fatty acids increase membrane fluidity, an increase in PUFA content in membrane lipids of ZG may assist in the observed volume increase (Konings et al. 1985). Additionally, PUFA released by PLA_2 serve as substrates for the biosynthesis of lipid mediators of inflammation catalyzed by cyclooxygenases and lipoxygenases, resulting in inflammatory response in acute pancreatitis (Smith et al. 2011, Haegstrom et al. 2011, Serhan and Petasis 2011).

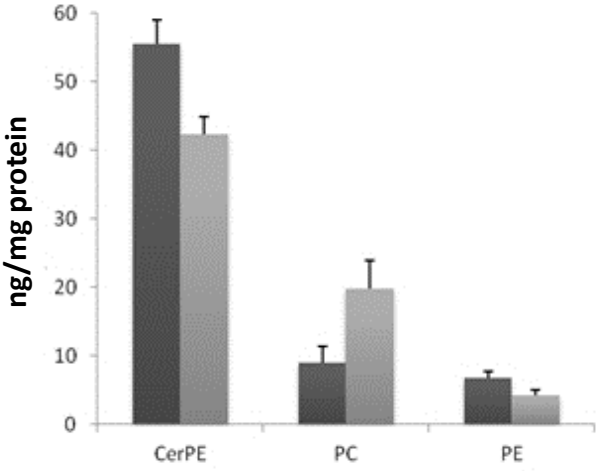

Figure 19. Lipid class profiles in ZG isolated from control and 2h post caerulein administered rats. Lipid profiles were generated by shotgun MS analysis, and data analysis was performed using LipidView (ABXCIEX). Classes of lipids were pooled based on the head groups detected by neutral loss scan MS and only the lipid classes that differed between the two groups with statistical significance ($p \leq 0.05$) are shown. Data represents mean ± SEM.

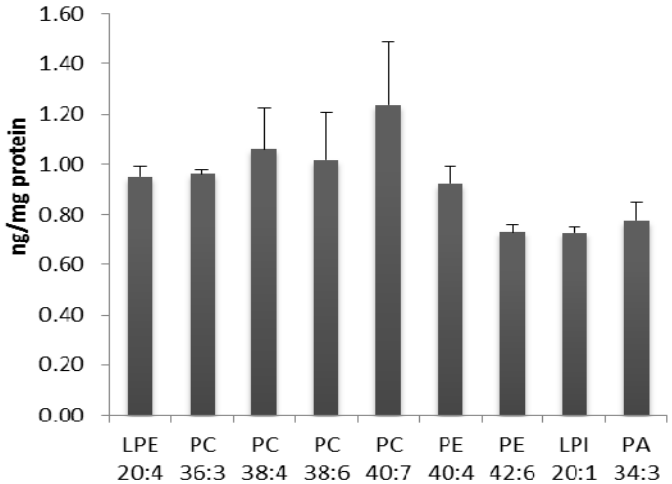

Figure 20. Lipid species that exclusively appear in the 2h ZG of the experimental group (2h post caerulein administered rats). Lipid classes were identified by shotgun MS analysis. Individual lipid species identification was from fatty acids detected by ms/ms of the detected lipids. Data is presented as mean ± SEM.

Two major cellular parameters are altered in acute pancreatitis. First, there is sharp rise in intracellular calcium, and second, a drop in intracellular pH is documented. Since cytosolic PLA_2 ($cPLA_2$) present in the exocrine pancreas is a calcium-dependent PLA_2 requiring Ca^{2+} for both its activity and translocation to a target membrane (Burke et al. 2009), its recruitment to the ZGM following supramaximal caerulein exposure is hypothesized. Immunoblot and immunocytochemistry demonstrate the enriched presence of $cPLA_2$ in ZG obtain from pancreas exposed to a supramaximal dose of caerulein (Figure 22). Using 2',7'-bis(2-carboxyethyl)-5(6)-carboxyfluorescein (BCECF), one of the most common methods of determining intracellular pH, low pH was demonstrated in the apical portion of control acinar cells where ZGs are located (Figure 21A). However, following a 2h exposure to a supramaximal dose of caerulein, a drop in intracellular pH is demonstrated, which is expressed as a diffused BCECF fluorescence throughout the cell (Figure 21B).

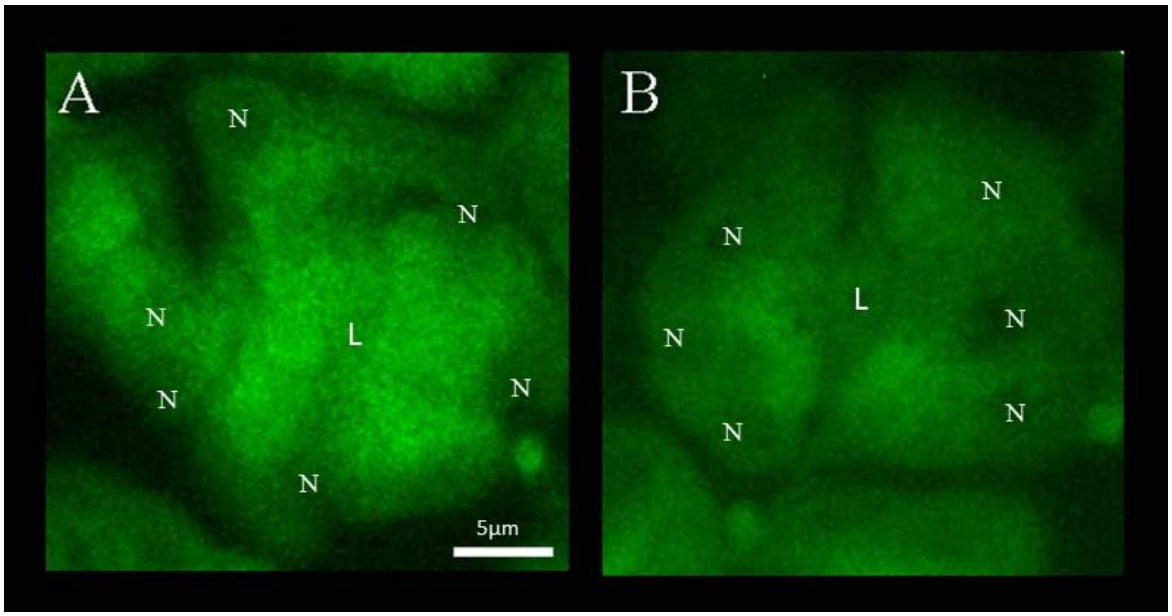

Figure 21. BCECF stain indicates near neutral pH (~6.5) in acinar cells examined from saline treated control animals (**A**), however the BCECF fluorescence is markedly reduced in acinar cells examined from pancreata of the 2h experimental group **(B)**, as a result in drop of intracellular pH following a 2h supramaximal caerulein exposure. (N=nucleus, L=lumen) *Scale Bar = 5µm*.

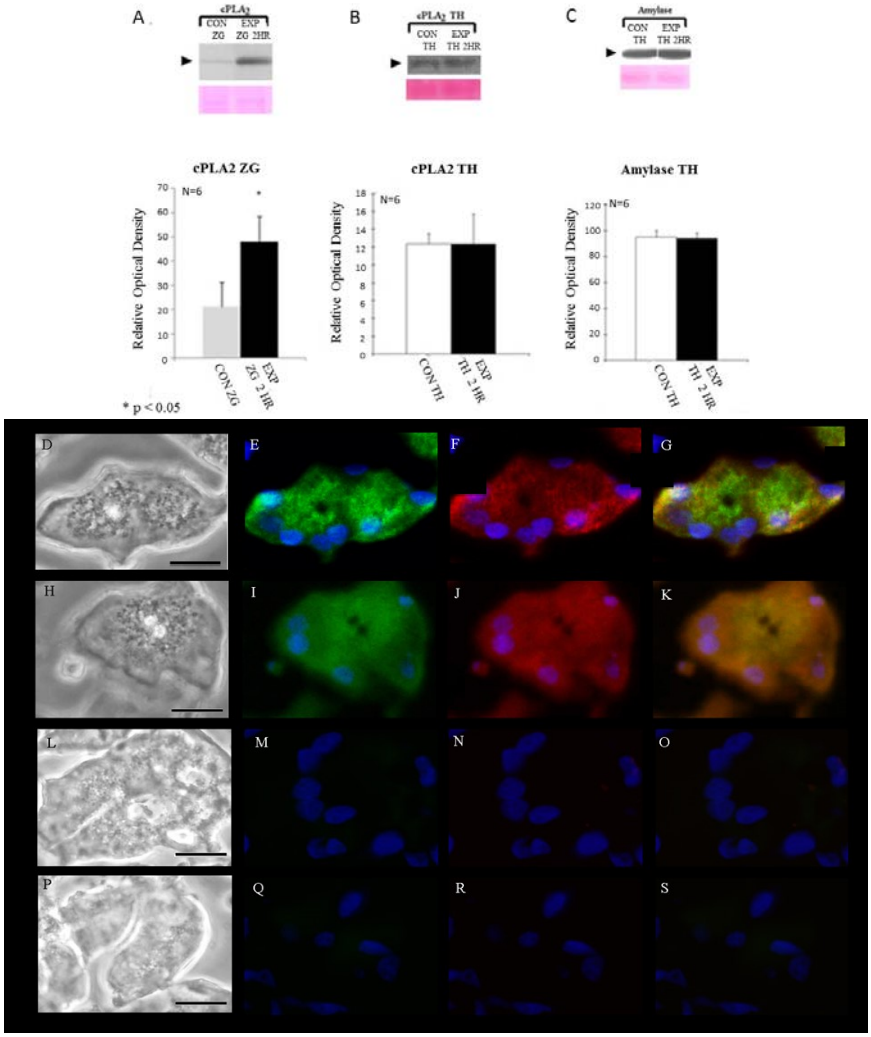

Figure 22. Altered distribution of $cPLA_2$ in acute pancreatitis. Demonstration of its increased association with ZG. (**A**) Immunoblot analysis of 5µg of SDS-PAGE resolved ZG protein per lane, demonstrates a significant increase in $cPLA_2$ in ZGs isolated from pancreata of the 2h experimental rat over control (N=6 *$p < 0.05$). (**B**) No change in total $cPLA_2$ levels are observed in both the control and experimental groups. (**C**) There was also no significant difference in amylase quantity in the total homogenate fraction as examined by Western blot analysis (5ug of resolved protein per lane). In agreement with the Western blot assays, immunocytochemistry (D-S) demonstrate increased association of $cPLA_2$ levels in ZG in acute pancreatitis. Immunocytochemistry demonstrating enriched presence of cPLA2 in ZG in pancreas exposed to a 2h supramaximal dose of caerulein. Phase contrast images indicate the shape of pancreatic acinar cells with apical poles located surrounding a luminal center in both control and 2h experimental rat tissue. Immuno staining verifies VAMP-2 localization in both the control (**D,E**) and experimental (**H,I**) group In contrast, the $cPLA_2$ immunoreactivity is much greater in the apical region of the 2h experimental acini (**J,K**) over control (**F,G)** Very little co-localization is noticed in the control acinar cells (**G**) where as a greater overlap of VAMP-2 and $cPLA_2$ proteins is present in the experimental tissue (**K**). Negative secondary staining controls (**M**,**N** with merged images **O**) for tissue isolated from control pancreata and (**Q**,**R** with merged images **S**) from 2h experimental pancreata demonstrate labeling specificity. PonchuS staining of nitrocellulose membranes confirms equal quantities of protein loaded per each lane. *Scale bar = 5µm.*

Since the involvement of lysosomes in zymogen activation in acute pancreatitis has previously been reported (Saluja et al. 1985, Saluja et al. 1997a, Saluja et al. 1997b, Saluja et al. 1999, Dawra et al. 2011, Saluja et al. 1987, Saluja et al. 1991, Gorelick et al. 1995), the translocation of the lysosomal cysteine protease cathepsin B to ZG, and the activation of certain Ca^{2+}-independent $iPLA_2$ requires a low pH optimum (pH 4.5) including lysosomal PLA_2, the elevation of $iPLA_2$ at the ZGM, and its involvement in lipid modeling at the ZGM in acute pancreatitis was suggested (Figure 23). Both Western blots and immunocytochemistry (Figure 24) confirms the increased presence of cathepsin B with ZG in 2h caerulein exposed pancreas, suggesting the possible fusion of lysosome-derived vesicles with the ZG in acute pancreatitis as previously reported (Saluja et al. 1985, Saluja et al. 1997a, Saluja et al. 1997b, Saluja et al. 1999, Dawra et al. 2011, Saluja et al. 1987, Saluja et al. 1991, Gorelick et al. 1995). Similarly, Western blots and immunocytochemistry (Figure 23) also demonstrated the increased presence of $iPLA_2$ with ZG in the 2h caerulein exposed pancreas.

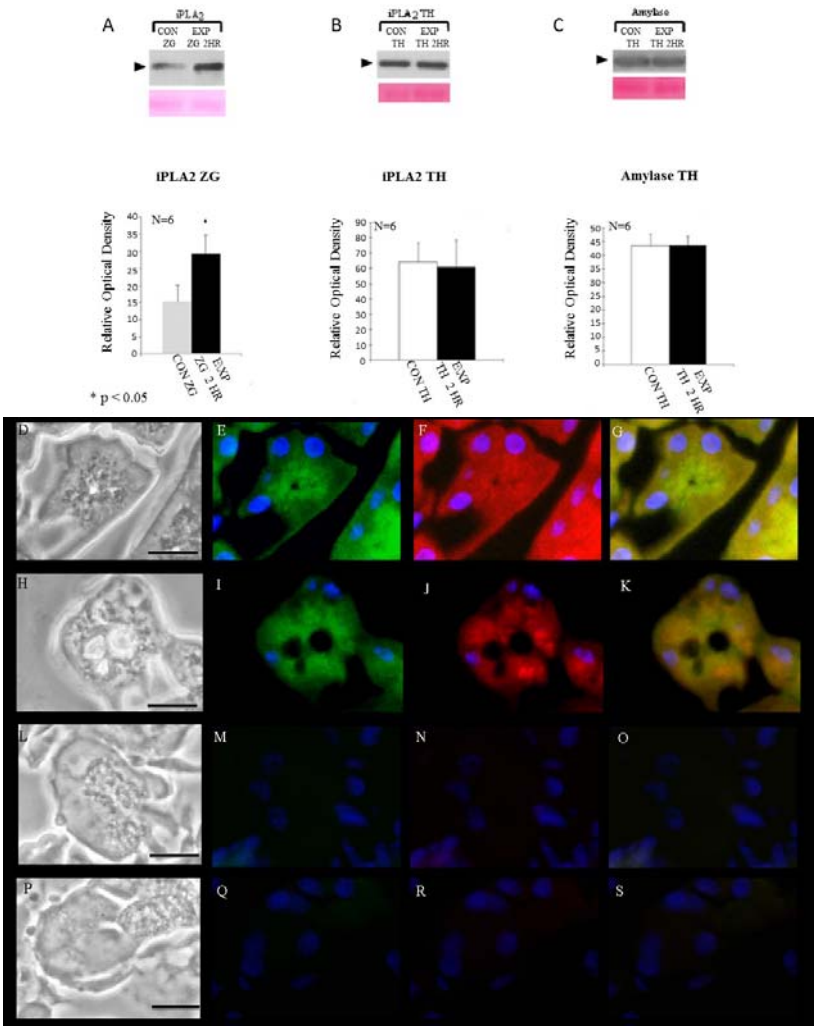

Figure 23. Altered distribution of $iPLA_2$ in acute pancreatitis. Demonstration of its increased association with ZG. (**A**) Immunoblot analysis of 5µg of SDS-PAGE resolved ZG protein per lane, demonstrates a significant increase in $iPLA_2$ in ZGs isolated from pancreata of the 2h experimental rat over control (N=6 *$p < 0.05$). (**B**) No change in total $iPLA_2$ levels are observed in both the control and experimental groups. (**C**) There was also no significant difference in amylase quantity in the total homogenate fraction as examined by Western blot analysis (5ug of resolved protein per lane). In agreement with the Western blot assays, immunocytochemistry (D-S) demonstrate increased association of $iPLA_2$ levels in ZG in acute pancreatitis. Immunocytochemistry demonstrating enriched presence of iPLA2 in ZG in pancreas exposed to a 2h supramaximal dose of caerulein. Phase contrast images indicate the shape of pancreatic acinar cells with apical poles located surrounding a luminal center in both control and 2h experimental rat tissue. Immuno staining verifies VAMP-2 localization in both the control (**D,E**) and experimental (**H,I**) group In contrast, the $iPLA_2$ immunoreactivity is much greater in the apical region of the 2h experimental acini (**J,K**) over control (**F,G)** Very little co-localization is noticed in the control acinar cells (**G**) where as a greater overlap of VAMP-2 and $iPLA_2$ proteins is present in the experimental tissue (**K**). Negative secondary staining controls (**M**,**N** with merged images **O**) for tissue isolated from control pancreata and (**Q**,**R** with merged images **S**) from 2h experimental pancreata demonstrate labeling specificity. PonchuS staining of nitrocellulose membranes confirms equal quantities of protein loaded per each lane. *Scale bar = 5µm*

Discussion

Since the major molecule known to impart volume increase in ZG is water, and the bidirectional water channel AQP1 present at the ZGM is implicated in the process (Cho et al. 2002), ZG swelling in acute pancreatitis may occur prior to the observed loss of AQP1 and other ZG volume regulatory proteins in pancreatitis. Furthermore, the enriched presence of the lysosomal cysteine protease cathepsin B in pancreatitic ZG (Figure 24) as well as an increase in co-localization seen in experimental tissue with the LAMP-1 protein (Figure 25) supports the likelihood of lysosomal vesicle fusion with ZG. These results suggest that ZG swelling in acute pancreatitis may involve water and ion transport into ZG as well as the fusion of lysosome-derived vesicles.

The loss of proteins from the ZGM could occur via cytosolic proteins such as chaperones that are known to bind and dislodge membrane proteins. Molecular chaperones for example, besides protein folding and transport, are also involved in the association-dissociation of proteins into and out of cellular membranes (Young et al. 2003). In eukaryotic cytosol, the chaperones belonging to the heat shock protein family: Hsp70, Hsc70, Hsp90, act through cycles of substrate binding and release governed by ATP hydrolysis (Young et al. 2003). For example, the heat shock protein Hsp70 chaperone machinery has been implicated in the processing and transport of G-protein coupled receptors (Meimaridav et al. 2011). Elevated levels of Hsp70, is known to protect pancreas from caerulein-induced pancreatitis (Bhagat et al. 2002) and heat shock promotes expression of both Hsp70 and AQP1 in cells (Umenishi et al. 2005). Additionally, AQP12 null mice demonstrate increased susceptibility to caerulein-induced acute pancreatitis (Ohta et al. 209), and the direct physical interaction between Hsp70 and AQP2 has also been reported (Lu et al. 2007).

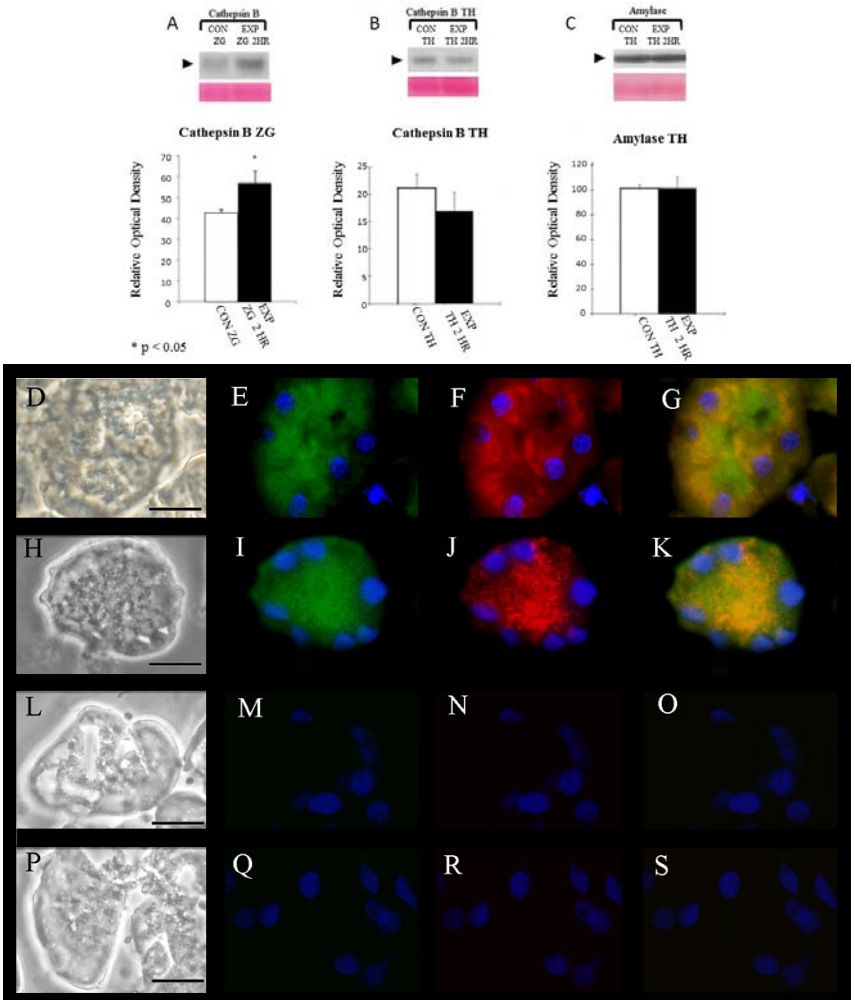

Figure 24. Altered distribution of cathepsin B in acute pancreatitis. Demonstration of its increased association with ZG. (**A**) Immunoblot analysis of 5µg of SDS-PAGE resolved ZG protein per lane, demonstrates a significant increase in cathepsin B in ZGs isolated from pancreata of the 2h experimental rat over control (N=6 *p < 0.05). (**B**) No change in total cathepsin B levels are observed in both the control and experimental groups. (**C**) There was also no significant difference in amylase quantity in the total homogenate fraction as examined by Western blot analysis (5ug of resolved protein per lane). In agreement with the Western blot assays, immunocytochemistry (D-S) demonstrate increased association of cathepsin B levels in ZG in acute pancreatitis. Immunocytochemistry demonstrating enriched presence of cathepsin B in ZG in pancreas exposed to a 2h supramaximal dose of caerulein. Phase contrast images indicate the shape of pancreatic acinar cells with apical poles located surrounding a luminal center in both control and 2h experimental rat tissue. Immuno staining verifies VAMP-2 localization in both the control (**D,E**) and experimental (**H,I**) group In contrast, the cathepsin B immunoreactivity is much greater in the apical region of the 2h experimental acini (**J,K**) over control (**F,G)** Very little co-localization is noticed in the control acinar cells (**G**) where as a greater overlap of VAMP-2 and cathepsin B proteins is present in the experimental tissue (**K**). Negative secondary staining controls (**M**,**N** with merged images **O**) for tissue isolated from control pancreata and (**Q**,**R** with merged images **S**) from 2h experimental pancreata demonstrate labeling specificity. PonchuS staining of nitrocellulose membranes confirms equal quantities of protein loaded per each lane. *Scale bar = 5µm*

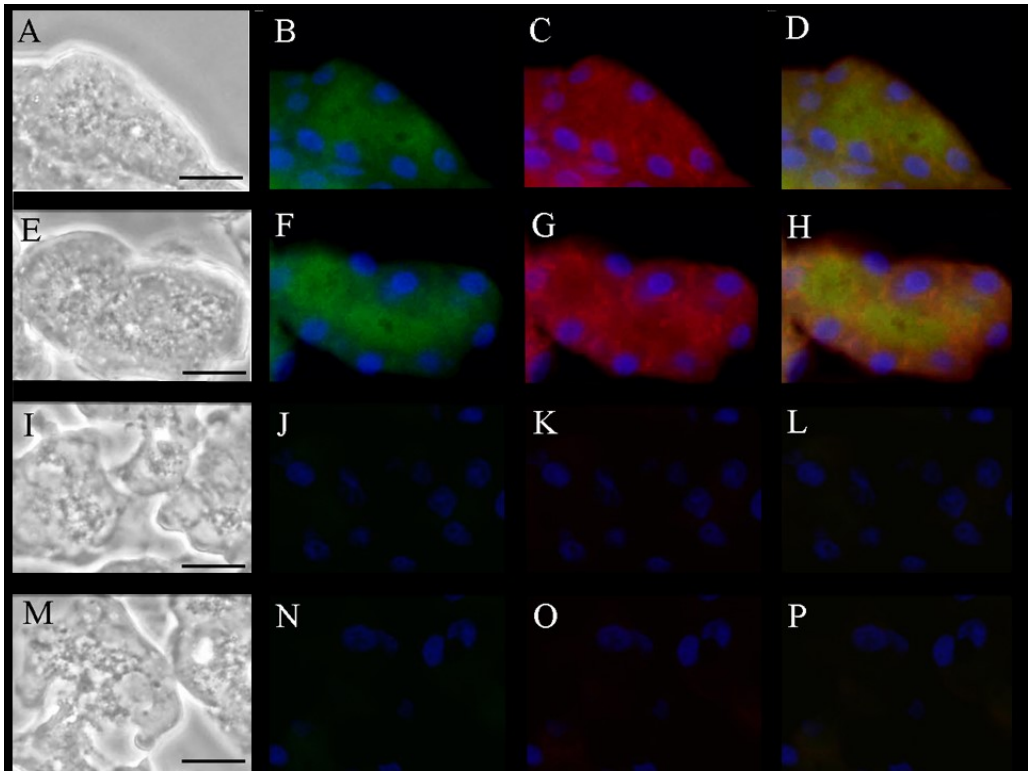

Figure 25. Altered distribution of LAMP-1 in acute pancreatitis. Immunocytochemistry demonstrating enriched presence of LAMP-1 in pancreas exposed to a 2h supramaximal dose of caerulein. Phase contrast images indicate the shape of pancreatic acinar cells with apical poles located surrounding a luminal center in both control and 2h experimental rat tissue. Immuno staining verifies VAMP-2 localization in both the control (**A,B**) and experimental (**E,F**) group In contrast, the LAMP-1 immunoreactivity is much greater in the 2h experimental acini (**G,H**) over control (**C,D)** Very little co-localization is noticed in the control acinar cells (**D**) where as a greater overlap of VAMP-2 and LAMP-1 proteins is present in the experimental tissue (**H**). Negative secondary staining controls (**J,K** with merged image **L**) for tissue isolated from control pancreata and (**N,O** with merged image **P**) from 2h experimental pancreata demonstrate labeling specificity. *Scale bar = 5μm*

These studies suggest that heat shock proteins could modulate ZG volume either by the removal of certain volume regulatory proteins from the ZGM or by direct binding to modulate activity of proteins at the ZGM. Similarly, the loss of ZGM-associated $G_{\alpha i3}$ could also be due to lipid modifications of the G proteins (Cabrera-Vera et al. 2008). It is well established that fatty acid acylation serve as hydrophobic membrane anchor for G-proteins. In the G_i family of G_α subunits for example, both myristoylation and palmitoylation contribute to membrane association (Degtyarev et al. 1994, Morales et al. 1998, Mumby et al. 1994, Wise et al. 1997). While myristoylation is relatively stable, palmitoylation is readily reversible. Removal of

palmitoylation results in a partial shift in localization of the $G_{\alpha i}$ subunit from membrane to the cytoplasm (Degtyarev et al. 1994, Morales et al. 1998, Mumby et al. 1994, Wise et al. 1997, Cabrera-Vera et al. 2003). Based on this information, possible changes in palmitoylation of ZG-associated $G_{\alpha i3}$, and or the involvement of Hsp70/Hsc70 in $G_{\alpha i3}$, v-H^+ATPase, and AQP1 loss from the ZGM, was hypothesized. The involvement of Hsp70/Hsc70 on $G_{\alpha i3}$, v-H+ATPase, and AQP1 loss from the ZGM was therefore tested (Figure 15).

Identification for the first time of the presence of G-protein coupled receptor 98 (GRP98) and the guanine nucleotide exchange factor (vav3) in ZG, and the involvement of GRP98 in $G_{\alpha i3}$-mediated ZG volume regulation, was a surprise find that progressed our understanding of ZG volume regulation in pancreatic acinar cells. Although the ligand for GRP98 is yet to be identified, the receptor possesses 35 calcium binding Calx-beta domains that could be involved in the signaling and regulation of the receptor. Since caerulein-induced acute pancreatitis results in a significant increase in basal intracellular calcium (135 nmol/l, opposed to 72 nmol/l in control cells) (Bragado et al. 1996), the role of elevated calcium on the interaction between GRP98 and $G_{\alpha i3}$ at the ZGM will need to be explored. Earlier studies (Jena et al. 1997) report that calcium has no effect on GTP-mediated ZG swelling, suggesting that the calcium binding sites in GRP98 may regulate binding of the endogenous ligand to the receptor. Hence, the endogenous ligand for ZG associated GRP98 needs to be identified. Since calcium-dependent PLA_2 and acyltransferase activity have been demonstrated to be present in ZGM (Rubin et al. 1990), and ZGM-associated $G_{\alpha i3}$ G-protein is implicated in this PLA_2 function (Jena et al. 1997, Cho et al. 2002, Abu-Hamdah et al. 2004, Kelly et al. 2004a, Kelly et al. 2004b, Rubin et al. 1991), the calcium-mediated interactions between GRP98, $G_{\alpha i3}$, and PLA_2, at the ZGM is hypothesized. The involvement of GRP98 in $G_{\alpha i3}$-mediated ZG volume regulation may be similar to the $G_{\alpha o}$ protein-coupled β-adrenergic receptor identified at the synaptic vesicle

membrane in neurons for regulated synaptic vesicle swelling and neurotransmitter release at the nerve terminal (Chen et al. 2011).

Since results from the study demonstrate binding of Hsp70 and Hsc70 with the ZGM-associated volume regulatory water channel AQP1, their involvement in the association-dissociation of AQP1 at the ZGM is suggested. Due to the previously reported protective power of Hsp70 against acute pancreatitis in rats (Bhagat et al. 2002), a possible role of Hsp70 may involve binding and stabilization of the associated AQP1 and other volume regulatory proteins at the ZGM. The altered lipid composition of ZG in acute pancreatitis demonstrated from the study, and the reported interaction of Hsp70 with specific membrane lipids (Zhu et al. 2012, Arispe et al. 2004), suggests that this change in ZG membrane lipids possibly influences the binding of Hsp70 to AQP1 or other ZG volume regulatory proteins, resulting in their loss from the ZGM.

The pH regulating vacuolar ATPase has been implicated in triggering zymogen activation in pancreatic acinar cells (Ohta et al. 2009), and the water channel aquaporin 1 (AQP1) is over expressed in the plasma membranes of pancreatic ducts in patients with autoimmune pancreatitis (AIP) (Waterford et al. 2005). Hence the altered ZG volume regulation observed in acute pancreatitis may represent an early event in the etiology of the disease. This hypothesis is further supported by the observation that AQP12 null mice show increased susceptibility to caerulein-induced acute pancreatitis (Ko et al. 2009). Since, $G_{\alpha i3}$, PLA_2, AQP1, and vH-ATPase are present in the ZG membrane, and their involvement in granule volume regulation is well established, the ZG size increase in acute pancreatitis appears to result from fluid entry rather than fusion between ZGs, since no loss in ZG number is demonstrated in acute pancreatitis. This however does not preclude the fusion of small lysosomal vesicles with the ZG in acute pancreatitis, and therefore both water entry and lysosome fusion could reflect the observed ZG

volume increase. The fusion of small 200 nm in diameter lysosomes, or 50-100 nm in diameter primary lysosomes or lysosome-derived vesicles with a certain population of ZG is likely.

Moreover, to activate zymogen within ZGs would require initial hydration followed by activation via lysosomal enzymes. Therefore preceding zymogen activation, there are critical changes at the ZGM, altering ZG function, leading to ZG hydration and ZG-lysozome fusion, consequently leading to the activation of zymogen within pancreatic acinar cells. Changes in ZG volume could also be assisted by changes in the lipid composition of the ZGM in acute pancreatitis. The significant increase in PC and lyso-PC in pancreatitic ZG would increase the positive membrane curvature (Fuller and Rand 2001), introducing packing stress, effecting membrane integrity (Cullis et al. 1979, Gruner et al. 1985, Zhelev et al. 1998), and the conformation and activity of membrane proteins (Bezrukov et al. 1999). Similarly, since polyunsaturated fatty acid contents are elevated in pancreatitic ZG, and polyunsaturated fatty acids are known to increase membrane fluidity, they are likely to assist in ZG volume increase.

Based on these results and reported studies, impaired water transport at the ZGM, due in part to alteration in the GRP98-$G_{\alpha i3}$–meadiated ZG volume regulation, a new paradigm in the pathophysiology leading to acute pancreatitis. The fusion of lysosome with ZG in acute pancreatitis is further suggested from the study since the lysosomal cysteine protease cathepsin B is enriched in the ZG, and a 14% increase in average ZG diameter measuring 553 ± 8.04 nm would reflect the fusion of just two 200 nm in diameter lysosomes or nine 100 nm in diameter primary lysosomes or lysosome-derived vesicles. The next objective is to determine the ligand for the ZG-associated GRP98, to be able to elucidate the entire signaling cascade at the ZGM involved in ZG volume regulation.

CHAPTER 4

ZG MEMBRANE CHOLESTEROL ALTERS SWELLING COMPETENCY

Abstract

Cholesterol is critically important and has many functions in the body in a normal and healthy physiological state. It ranges from a precursor of steroid hormones to being an integral component in cellular signaling and lipid raft formation. This study has examined the effects of cholesterol on ZG swelling, and has specifically highlighted that excessive cholesterol presence or its depletion in the ZG membrane leads (ZGM) to a decrease in vesicle swelling competency. Vesicle swelling was measured by light scattering intensity was measured over time. ZGs pre-incubated in cholesterol or methyl-β-cyclodextran swelled to a lesser degree and more slowly than untreated control ZGs. This suggests the need for a precision balance in cholesterol homeostasis in the pancreas.

Introduction

Previous studies have shown membrane composition to be an integral component in membrane fusion (Jeremic et al. 2006, Cho et al. 2007). Integral membrane lipids like cholesterol and lysophosphatidylcholine (LPC) effect the positive and negative curvature, respectively, of lipid vesicles (McMahon and Gallop 2005). They also alter the ability of SNARE proteins to disassemble after a secretory event. It has been shown that when artificial vesicles enriched in v-SNAREs meet artificial vesicles enriched in t-SNAREs in solution they will freely form a ring complex and when n-ethylmaleimide-sensitive factor (NSF) plus ATP are added the SNARE proteins disassemble. When LPC is added to the t- and v-SNARE enriched vesicles there is a lack of disassembly, but when cholesterol is added disassembly is not affected (Shin et al. 2011).

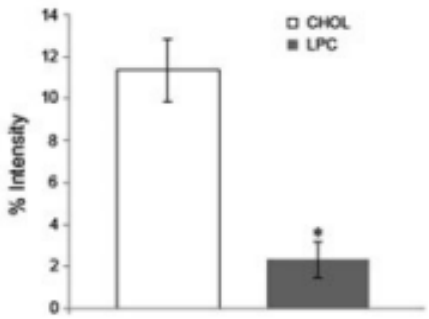

Figure 26. Dynamic Light Scattering Studies indicate a lack of SNARE disassembly with NSF-ATP when the artificial vesicles, liposomes, are enriched in LPC. However, in cholesterol enriched vesicles disassembly occurs normally (Shin et al. 2012).

Cholesterol is also important for ideal secretory release at the porosome. It has been established that syntaxin-1, a t-SNARE protein, co-localizes with cholesterol in synaptosomal membranes. Further depletion of cholesterol from the synaptosomal membrane results in dissociation of N-type calcium channels and syntaxin-1 from the porosomal complex in the plasma membrane (Jeremic et al. 2006). It has also been previously demonstrated that t-SNAREs demonstrate a physical connection with calcium channels in the brain. When cholesterol is depleted and t-SNAREs and calcium channels lose their direct interaction the porosomal machinery becomes unstable. Loss of calcium channels at the porosome leads to loss of the primary fusogen (Jeremic et al. 2004) therefore transient docking of vesicles at the plasma membrane is not favorable (Cho et al. 2007).

It has been established that cholesterol is required for more than membrane fusion alone. Synaptic vesicles (SVs) isolated from rat brain cortex swell after GTP and mastoparan stimulation (Lee et al. 2010, Chen et al. 2011). It has been demonstrated that cholesterol is a requirement for vesicle swelling in SVs. In isolated SVs where cholesterol has been depleted via methyl-β-cyclodextran (MβCD), GTP and mastoparan stimulable swelling is significantly abrogated. Co-immunoisolations reveal the $G_{\alpha o}$ protein is associated with both the v-H^+ATPase proton pump required for vesicle acidification and with AQP6. However, after the SVs were incubated with the cholesterol removing detergent saponin, the association between $G_{\alpha o}$ and v-

H^+ATPase and the association between $G_{\alpha o}$ and AQP6 was significantly decreased. These data indicate that cholesterol is necessary for synaptic vesicle swelling (Lee et al. 2010).

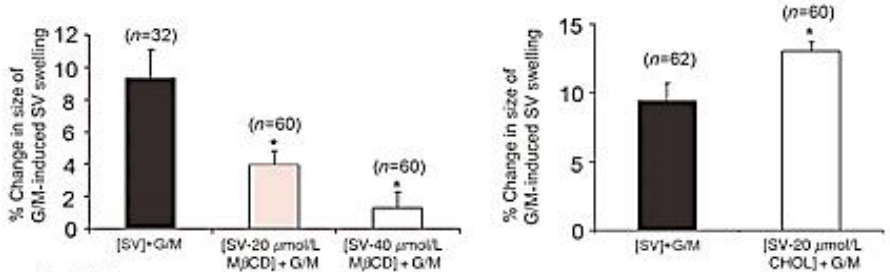

Figure 27. Isolated SVs swell when stimulated with GTP and mastoparan. Exposure of SVs to 40μM MβCD significantly inhibits GTP and mastoparan-induced vesicle swelling and is dose dependant. In contrast, exposure of SVs to 20μM cholesterol demonstrates a significant increase in GTP and mastoparan stimulated swelling (Lee et al. 2010).

Determining the role of cholesterol as it affects health and disease is increasingly important. In cells containing AQP4, vesicles swell at a slower rate when cholesterol is present. The permeability of AQP4 is also altered by cholesterol presence. In the presence of high concentrations of cholesterol, AQP4 permeability is diminished (Tong et al. 2012). In light of this the hypothesis that cholesterol may alter AQP-mediated swelling in pancreatic ZGs is suggested. My research has highlighted the importance of tight cholesterol regulation in the body. Specifically, the effects of cholesterol on ZG swelling is examined and I have shown that excessive cholesterol presence at the ZGM or its depletion leads to a decrease in vesicle swelling ability. This is key in understanding how metabolic disorders like high cholesterol predispose individuals to disease. A lack of secretion is demonstrated in acinar cells during the course of pancreatitis. It has therefore been important to examine one of the ways cellular secretion can be altered leading to potential disease states.

The causes of pancreatitis on a global scale range from gall stones and alcohol abuse to metabolic disorders. While physical or behavioral changes may ameliorate disease symptoms and improve prognosis associated with alcoholic or gall stone-induced pacreatitis (National Pancreas Foundation 2013, NIDDK 2012) metabolic disorders like altered lipid states are more

difficult to control systemically. Much less is known about how these factors contribute to cellular dysfunction that can potentially lead to disease states like pancreatitis (Pandol et al. 2007). Therefore my research goal has been to examine how the addition of exogenous cholesterol or the depletion of ZG membrane cholesterol effects the ability of the isolated ZG to swell when stimulated with GTP and mastoparan. When vesicles are pre-incubated with exogenous cholesterol there appears to be a significant decline in the ability of the ZG to swell after being challenged with GTP and mastoparan.

Cholesterol homeostasis in the pancreas is essential for proper ZG content release (Lee et al. 2010, Ravnskov 2002). The swelling ability of the ZG is markedly altered when cholesterol levels are changed. The addition or subtraction of cholesterol may serve to geographically isolate some of the key secretory cascade proteins from one another or interfere with their ability to function properly during a secretory event although currently this is only hypothesized. High cholesterol and other lipids have been demonstrated to cause significant impairment in human physiology in more than one tissue bed (Ravnskov 2002). Therefore it has been my goal to examine the effects of altered cholesterol levels in isolated ZGs and subsequent swelling competency.

Materials & Methods

Isolation of Zymogen granules (ZG):

Zymogen granules were isolated as previously outlined in Chapter 2.

Right Angle Light Scattering:

Kinetics of ZG vesicle swelling was monitored using right angle light scattering with excitation and emission set at 600nm in a Hitachi F-2000 spectrophotometer as previously established (Jeremic et al. 2003, Shin et al. 2011). A 5μL ZG suspension was injected into cuvettes containing 700μL assay buffer (100mM Mes, 25mM KCl, pH 6.5) under continuous

stirring. ZGs were assessed for swelling capability with and without the presence of the GRP-98 (MASS-1) (Santa Cruz Biotechnology, Dallas, TX) antibody. Light scattering was monitored in baseline conditions for 100 seconds then 40μM GTP and 40μM Mas7 were added to the suspension. The ZG suspension was then monitored for 100 more seconds with average light scattering intensities averaged every two seconds. Values are expressed in arbitrary units as percent light scattered over control (n=6). Student's t test was used comparisons between groups with significance established at $p < 0.05$.

Results

Isolated ZGs were then examined with right angle light scattering. ZGs were stimulated to swell with increasing concentrations of GTP and mastoparan. The greatest degree of swelling was observed with 40μM GTP and mastoparan (Figure 28A). These data indicate the viability and functionality of the isolated ZGs suspended in assay buffer. ZGs stimulated to swell with 40μM GTP and mastoparan but pre-incubated with cholesterol demonstrated a significant decrease in vesicle swelling (Figure 28B) as indicated by a decrease in light scattering intensity.

Kinetics were also measured and the cholesterol pre-incubated ZGs swelled at a slower rate than their untreated ZG counterparts (Figure 28C). Vesicle swelling was measured by light scattering intensity over time and averaged every five seconds. As the vesicles swell it is represented by an increase in light scattering intensity. The slope of the curve generated by the light scattering intensity over time was significantly decreased when compared to the slope of the curve generated from isolated ZGs that did not undergo cholesterol pre-incubation.

Interestingly, when isolated ZGs were pre-incubated in MβCD then stimulated 40μM GTP and mastoparan there was also a deficit (Figure 28 B) in swelling degree when compared control values. This suggests that while the addition of copious amounts of cholesterol are detrimental for secretory vesicle swelling in the pancreas, the removal of cholesterol also impairs

vesicle swelling. While the ZGs swelled to a lesser degree than control as seen by light scattering they also swelled at a slower rate than control, untreated ZGs (Figure 28D). Raw data traces (Figure 28E) indicate the differences in light scattering over time.

Discussion

While cholesterol has been shown to be imperative in neuronal vesicle content release (Lee et al. 2010) in that it potentiates membrane fusion (Shin et al. 2011) and complete loss of cholesterol due to MβCD significantly inhibits synaptic vesicle swelling (Lee et al. 2010), my research indicates that excess cholesterol presence in the pancreas is detrimental to proper secretory function (Figure 28 B & C). When these data are paired with that data showing a lack in vesicle swelling with the addition of MβCD these results indicate that the levels of cholesterol must be tightly regulated and that the presence or absence of excess cholesterol may allow symptoms including impaired cellular secretion from pancreatic acinar cells.

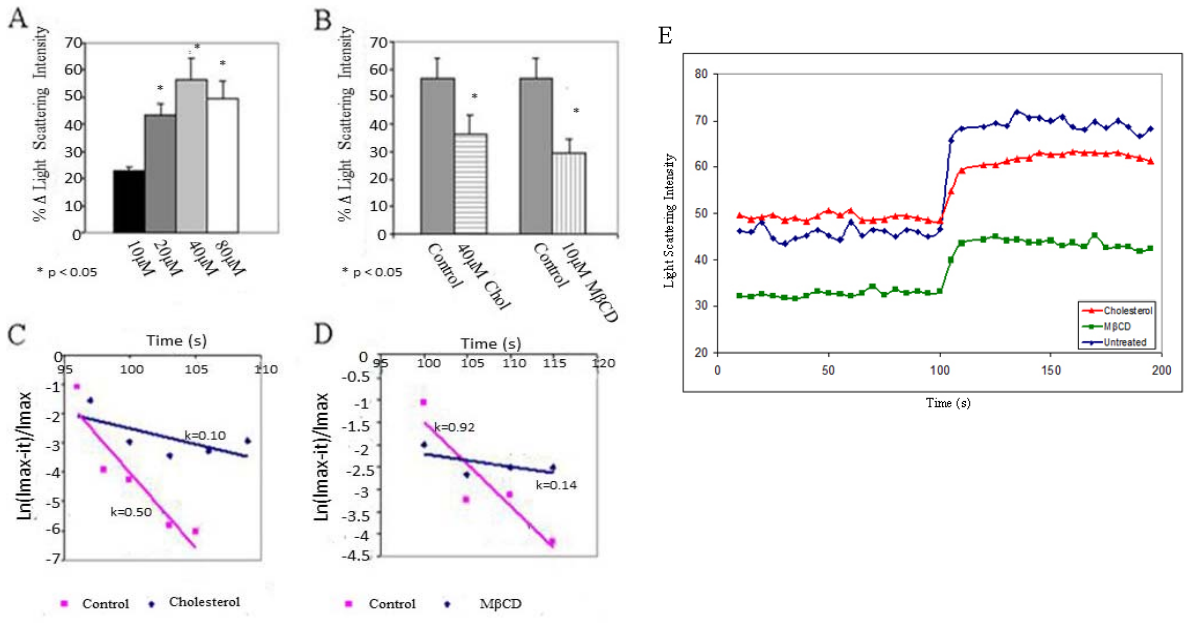

Figure 28. Excess Cholesterol or depletion of membrane cholesterol inhibits GTP and mastoparan induced swelling. Untreated isolated ZGs swell in response to GTP and mastoparan is demonstrated by right angle lights scattering (**A**). However after pretreatment (**B**) with exogenous cholesterol or methyl-β-cyclodextran swelling is significantly abrogated (N=6, $p < 0.05$). Initial kinetics of GTP and mastoparan induced swelling (**C-E**) are first order. The pretreated ZGs swell to a lesser extent and do so in a slower manner (**B-D**) than do their untreated counterparts.

Figure 28 C & D also indicate that when compared with control untreated ZGs the poor swelling response of ZGs due to the administration of excess cholesterol or the depletion of membrane cholesterol due to MβCD is accompanied with a swelling rate slower than control. Previous research indicates that cholesterol promotes membrane fusion where other molecules like LPC facilitate the longevity of a secretory event by inhibition of SNARE complex disassembly (Shin et al. 2011). This suggests that in-vivo membrane-membrane fusion may not be altered, but cholesterol inhibits some other portion of the swelling cascade. Cholesterol has also been demonstrated to decrease the permeability (Pf) of a plasma membrane but it is more likely that the water channel (Knepper et al. 1994), AQP1, is effected by the excess cholesterol presence in both the cholesterol (red trace) pre-incubation group and the MβCD (green trace) pre-incubation group.

Other research has shown that alteration in the lipid bilayer can effect protein conformation and activity of proteins housed therein (Yuan et al. 2007, Perozo et al. 2002). Studies using artificial vesicles enriched in AQP-4 have demonstrated a decrease in water permeability when the membrane is also enriched in exogenous cholesterol over unaltered lipid content (Tong et al. 2012). This occurs due to a mismatch in hydrophobic and hydrophilic regions in the protein and the lipid membrane when excess foreign lipids are added (Mouritsen and Bloom 1984, Nyholm et al. 2007, Dumas et al. 2000). When this mismatch occurs the unit bilayer then responds in one of two ways: 1) the protein changes conformation to realign hydrophobic regions or 2) the local thickness of the bilayer changes to overcome hydrophobic misalignment (Lundbaek 2008).

While cholesterol is essential for proper cellular function (Cho et al. 2005, Jeremic et al. 2006,) deviations from homeostasis result in pathophysiological conditions. Without cholesterol cellular membranes lose rigidity and lipid rafts lose segregating ability (Simons and Ehehalt

2002). However, when the biological level of cholesterol varies widely from what is considered healthy, aberrant conditions arise. The American Heart association, among others, warns of increased cardiovascular risk (American Heart Association 2013).

Lack of cholesterol control contributes to other pathophysiological states including those that effect the pancreas (NIDDK 2011, Uimari et al. 2011). The current research with ZGs isolated from the acinar cells of the pancreas illustrates the need for precise cholesterol balance in the pancreas. ZG swelling function is significantly decreased in conditions of excess or decreased vesicle membrane cholesterol (Figure 28). These data suggest that the alteration in lipid composition, specifically that of cholesterol, disallow GTP and mastoparan stimulable swelling via a mechanism that is currently unknown.

While it has been demonstrated that excessive cholesterol levels impair vesicle swelling the course of hypercholesterolemia in the pancreas may be further reaching. States of increased cholesterol and triglycerides may lead to more extensive damage in the pancreas. Fat deposits are often found in pancreatic tissue from patients with acute or chronic pancreatitis and high serum lipid levels predispose patients for pancreatitis (Conwell et al. 2011, NIDDK 2011, Uimara et al. 2011). Increased cholesterol levels have been linked to inflammatory mediator release that has been independently seen in cases of pancreatitis and pancreatic disease (Ding et al. 2003).

APPENDIX A

IACUC Approval Letter

WAYNE STATE UNIVERSITY

INSTITUTIONAL ANIMAL
CARE AND USE COMMITTEE
87 E. Canfield, Second Floor
Detroit, MI 48201-2011
Telephone: (313) 577-1629
Fax Number: (313) 577-1941

ANIMAL WELFARE ASSURANCE # A 3310-01

PROTOCOL # A 05-11-11

Protocol Effective Period: July 12, 2011 – May 31, 2014

TO: Dr. Xuequn Chen
Physiology
5215 Scott Hall

FROM: Lisa Anne Polin, Ph.D.
Chairperson
Institutional Animal Care and Use Committee

SUBJECT: Approval of Protocol # A 05-11-11
"ZYMOGEN GRANULE BIOGENESIS - ER TO GOLGI TRANSPORT"

DATE: July 12, 2011

Your animal research protocol has been reviewed by the Wayne State University Institutional Animal Care and Use Committee, and given final approval for the period effective **July 12, 2011** through **May 31, 2014**. The listed source of funding for the protocol is **Start-up Funds**. The species and number of animals approved for the duration of this protocol are listed below.

Species	Strain	Qty.	USDA Cat.
MICE	ICR, M, 4-5 weeks/21-24g	450	C
RATS	Sprague Dawley, 5-6 weeks/125-149g	216	C

Be advised that this protocol must be reviewed by the IACUC on an annual basis to remain active. Any change in procedures, change in lab personnel, change in species, or additional numbers of animals requires prior approval by the IACUC. Any animal work on this research protocol beyond the expiration date will require the submission of a new IACUC protocol form and full committee review.

The Guide for the Care and Use of Laboratory Animals is the primary reference used for standards of animal care at Wayne State University. The University has submitted an appropriate assurance statement to the Office for Laboratory Animal Welfare (OLAW) of the National Institutes of Health. The animal care program at Wayne State University is accredited by the Association for Assessment and Accreditation of Laboratory Animal Care International (AAALAC).

APPENDIX B

Unabridged Mass Spectrometry Data

BAND 1 CONTROL:

MS data file : Jena ZG band 1.tmp.tmp
Database : SwissProt 2012_04 (535698 sequences; 190107059 residues)
Taxonomy : Mus musculus (house mouse) (16528 sequences)
Timestamp : 8 May 2012 at 16:36:37 GMT
Protein hits :

GRP78_MOUSE	78 kDa glucose-regulated protein OS=Mus musculus GN=Hspa5 PE=1 SV=3
HSP7C_MOUSE	Heat shock cognate 71 kDa protein OS=Mus musculus GN=Hspa8 PE=1 SV=1
CEL_MOUSE	Bile salt-activated lipase OS=Mus musculus GN=Cel PE=1 SV=1
K1C10_MOUSE	Keratin, type I cytoskeletal 10 OS=Mus musculus GN=Krt10 PE=1 SV=3
PDIA2_MOUSE	Protein disulfide-isomerase A2 OS=Mus musculus GN=Pdia2 PE=1 SV=1
K2C1_MOUSE	Keratin, type II cytoskeletal 1 OS=Mus musculus GN=Krt1 PE=1 SV=4
ACTB_MOUSE	Actin, cytoplasmic 1 OS=Mus musculus GN=Actb PE=1 SV=1
SYG_MOUSE	Glycine--tRNA ligase OS=Mus musculus GN=Gars PE=1 SV=1
GRP75_MOUSE	Stress-70 protein, mitochondrial OS=Mus musculus GN=Hspa9 PE=1 SV=2
SYK_MOUSE	Lysine--tRNA ligase OS=Mus musculus GN=Kars PE=1 SV=1
LIPR1_MOUSE	Pancreatic lipase-related protein 1 OS=Mus musculus GN=Pnliprp1 PE=2 SV=2
LIPP_MOUSE	Pancreatic triacylglycerol lipase OS=Mus musculus GN=Pnlip PE=1 SV=1
AMYP_MOUSE	Pancreatic alpha-amylase OS=Mus musculus GN=Amy2 PE=1 SV=2
AMY1_MOUSE	Alpha-amylase 1 OS=Mus musculus GN=Amy1 PE=1 SV=2
SYTL1_MOUSE	Synaptotagmin-like protein 1 OS=Mus musculus GN=Sytl1 PE=1 SV=2
SPI2_MOUSE	Serpin I2 OS=Mus musculus GN=Serpini2 PE=1 SV=1
K2C5_MOUSE	Keratin, type II cytoskeletal 5 OS=Mus musculus GN=Krt5 PE=1 SV=1
ALBU_MOUSE	Serum albumin OS=Mus musculus GN=Alb PE=1 SV=3
K1C42_MOUSE	Keratin, type I cytoskeletal 42 OS=Mus musculus GN=Krt42 PE=1 SV=1
ACTC_MOUSE	Actin, alpha cardiac muscle 1 OS=Mus musculus GN=Actc1 PE=1 SV=1
ANXA6_MOUSE	Annexin A6 OS=Mus musculus GN=Anxa6 PE=1 SV=3
K1C15_MOUSE	Keratin, type I cytoskeletal 15 OS=Mus musculus GN=Krt15 PE=1 SV=2
K2C73_MOUSE	Keratin, type II cytoskeletal 73 OS=Mus musculus GN=Krt73 PE=1 SV=1
K2C1B_MOUSE	Keratin, type II cytoskeletal 1b OS=Mus musculus GN=Krt77 PE=1 SV=1
K2C79_MOUSE	Keratin, type II cytoskeletal 79 OS=Mus musculus GN=Krt79 PE=1 SV=2
PABP1_MOUSE	Polyadenylate-binding protein 1 OS=Mus musculus GN=Pabpc1 PE=1 SV=2
HBA_MOUSE	Hemoglobin subunit alpha OS=Mus musculus GN=Hba PE=1 SV=2
K22E_MOUSE	Keratin, type II cytoskeletal 2 epidermal OS=Mus musculus GN=Krt2 PE=1 SV=1
K2C6A_MOUSE	Keratin, type II cytoskeletal 6A OS=Mus musculus GN=Krt6a PE=2 SV=3
K2C4_MOUSE	Keratin, type II cytoskeletal 4 OS=Mus musculus GN=Krt4 PE=1 SV=2
ACTBL_MOUSE	Beta-actin-like protein 2 OS=Mus musculus GN=Actbl2 PE=1 SV=1
RPN1_MOUSE	Dolichyl-diphosphooligosaccharide--protein glycosyltransferase subunit 1

	OS=Mus musculus GN=Rpn1 PE=2 SV=1
SYFB_MOUSE	Phenylalanine--tRNA ligase beta subunit OS=Mus musculus GN=Farsb PE=2 SV=2
K1C13_MOUSE	Keratin, type I cytoskeletal 13 OS=Mus musculus GN=Krt13 PE=1 SV=2
GP2_MOUSE	Pancreatic secretory granule membrane major glycoprotein GP2 OS=Mus musculus GN=Gp2 PE=2 SV=3
HS90B_MOUSE	Heat shock protein HSP 90-beta OS=Mus musculus GN=Hsp90ab1 PE=1 SV=3
HS90A_MOUSE	Heat shock protein HSP 90-alpha OS=Mus musculus GN=Hsp90aa1 PE=1 SV=4
TRAP1_MOUSE	Heat shock protein 75 kDa, mitochondrial OS=Mus musculus GN=Trap1 PE=1 SV=1
TERA_MOUSE	Transitional endoplasmic reticulum ATPase OS=Mus musculus GN=Vcp PE=1 SV=4
CBPA2_MOUSE	Carboxypeptidase A2 OS=Mus musculus GN=Cpa2 PE=2 SV=1
SYRC_MOUSE	Arginine--tRNA ligase, cytoplasmic OS=Mus musculus GN=Rars PE=2 SV=2
PCCA_MOUSE	Propionyl-CoA carboxylase alpha chain, mitochondrial OS=Mus musculus GN=Pcca PE=2 SV=2
SPAT5_MOUSE	Spermatogenesis-associated protein 5 OS=Mus musculus GN=Spata5 PE=2 SV=2
K2C8_MOUSE	
EF1A1_MOUSE	Elongation factor 1-alpha 1 OS=Mus musculus GN=Eef1a1 PE=1 SV=3
PDIA4_MOUSE	Protein disulfide-isomerase A4 OS=Mus musculus GN=Pdia4 PE=1 SV=3
ENPL_MOUSE	Endoplasmin OS=Mus musculus GN=Hsp90b1 PE=1 SV=2
CBPA1_MOUSE	Carboxypeptidase A1 OS=Mus musculus GN=Cpa1 PE=2 SV=1
SWAP1_MOUSE	ATPase SWSAP1 OS=Mus musculus GN=Swsap1 PE=2 SV=2
ERF3A_MOUSE	Eukaryotic peptide chain release factor GTP-binding subunit ERF3A OS=Mus musculus GN=Gspt1 PE=1 SV=1
LIPR2_MOUSE	Pancreatic lipase-related protein 2 OS=Mus musculus GN=Pnliprp2 PE=2 SV=1
HAOX2_MOUSE	Hydroxyacid oxidase 2 OS=Mus musculus GN=Hao2 PE=2 SV=1
NASP_MOUSE	Nuclear autoantigenic sperm protein OS=Mus musculus GN=Nasp PE=1 SV=2
MFTC_MOUSE	Mitochondrial folate transporter/carrier OS=Mus musculus GN=Slc25a32 PE=2 SV=1
DUS3_MOUSE	Dual specificity protein phosphatase 3 OS=Mus musculus GN=Dusp3 PE=1 SV=1
CP135_MOUSE	
ETUD1_MOUSE	Elongation factor Tu GTP-binding domain-containing protein 1 OS=Mus musculus GN=Eftud1 PE=2 SV=1
ZN322_MOUSE	Zinc finger protein 322 OS=Mus musculus GN=Znf322 PE=2 SV=1
TF_MOUSE	
GLGB_MOUSE	1,4-alpha-glucan-branching enzyme OS=Mus musculus GN=Gbe1 PE=2 SV=1
HBE_MOUSE	Hemoglobin subunit epsilon-Y2 OS=Mus musculus GN=Hbb-y PE=1 SV=2
CES1D_MOUSE	Carboxylesterase 1D OS=Mus musculus GN=Ces1d PE=1 SV=1
YPEL5_MOUSE	Protein yippee-like 5 OS=Mus musculus GN=Ypel5 PE=2 SV=1
POC1A_MOUSE	

Mascot Score Histogram

Ions score is -10*Log(P), where P is the probability that the observed match is a random event.
Individual ions scores > 28 indicate identity or extensive homology (p<0.05).
Protein scores are derived from ions scores as a non-probabilistic basis for ranking protein hits.

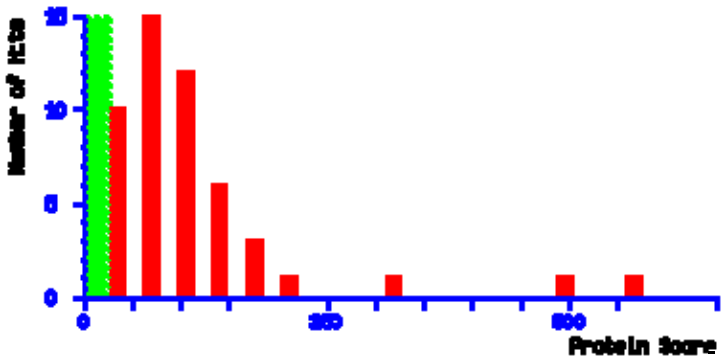

BAND 2 CONTROL:

MS data file : Jena ZG band 2.tmp.tmp
Database : SwissProt 2012_04 (535698 sequences; 190107059 residues)
Taxonomy : Mus musculus (house mouse) (16528 sequences)
Timestamp : 8 May 2012 at 16:49:36 GMT
Protein hits :

GRP78_MOUSE	78 kDa glucose-regulated protein OS=Mus musculus GN=Hspa5 PE=1 SV=3
HSP7C_MOUSE	Heat shock cognate 71 kDa protein OS=Mus musculus GN=Hspa8 PE=1 SV=1
CEL_MOUSE	Bile salt-activated lipase OS=Mus musculus GN=Cel PE=1 SV=1
K1C10_MOUSE	Keratin, type I cytoskeletal 10 OS=Mus musculus GN=Krt10 PE=1 SV=3
GRP75_MOUSE	Stress-70 protein, mitochondrial OS=Mus musculus GN=Hspa9 PE=1 SV=2
ALBU_MOUSE	Serum albumin OS=Mus musculus GN=Alb PE=1 SV=3
K1C14_MOUSE	Keratin, type I cytoskeletal 14 OS=Mus musculus GN=Krt14 PE=1 SV=2
K1C17_MOUSE	Keratin, type I cytoskeletal 17 OS=Mus musculus GN=Krt17 PE=1 SV=3
K2C1_MOUSE	Keratin, type II cytoskeletal 1 OS=Mus musculus GN=Krt1 PE=1 SV=4
PDIA2_MOUSE	Protein disulfide-isomerase A2 OS=Mus musculus GN=Pdia2 PE=1 SV=1
K2C5_MOUSE	Keratin, type II cytoskeletal 5 OS=Mus musculus GN=Krt5 PE=1 SV=1
CBPA1_MOUSE	Carboxypeptidase A1 OS=Mus musculus GN=Cpa1 PE=2 SV=1
ACTB_MOUSE	Actin, cytoplasmic 1 OS=Mus musculus GN=Actb PE=1 SV=1
ANXA6_MOUSE	Annexin A6 OS=Mus musculus GN=Anxa6 PE=1 SV=3
K1C42_MOUSE	Keratin, type I cytoskeletal 42 OS=Mus musculus GN=Krt42 PE=1 SV=1
K1C15_MOUSE	Keratin, type I cytoskeletal 15 OS=Mus musculus GN=Krt15 PE=1 SV=2
AMYP_MOUSE	Pancreatic alpha-amylase OS=Mus musculus GN=Amy2 PE=1 SV=2
K2C6A_MOUSE	Keratin, type II cytoskeletal 6A OS=Mus musculus GN=Krt6a PE=2 SV=3
K2C73_MOUSE	Keratin, type II cytoskeletal 73 OS=Mus musculus GN=Krt73 PE=1 SV=1
TRFE_MOUSE	Serotransferrin OS=Mus musculus GN=Tf PE=1 SV=1
LIPP_MOUSE	Pancreatic triacylglycerol lipase OS=Mus musculus GN=Pnlip PE=1 SV=1
AMY1_MOUSE	Alpha-amylase 1 OS=Mus musculus GN=Amy1 PE=1 SV=2
K2C79_MOUSE	Keratin, type II cytoskeletal 79 OS=Mus musculus GN=Krt79 PE=1 SV=2
K1C13_MOUSE	Keratin, type I cytoskeletal 13 OS=Mus musculus GN=Krt13 PE=1 SV=2
K2C71_MOUSE	Keratin, type II cytoskeletal 71 OS=Mus musculus GN=Krt71 PE=1 SV=1

LIPR1_MOUSE	Pancreatic lipase-related protein 1 OS=Mus musculus GN=Pnliprp1 PE=2 SV=2
GP2_MOUSE	Pancreatic secretory granule membrane major glycoprotein GP2 OS=Mus musculus GN=Gp2 PE=2 SV=3
HS90B_MOUSE	Heat shock protein HSP 90-beta OS=Mus musculus GN=Hsp90ab1 PE=1 SV=3
RPN1_MOUSE	Dolichyl-diphosphooligosaccharide--protein glycosyltransferase subunit 1 OS=Mus musculus GN=Rpn1 PE=2 SV=1
K2C7_MOUSE	Keratin, type II cytoskeletal 7 OS=Mus musculus GN=Krt7 PE=1 SV=1
TRAP1_MOUSE	Heat shock protein 75 kDa, mitochondrial OS=Mus musculus GN=Trap1 PE=1 SV=1
HS90A_MOUSE	Heat shock protein HSP 90-alpha OS=Mus musculus GN=Hsp90aa1 PE=1 SV=4
K22E_MOUSE	Keratin, type II cytoskeletal 2 epidermal OS=Mus musculus GN=Krt2 PE=1 SV=1
EF1A1_MOUSE	Elongation factor 1-alpha 1 OS=Mus musculus GN=Eef1a1 PE=1 SV=3
K1C16_MOUSE	Keratin, type I cytoskeletal 16 OS=Mus musculus GN=Krt16 PE=1 SV=3
K1C25_MOUSE	Keratin, type I cytoskeletal 25 OS=Mus musculus GN=Krt25 PE=1 SV=1
SYRC_MOUSE	Arginine--tRNA ligase, cytoplasmic OS=Mus musculus GN=Rars PE=2 SV=2
K2C4_MOUSE	Keratin, type II cytoskeletal 4 OS=Mus musculus GN=Krt4 PE=1 SV=2
SPAT5_MOUSE	Spermatogenesis-associated protein 5 OS=Mus musculus GN=Spata5 PE=2 SV=2
TERA_MOUSE	Transitional endoplasmic reticulum ATPase OS=Mus musculus GN=Vcp PE=1 SV=4
ACTC_MOUSE	Actin, alpha cardiac muscle 1 OS=Mus musculus GN=Actc1 PE=1 SV=1
SAHH_MOUSE	Adenosylhomocysteinase OS=Mus musculus GN=Ahcy PE=1 SV=3
SPI2_MOUSE	Serpin I2 OS=Mus musculus GN=Serpini2 PE=1 SV=1
K2C8_MOUSE	
K2C72_MOUSE	
CALX_MOUSE	Calnexin OS=Mus musculus GN=Canx PE=1 SV=1
PABP1_MOUSE	Polyadenylate-binding protein 1 OS=Mus musculus GN=Pabpc1 PE=1 SV=2
LIPR2_MOUSE	Pancreatic lipase-related protein 2 OS=Mus musculus GN=Pnliprp2 PE=2 SV=1
SYK_MOUSE	Lysine--tRNA ligase OS=Mus musculus GN=Kars PE=1 SV=1
SARNP_MOUSE	
LMNA_MOUSE	Prelamin-A/C OS=Mus musculus GN=Lmna PE=1 SV=2
DVL1_MOUSE	
MTA70_MOUSE	N6-adenosine-methyltransferase 70 kDa subunit OS=Mus musculus GN=Mettl3 PE=2 SV=2
PCCA_MOUSE	Propionyl-CoA carboxylase alpha chain, mitochondrial OS=Mus musculus GN=Pcca PE=2 SV=2
QN1_MOUSE	Protein QN1 homolog OS=Mus musculus GN=Kiaa1009 PE=1 SV=2
ACOX2_MOUSE	
GLGB_MOUSE	1,4-alpha-glucan-branching enzyme OS=Mus musculus GN=Gbe1 PE=2 SV=1
CES1D_MOUSE	Carboxylesterase 1D OS=Mus musculus GN=Ces1d PE=1 SV=1
RBM44_MOUSE	RNA-binding protein 44 OS=Mus musculus GN=Rbm44 PE=2 SV=1
ACTBL_MOUSE	
GNN_MOUSE	Tetratricopeptide repeat protein GNN OS=Mus musculus GN=Gnn PE=1 SV=1
GALP_MOUSE	Galanin-like peptide OS=Mus musculus GN=Galp PE=2 SV=1
SYFB_MOUSE	Phenylalanine--tRNA ligase beta subunit OS=Mus musculus GN=Farsb PE=2 SV=2
MACF1_MOUSE	Microtubule-actin cross-linking factor 1 OS=Mus musculus GN=Macf1 PE=1 SV=2
HEY2_MOUSE	Hairy/enhancer-of-split related with YRPW motif protein 2 OS=Mus musculus GN=Hey2 PE=1 SV=1
CANT1_MOUSE	Soluble calcium-activated nucleotidase 1 OS=Mus musculus GN=Cant1 PE=2 SV=1

GLU2B_MOUSE	Glucosidase 2 subunit beta OS=Mus musculus GN=Prkcsh PE=1 SV=1
SELS_MOUSE	Selenoprotein S OS=Mus musculus GN=Sels PE=2 SV=3
UBP25_MOUSE	
TJAP1_MOUSE	Tight junction-associated protein 1 OS=Mus musculus GN=Tjap1 PE=1 SV=1
SPG7_MOUSE	

Mascot Score Histogram

Ions score is -10*Log(P), where P is the probability that the observed match is a random event.
Individual ions scores > 28 indicate identity or extensive homology (p<0.05).
Protein scores are derived from ions scores as a non-probabilistic basis for ranking protein hits.

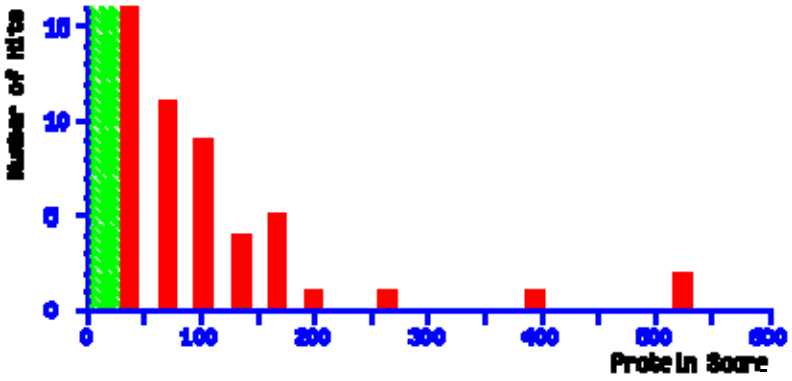

BAND 3 CONTROL:

MS data file : Jena ZG band 3.tmp.tmp
Database : SwissProt 2012_04 (535698 sequences; 190107059 residues)
Taxonomy : Mus musculus (house mouse) (16528 sequences)
Timestamp : 8 May 2012 at 16:52:05 GMT
Protein hits :

LIPP_MOUSE	Pancreatic triacylglycerol lipase OS=Mus musculus GN=Pnlip PE=1 SV=1
K1C10_MOUSE	Keratin, type I cytoskeletal 10 OS=Mus musculus GN=Krt10 PE=1 SV=3
LIPR1_MOUSE	Pancreatic lipase-related protein 1 OS=Mus musculus GN=Pnliprp1 PE=2 SV=2
K22E_MOUSE	Keratin, type II cytoskeletal 2 epidermal OS=Mus musculus GN=Krt2 PE=1 SV=1
AMY1_MOUSE	Alpha-amylase 1 OS=Mus musculus GN=Amy1 PE=1 SV=2
K2C5_MOUSE	Keratin, type II cytoskeletal 5 OS=Mus musculus GN=Krt5 PE=1 SV=1
VAT1_MOUSE	Synaptic vesicle membrane protein VAT-1 homolog OS=Mus musculus GN=Vat1 PE=1 SV=3
K2C1_MOUSE	Keratin, type II cytoskeletal 1 OS=Mus musculus GN=Krt1 PE=1 SV=4
K2C75_MOUSE	Keratin, type II cytoskeletal 75 OS=Mus musculus GN=Krt75 PE=1 SV=1
K2C6A_MOUSE	Keratin, type II cytoskeletal 6A OS=Mus musculus GN=Krt6a PE=2 SV=3
PDIA6_MOUSE	Protein disulfide-isomerase A6 OS=Mus musculus GN=Pdia6 PE=1 SV=3
AMYP_MOUSE	Pancreatic alpha-amylase OS=Mus musculus GN=Amy2 PE=1 SV=2
EF1A1_MOUSE	Elongation factor 1-alpha 1 OS=Mus musculus GN=Eef1a1 PE=1 SV=3
ATPB_MOUSE	ATP synthase subunit beta, mitochondrial OS=Mus musculus GN=Atp5b PE=1 SV=2
CBPA1_MOUSE	Carboxypeptidase A1 OS=Mus musculus GN=Cpa1 PE=2 SV=1
K22O_MOUSE	Keratin, type II cytoskeletal 2 oral OS=Mus musculus GN=Krt76 PE=2 SV=1
K2C7_MOUSE	Keratin, type II cytoskeletal 7 OS=Mus musculus GN=Krt7 PE=1 SV=1

CEL_MOUSE	Bile salt-activated lipase OS=Mus musculus GN=Cel PE=1 SV=1
ENOA_MOUSE	Alpha-enolase OS=Mus musculus GN=Eno1 PE=1 SV=3
K1C13_MOUSE	Keratin, type I cytoskeletal 13 OS=Mus musculus GN=Krt13 PE=1 SV=2
K1C17_MOUSE	Keratin, type I cytoskeletal 17 OS=Mus musculus GN=Krt17 PE=1 SV=3
K2C73_MOUSE	Keratin, type II cytoskeletal 73 OS=Mus musculus GN=Krt73 PE=1 SV=1
K2C4_MOUSE	Keratin, type II cytoskeletal 4 OS=Mus musculus GN=Krt4 PE=1 SV=2
K2C79_MOUSE	Keratin, type II cytoskeletal 79 OS=Mus musculus GN=Krt79 PE=1 SV=2
K2C1B_MOUSE	Keratin, type II cytoskeletal 1b OS=Mus musculus GN=Krt77 PE=1 SV=1
K1C14_MOUSE	Keratin, type I cytoskeletal 14 OS=Mus musculus GN=Krt14 PE=1 SV=2
K1C15_MOUSE	Keratin, type I cytoskeletal 15 OS=Mus musculus GN=Krt15 PE=1 SV=2
KRT84_MOUSE	Keratin, type II cuticular Hb4 OS=Mus musculus GN=Krt84 PE=2 SV=2
LIPR2_MOUSE	Pancreatic lipase-related protein 2 OS=Mus musculus GN=Pnliprp2 PE=2 SV=1
K2C8_MOUSE	Keratin, type II cytoskeletal 8 OS=Mus musculus GN=Krt8 PE=1 SV=4
ENOB_MOUSE	Beta-enolase OS=Mus musculus GN=Eno3 PE=1 SV=3
KRT85_MOUSE	Keratin, type II cuticular Hb5 OS=Mus musculus GN=Krt85 PE=2 SV=2
K2C72_MOUSE	Keratin, type II cytoskeletal 72 OS=Mus musculus GN=Krt72 PE=2 SV=1
EIF3F_MOUSE	Eukaryotic translation initiation factor 3 subunit F OS=Mus musculus GN=Eif3f PE=1 SV=2
RHG01_MOUSE	Rho GTPase-activating protein 1 OS=Mus musculus GN=Arhgap1 PE=1 SV=1
AL9A1_MOUSE	4-trimethylaminobutyraldehyde dehydrogenase OS=Mus musculus GN=Aldh9a1 PE=1 SV=1
K1C25_MOUSE	Keratin, type I cytoskeletal 25 OS=Mus musculus GN=Krt25 PE=1 SV=1
EF1G_MOUSE	Elongation factor 1-gamma OS=Mus musculus GN=Eef1g PE=1 SV=3
ACTB_MOUSE	Actin, cytoplasmic 1 OS=Mus musculus GN=Actb PE=1 SV=1
NUCB2_MOUSE	Nucleobindin-2 OS=Mus musculus GN=Nucb2 PE=1 SV=2
CD1D1_MOUSE	Antigen-presenting glycoprotein CD1d1 OS=Mus musculus GN=Cd1d1 PE=1 SV=3
SPI2_MOUSE	Serpin I2 OS=Mus musculus GN=Serpini2 PE=1 SV=1
MTOR_MOUSE	
CA087_MOUSE	
NFH_MOUSE	Neurofilament heavy polypeptide OS=Mus musculus GN=Nefh PE=1 SV=3
GGLO_MOUSE	
LR16C_MOUSE	
CBPA2_MOUSE	Carboxypeptidase A2 OS=Mus musculus GN=Cpa2 PE=2 SV=1
YBOX1_MOUSE	Nuclease-sensitive element-binding protein 1 OS=Mus musculus GN=Ybx1 PE=1 SV=3
VAV3_MOUSE	Guanine nucleotide exchange factor VAV3 OS=Mus musculus GN=Vav3 PE=1 SV=2
GGT1_MOUSE	Gamma-glutamyltranspeptidase 1 OS=Mus musculus GN=Ggt1 PE=1 SV=1
METK2_MOUSE	S-adenosylmethionine synthase isoform type-2 OS=Mus musculus GN=Mat2a PE=2 SV=2
OST48_MOUSE	Dolichyl-diphosphooligosaccharide--protein glycosyltransferase 48 kDa subunit OS=Mus musculus GN=Ddost PE=1 SV=2
RL4_MOUSE	60S ribosomal protein L4 OS=Mus musculus GN=Rpl4 PE=1 SV=3
RAE1D_MOUSE	
DUS11_MOUSE	RNA/RNP complex-1-interacting phosphatase OS=Mus musculus GN=Dusp11 PE=2 SV=1
K1C20_MOUSE	
ASAP2_MOUSE	Arf-GAP with SH3 domain, ANK repeat and PH domain-containing protein 2 OS=Mus musculus GN=Asap2 PE=1 SV=3
MYH1_MOUSE	Myosin-1 OS=Mus musculus GN=Myh1 PE=1 SV=1

IQUB_MOUSE	
GPR98_MOUSE	G-protein coupled receptor 98 OS=Mus musculus GN=Gpr98 PE=2 SV=1
ILEUB_MOUSE	Leukocyte elastase inhibitor B OS=Mus musculus GN=Serpinb1b PE=1 SV=1
F207A_MOUSE	Protein FAM207A OS=Mus musculus GN=Fam207a PE=1 SV=1
PSMD1_MOUSE	26S proteasome non-ATPase regulatory subunit 1 OS=Mus musculus GN=Psmd1 PE=1 SV=1
CCNC_MOUSE	
SMC5_MOUSE	
COT1_MOUSE	COUP transcription factor 1 OS=Mus musculus GN=Nr2f1 PE=2 SV=2
PO2F1_MOUSE	
TDG_MOUSE	G/T mismatch-specific thymine DNA glycosylase OS=Mus musculus GN=Tdg PE=2 SV=1
SMC3_MOUSE	Structural maintenance of chromosomes protein 3 OS=Mus musculus GN=Smc3 PE=1 SV=2
DNPEP_MOUSE	Aspartyl aminopeptidase OS=Mus musculus GN=Dnpep PE=2 SV=2
FBW10_MOUSE	F-box/WD repeat-containing protein 10 OS=Mus musculus GN=Fbxw10 PE=2 SV=1
RADI_MOUSE	Radixin OS=Mus musculus GN=Rdx PE=1 SV=3
GATM_MOUSE	Glycine amidinotransferase, mitochondrial OS=Mus musculus GN=Gatm PE=1 SV=1
HUTH_MOUSE	Histidine ammonia-lyase OS=Mus musculus GN=Hal PE=1 SV=1
ALBU_MOUSE	Serum albumin OS=Mus musculus GN=Alb PE=1 SV=3
SHRM3_MOUSE	Protein Shroom3 OS=Mus musculus GN=Shroom3 PE=1 SV=2
TXD11_MOUSE	Thioredoxin domain-containing protein 11 OS=Mus musculus GN=Txndc11 PE=2 SV=1

Mascot Score Histogram

Ions score is -10*Log(P), where P is the probability that the observed match is a random event.
Individual ions scores > 28 indicate identity or extensive homology (p<0.05).
Protein scores are derived from ions scores as a non-probabilistic basis for ranking protein hits.

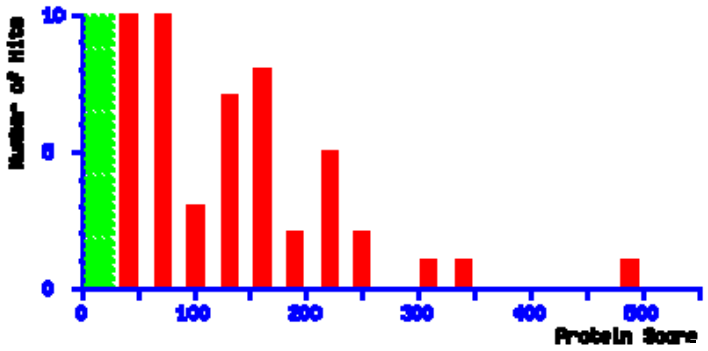

BAND 4 CONTROL:

MS data file : Jena ZG band 4.tmp.tmp
Database : SwissProt 2012_04 (535698 sequences; 190107059 residues)
Taxonomy : Mus musculus (house mouse) (16528 sequences)
Timestamp : 8 May 2012 at 16:55:32 GMT
Protein hits :

LIPP_MOUSE	Pancreatic triacylglycerol lipase OS=Mus musculus GN=Pnlip PE=1 SV=1
LIPR1_MOUSE	Pancreatic lipase-related protein 1 OS=Mus musculus GN=Pnliprp1 PE=2 SV=2

AMYP_MOUSE	Pancreatic alpha-amylase OS=Mus musculus GN=Amy2 PE=1 SV=2
PDIA6_MOUSE	Protein disulfide-isomerase A6 OS=Mus musculus GN=Pdia6 PE=1 SV=3
VAT1_MOUSE	Synaptic vesicle membrane protein VAT-1 homolog OS=Mus musculus GN=Vat1 PE=1 SV=3
AMY1_MOUSE	Alpha-amylase 1 OS=Mus musculus GN=Amy1 PE=1 SV=2
ATPB_MOUSE	ATP synthase subunit beta, mitochondrial OS=Mus musculus GN=Atp5b PE=1 SV=2
K1C10_MOUSE	Keratin, type I cytoskeletal 10 OS=Mus musculus GN=Krt10 PE=1 SV=3
ENOA_MOUSE	Alpha-enolase OS=Mus musculus GN=Eno1 PE=1 SV=3
TBB4B_MOUSE	Tubulin beta-4B chain OS=Mus musculus GN=Tubb4b PE=1 SV=1
CBPA1_MOUSE	Carboxypeptidase A1 OS=Mus musculus GN=Cpa1 PE=2 SV=1
EF1A1_MOUSE	Elongation factor 1-alpha 1 OS=Mus musculus GN=Eef1a1 PE=1 SV=3
CEL_MOUSE	Bile salt-activated lipase OS=Mus musculus GN=Cel PE=1 SV=1
K2C1_MOUSE	Keratin, type II cytoskeletal 1 OS=Mus musculus GN=Krt1 PE=1 SV=4
K1C17_MOUSE	Keratin, type I cytoskeletal 17 OS=Mus musculus GN=Krt17 PE=1 SV=3
K1C14_MOUSE	Keratin, type I cytoskeletal 14 OS=Mus musculus GN=Krt14 PE=1 SV=2
K1C15_MOUSE	Keratin, type I cytoskeletal 15 OS=Mus musculus GN=Krt15 PE=1 SV=2
K1C18_MOUSE	Keratin, type I cytoskeletal 18 OS=Mus musculus GN=Krt18 PE=1 SV=5
K2C5_MOUSE	Keratin, type II cytoskeletal 5 OS=Mus musculus GN=Krt5 PE=1 SV=1
LIPR2_MOUSE	Pancreatic lipase-related protein 2 OS=Mus musculus GN=Pnliprp2 PE=2 SV=1
K1C19_MOUSE	Keratin, type I cytoskeletal 19 OS=Mus musculus GN=Krt19 PE=1 SV=1
NUCB2_MOUSE	Nucleobindin-2 OS=Mus musculus GN=Nucb2 PE=1 SV=2
K1C42_MOUSE	Keratin, type I cytoskeletal 42 OS=Mus musculus GN=Krt42 PE=1 SV=1
ENOB_MOUSE	Beta-enolase OS=Mus musculus GN=Eno3 PE=1 SV=3
EF1G_MOUSE	Elongation factor 1-gamma OS=Mus musculus GN=Eef1g PE=1 SV=3
CBPA2_MOUSE	Carboxypeptidase A2 OS=Mus musculus GN=Cpa2 PE=2 SV=1
K1C16_MOUSE	Keratin, type I cytoskeletal 16 OS=Mus musculus GN=Krt16 PE=1 SV=3
HS90A_MOUSE	Heat shock protein HSP 90-alpha OS=Mus musculus GN=Hsp90aa1 PE=1 SV=4
TRAP1_MOUSE	Heat shock protein 75 kDa, mitochondrial OS=Mus musculus GN=Trap1 PE=1 SV=1
K2C6A_MOUSE	Keratin, type II cytoskeletal 6A OS=Mus musculus GN=Krt6a PE=2 SV=3
K2C74_MOUSE	Keratin, type II cytoskeletal 74 OS=Mus musculus GN=Krt74 PE=2 SV=1
VTDB_MOUSE	Vitamin D-binding protein OS=Mus musculus GN=Gc PE=1 SV=2
TBB1_MOUSE	Tubulin beta-1 chain OS=Mus musculus GN=Tubb1 PE=1 SV=1
TBA1A_MOUSE	Tubulin alpha-1A chain OS=Mus musculus GN=Tuba1a PE=1 SV=1
AL9A1_MOUSE	4-trimethylaminobutyraldehyde dehydrogenase OS=Mus musculus GN=Aldh9a1 PE=1 SV=1
K22E_MOUSE	Keratin, type II cytoskeletal 2 epidermal OS=Mus musculus GN=Krt2 PE=1 SV=1
CD1D1_MOUSE	Antigen-presenting glycoprotein CD1d1 OS=Mus musculus GN=Cd1d1 PE=1 SV=3
EIF3F_MOUSE	Eukaryotic translation initiation factor 3 subunit F OS=Mus musculus GN=Eif3f PE=1 SV=2
K1C24_MOUSE	
KRT35_MOUSE	
RHG01_MOUSE	Rho GTPase-activating protein 1 OS=Mus musculus GN=Arhgap1 PE=1 SV=1
DNPEP_MOUSE	Aspartyl aminopeptidase OS=Mus musculus GN=Dnpep PE=2 SV=2
CTRB1_MOUSE	
GDIB_MOUSE	Rab GDP dissociation inhibitor beta OS=Mus musculus GN=Gdi2 PE=1 SV=1
PDIA1_MOUSE	Protein disulfide-isomerase OS=Mus musculus GN=P4hb PE=1 SV=2

AMNLS_MOUSE	
K22O_MOUSE	Keratin, type II cytoskeletal 2 oral OS=Mus musculus GN=Krt76 PE=2 SV=1
GATM_MOUSE	Glycine amidinotransferase, mitochondrial OS=Mus musculus GN=Gatm PE=1 SV=1
CA087_MOUSE	
MTOR_MOUSE	
RL4_MOUSE	60S ribosomal protein L4 OS=Mus musculus GN=Rpl4 PE=1 SV=3
GGLO_MOUSE	
E2AK4_MOUSE	Eukaryotic translation initiation factor 2-alpha kinase 4 OS=Mus musculus GN=Eif2ak4 PE=1 SV=2
ATX3_MOUSE	
DUS11_MOUSE	RNA/RNP complex-1-interacting phosphatase OS=Mus musculus GN=Dusp11 PE=2 SV=1
LR16C_MOUSE	
RAE1D_MOUSE	
IQUB_MOUSE	
RN111_MOUSE	
CPNE5_MOUSE	
K1731_MOUSE	
RRAS_MOUSE	
RN169_MOUSE	
MATN4_MOUSE	
ASAP2_MOUSE	Arf-GAP with SH3 domain, ANK repeat and PH domain-containing protein 2 OS=Mus musculus GN=Asap2 PE=1 SV=3
GGH_MOUSE	Gamma-glutamyl hydrolase OS=Mus musculus GN=Ggh PE=1 SV=2
PLD1_MOUSE	
PO2F3_MOUSE	POU domain, class 2, transcription factor 3 OS=Mus musculus GN=Pou2f3 PE=2 SV=2
K1C20_MOUSE	
ODB2_MOUSE	Lipoamide acyltransferase component of branched-chain alpha-keto acid dehydrogenase complex, mitochondrial OS=Mus musculus GN=Dbt PE=2 SV=2
S41A3_MOUSE	
VWA2_MOUSE	
GGT1_MOUSE	Gamma-glutamyltranspeptidase 1 OS=Mus musculus GN=Ggt1 PE=1 SV=1
FBW10_MOUSE	F-box/WD repeat-containing protein 10 OS=Mus musculus GN=Fbxw10 PE=2 SV=1
SHP1L_MOUSE	SHC SH2 domain-binding protein 1-like protein OS=Mus musculus GN=Shcbp1l PE=2 SV=1
HMOX2_MOUSE	Heme oxygenase 2 OS=Mus musculus GN=Hmox2 PE=2 SV=1
SHRM3_MOUSE	Protein Shroom3 OS=Mus musculus GN=Shroom3 PE=1 SV=2
SHRM2_MOUSE	Protein Shroom2 OS=Mus musculus GN=Shroom2 PE=1 SV=1
ALBU_MOUSE	Serum albumin OS=Mus musculus GN=Alb PE=1 SV=3

Mascot Score Histogram

Ions score is -10*Log(P), where P is the probability that the observed match is a random event.
Individual ions scores > 28 indicate identity or extensive homology (p<0.05).
Protein scores are derived from ions scores as a non-probabilistic basis for ranking protein hits.

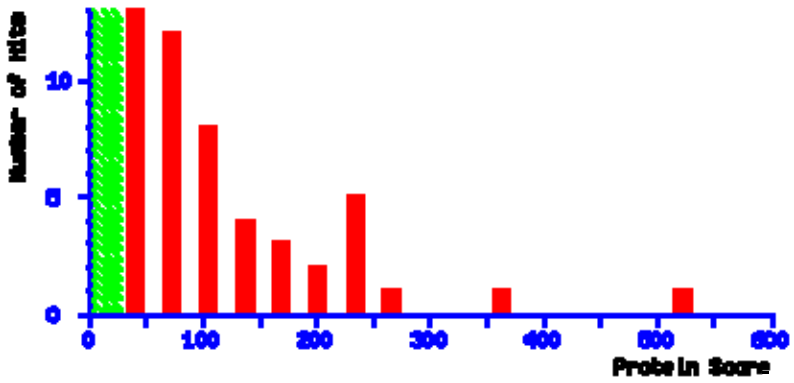

BAND 1 2h EXPERIMENTAL:

MS data file : Jena ZG band 5.tmp.tmp
Database : SwissProt 2012_04 (535698 sequences; 190107059 residues)
Taxonomy : Mus musculus (house mouse) (16528 sequences)
Timestamp : 8 May 2012 at 18:06:37 GMT
Protein hits :

LIPP_MOUSE	Pancreatic triacylglycerol lipase OS=Mus musculus GN=Pnlip PE=1 SV=1
LIPR1_MOUSE	Pancreatic lipase-related protein 1 OS=Mus musculus GN=Pnliprp1 PE=2 SV=2
K1C10_MOUSE	Keratin, type I cytoskeletal 10 OS=Mus musculus GN=Krt10 PE=1 SV=3
AMY1_MOUSE	Alpha-amylase 1 OS=Mus musculus GN=Amy1 PE=1 SV=2
AMYP_MOUSE	Pancreatic alpha-amylase OS=Mus musculus GN=Amy2 PE=1 SV=2
CBPA2_MOUSE	Carboxypeptidase A2 OS=Mus musculus GN=Cpa2 PE=2 SV=1
CEL_MOUSE	Bile salt-activated lipase OS=Mus musculus GN=Cel PE=1 SV=1
EF1A1_MOUSE	Elongation factor 1-alpha 1 OS=Mus musculus GN=Eef1a1 PE=1 SV=3
CBPA1_MOUSE	Carboxypeptidase A1 OS=Mus musculus GN=Cpa1 PE=2 SV=1
SPI2_MOUSE	Serpin I2 OS=Mus musculus GN=Serpini2 PE=1 SV=1
ENOA_MOUSE	Alpha-enolase OS=Mus musculus GN=Eno1 PE=1 SV=3
VAT1_MOUSE	Synaptic vesicle membrane protein VAT-1 homolog OS=Mus musculus GN=Vat1 PE=1 SV=3
K2C1_MOUSE	Keratin, type II cytoskeletal 1 OS=Mus musculus GN=Krt1 PE=1 SV=4
K2C5_MOUSE	Keratin, type II cytoskeletal 5 OS=Mus musculus GN=Krt5 PE=1 SV=1
ENOB_MOUSE	Beta-enolase OS=Mus musculus GN=Eno3 PE=1 SV=3
K22E_MOUSE	Keratin, type II cytoskeletal 2 epidermal OS=Mus musculus GN=Krt2 PE=1 SV=1
K1C15_MOUSE	Keratin, type I cytoskeletal 15 OS=Mus musculus GN=Krt15 PE=1 SV=2
IF4A1_MOUSE	Eukaryotic initiation factor 4A-I OS=Mus musculus GN=Eif4a1 PE=2 SV=1
K2C8_MOUSE	Keratin, type II cytoskeletal 8 OS=Mus musculus GN=Krt8 PE=1 SV=4
K1C42_MOUSE	Keratin, type I cytoskeletal 42 OS=Mus musculus GN=Krt42 PE=1 SV=1
K2C6A_MOUSE	Keratin, type II cytoskeletal 6A OS=Mus musculus GN=Krt6a PE=2 SV=3
K2C75_MOUSE	Keratin, type II cytoskeletal 75 OS=Mus musculus GN=Krt75 PE=1 SV=1

EF1G_MOUSE	Elongation factor 1-gamma OS=Mus musculus GN=Eef1g PE=1 SV=3
K2C73_MOUSE	Keratin, type II cytoskeletal 73 OS=Mus musculus GN=Krt73 PE=1 SV=1
K2C71_MOUSE	Keratin, type II cytoskeletal 71 OS=Mus musculus GN=Krt71 PE=1 SV=1
K1C16_MOUSE	Keratin, type I cytoskeletal 16 OS=Mus musculus GN=Krt16 PE=1 SV=3
PDIA6_MOUSE	Protein disulfide-isomerase A6 OS=Mus musculus GN=Pdia6 PE=1 SV=3
K1C13_MOUSE	Keratin, type I cytoskeletal 13 OS=Mus musculus GN=Krt13 PE=1 SV=2
K1C18_MOUSE	Keratin, type I cytoskeletal 18 OS=Mus musculus GN=Krt18 PE=1 SV=5
ILEUA_MOUSE	Leukocyte elastase inhibitor A OS=Mus musculus GN=Serpinb1a PE=1 SV=1
QCR1_MOUSE	Cytochrome b-c1 complex subunit 1, mitochondrial OS=Mus musculus GN=Uqcrc1 PE=1 SV=2
METK1_MOUSE	S-adenosylmethionine synthase isoform type-1 OS=Mus musculus GN=Mat1a PE=2 SV=1
IF2B_MOUSE	Eukaryotic translation initiation factor 2 subunit 2 OS=Mus musculus GN=Eif2s2 PE=1 SV=1
PKHA7_MOUSE	Pleckstrin homology domain-containing family A member 7 OS=Mus musculus GN=Plekha7 PE=1 SV=2
K1C24_MOUSE	Keratin, type I cytoskeletal 24 OS=Mus musculus GN=Krt24 PE=2 SV=2
AMNLS_MOUSE	
RM10_MOUSE	39S ribosomal protein L10, mitochondrial OS=Mus musculus GN=Mrpl10 PE=2 SV=2
K2C79_MOUSE	Keratin, type II cytoskeletal 79 OS=Mus musculus GN=Krt79 PE=1 SV=2
RL4_MOUSE	60S ribosomal protein L4 OS=Mus musculus GN=Rpl4 PE=1 SV=3
MTOR_MOUSE	
F10A1_MOUSE	Hsc70-interacting protein OS=Mus musculus GN=St13 PE=2 SV=1
METK2_MOUSE	S-adenosylmethionine synthase isoform type-2 OS=Mus musculus GN=Mat2a PE=2 SV=2
IF4A3_MOUSE	Eukaryotic initiation factor 4A-III OS=Mus musculus GN=Eif4a3 PE=2 SV=3
K2C4_MOUSE	Keratin, type II cytoskeletal 4 OS=Mus musculus GN=Krt4 PE=1 SV=2
K2C7_MOUSE	Keratin, type II cytoskeletal 7 OS=Mus musculus GN=Krt7 PE=1 SV=1
K2C72_MOUSE	
KRT84_MOUSE	
CA087_MOUSE	
LIPR2_MOUSE	Pancreatic lipase-related protein 2 OS=Mus musculus GN=Pnliprp2 PE=2 SV=1
YBOX1_MOUSE	Nuclease-sensitive element-binding protein 1 OS=Mus musculus GN=Ybx1 PE=1 SV=3
GATM_MOUSE	Glycine amidinotransferase, mitochondrial OS=Mus musculus GN=Gatm PE=1 SV=1
DUS11_MOUSE	RNA/RNP complex-1-interacting phosphatase OS=Mus musculus GN=Dusp11 PE=2 SV=1
NUP50_MOUSE	Nuclear pore complex protein Nup50 OS=Mus musculus GN=Nup50 PE=1 SV=3
GDF7_MOUSE	Growth/differentiation factor 7 OS=Mus musculus GN=Gdf7 PE=2 SV=2
ASAP2_MOUSE	Arf-GAP with SH3 domain, ANK repeat and PH domain-containing protein 2 OS=Mus musculus GN=Asap2 PE=1 SV=3
PCLO_MOUSE	Protein piccolo OS=Mus musculus GN=Pclo PE=1 SV=3
K1C20_MOUSE	
SAHH_MOUSE	Adenosylhomocysteinase OS=Mus musculus GN=Ahcy PE=1 SV=3
PHRF1_MOUSE	
GGH_MOUSE	Gamma-glutamyl hydrolase OS=Mus musculus GN=Ggh PE=1 SV=2
INHBA_MOUSE	
NDF2_MOUSE	

PO2F1_MOUSE	
DUS3_MOUSE	Dual specificity protein phosphatase 3 OS=Mus musculus GN=Dusp3 PE=1 SV=1
HNRPF_MOUSE	Heterogeneous nuclear ribonucleoprotein F OS=Mus musculus GN=Hnrnpf PE=1 SV=3
ADCYA_MOUSE	
GDIB_MOUSE	Rab GDP dissociation inhibitor beta OS=Mus musculus GN=Gdi2 PE=1 SV=1
ATX3_MOUSE	
PRS7_MOUSE	26S protease regulatory subunit 7 OS=Mus musculus GN=Psmc2 PE=1 SV=5
ANXA7_MOUSE	Annexin A7 OS=Mus musculus GN=Anxa7 PE=2 SV=2
FBW10_MOUSE	F-box/WD repeat-containing protein 10 OS=Mus musculus GN=Fbxw10 PE=2 SV=1
T3JAM_MOUSE	
SPG7_MOUSE	

Mascot Score Histogram

Ions score is -10*Log(P), where P is the probability that the observed match is a random event.
Individual ions scores > 27 indicate identity or extensive homology (p<0.05).
Protein scores are derived from ions scores as a non-probabilistic basis for ranking protein hits.

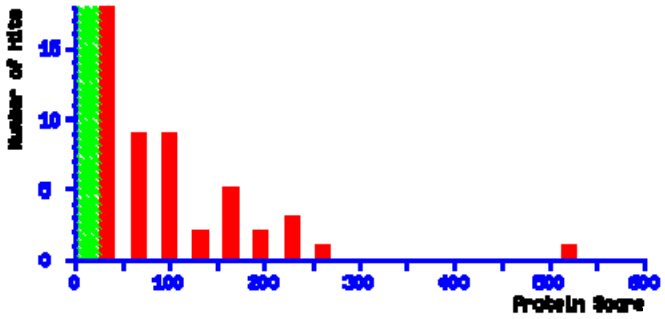

BAND 2 2h EXPERIMENTAL:

MS data file : Jena ZG band 6.tmp.tmp
Database : SwissProt 2012_04 (535698 sequences; 190107059 residues)
Taxonomy : Mus musculus (house mouse) (16528 sequences)
Timestamp : 8 May 2012 at 18:08:16 GMT
Protein hits :

LIPP_MOUSE	Pancreatic triacylglycerol lipase OS=Mus musculus GN=Pnlip PE=1 SV=1
VAT1_MOUSE	Synaptic vesicle membrane protein VAT-1 homolog OS=Mus musculus GN=Vat1 PE=1 SV=3
LIPR1_MOUSE	Pancreatic lipase-related protein 1 OS=Mus musculus GN=Pnliprp1 PE=2 SV=2
CEL_MOUSE	Bile salt-activated lipase OS=Mus musculus GN=Cel PE=1 SV=1
K1C10_MOUSE	Keratin, type I cytoskeletal 10 OS=Mus musculus GN=Krt10 PE=1 SV=3
CBPA1_MOUSE	Carboxypeptidase A1 OS=Mus musculus GN=Cpa1 PE=2 SV=1
AMY1_MOUSE	Alpha-amylase 1 OS=Mus musculus GN=Amy1 PE=1 SV=2
PDIA6_MOUSE	Protein disulfide-isomerase A6 OS=Mus musculus GN=Pdia6 PE=1 SV=3
AMYP_MOUSE	Pancreatic alpha-amylase OS=Mus musculus GN=Amy2 PE=1 SV=2
EF1A1_MOUSE	Elongation factor 1-alpha 1 OS=Mus musculus GN=Eef1a1 PE=1 SV=3
K2C1_MOUSE	Keratin, type II cytoskeletal 1 OS=Mus musculus GN=Krt1 PE=1 SV=4
K1C14_MOUSE	Keratin, type I cytoskeletal 14 OS=Mus musculus GN=Krt14 PE=1 SV=2

K2C5_MOUSE	Keratin, type II cytoskeletal 5 OS=Mus musculus GN=Krt5 PE=1 SV=1
SPI2_MOUSE	Serpin I2 OS=Mus musculus GN=Serpini2 PE=1 SV=1
K1C18_MOUSE	Keratin, type I cytoskeletal 18 OS=Mus musculus GN=Krt18 PE=1 SV=5
K1C17_MOUSE	Keratin, type I cytoskeletal 17 OS=Mus musculus GN=Krt17 PE=1 SV=3
K1C19_MOUSE	Keratin, type I cytoskeletal 19 OS=Mus musculus GN=Krt19 PE=1 SV=1
K1C15_MOUSE	Keratin, type I cytoskeletal 15 OS=Mus musculus GN=Krt15 PE=1 SV=2
CBPA2_MOUSE	Carboxypeptidase A2 OS=Mus musculus GN=Cpa2 PE=2 SV=1
ENOA_MOUSE	Alpha-enolase OS=Mus musculus GN=Eno1 PE=1 SV=3
TBB4A_MOUSE	Tubulin beta-4A chain OS=Mus musculus GN=Tubb4a PE=1 SV=3
K1C42_MOUSE	Keratin, type I cytoskeletal 42 OS=Mus musculus GN=Krt42 PE=1 SV=1
ENOB_MOUSE	Beta-enolase OS=Mus musculus GN=Eno3 PE=1 SV=3
K1C13_MOUSE	Keratin, type I cytoskeletal 13 OS=Mus musculus GN=Krt13 PE=1 SV=2
K2C6A_MOUSE	Keratin, type II cytoskeletal 6A OS=Mus musculus GN=Krt6a PE=2 SV=3
SAHH_MOUSE	Adenosylhomocysteinase OS=Mus musculus GN=Ahcy PE=1 SV=3
K1C16_MOUSE	Keratin, type I cytoskeletal 16 OS=Mus musculus GN=Krt16 PE=1 SV=3
ERP44_MOUSE	Endoplasmic reticulum resident protein 44 OS=Mus musculus GN=Erp44 PE=1 SV=1
TBA1A_MOUSE	Tubulin alpha-1A chain OS=Mus musculus GN=Tuba1a PE=1 SV=1
EF1G_MOUSE	Elongation factor 1-gamma OS=Mus musculus GN=Eef1g PE=1 SV=3
K2C1B_MOUSE	Keratin, type II cytoskeletal 1b OS=Mus musculus GN=Krt77 PE=1 SV=1
K2C73_MOUSE	Keratin, type II cytoskeletal 73 OS=Mus musculus GN=Krt73 PE=1 SV=1
K1C25_MOUSE	Keratin, type I cytoskeletal 25 OS=Mus musculus GN=Krt25 PE=1 SV=1
IF4A1_MOUSE	Eukaryotic initiation factor 4A-I OS=Mus musculus GN=Eif4a1 PE=2 SV=1
LIPR2_MOUSE	Pancreatic lipase-related protein 2 OS=Mus musculus GN=Pnliprp2 PE=2 SV=1
K1C24_MOUSE	Keratin, type I cytoskeletal 24 OS=Mus musculus GN=Krt24 PE=2 SV=2
K1C40_MOUSE	
K22E_MOUSE	Keratin, type II cytoskeletal 2 epidermal OS=Mus musculus GN=Krt2 PE=1 SV=1
F10A1_MOUSE	Hsc70-interacting protein OS=Mus musculus GN=St13 PE=2 SV=1
METK1_MOUSE	S-adenosylmethionine synthase isoform type-1 OS=Mus musculus GN=Mat1a PE=2 SV=1
RM10_MOUSE	39S ribosomal protein L10, mitochondrial OS=Mus musculus GN=Mrpl10 PE=2 SV=2
RL3_MOUSE	60S ribosomal protein L3 OS=Mus musculus GN=Rpl3 PE=2 SV=3
CTRB1_MOUSE	
TBB1_MOUSE	Tubulin beta-1 chain OS=Mus musculus GN=Tubb1 PE=1 SV=1
DUS11_MOUSE	RNA/RNP complex-1-interacting phosphatase OS=Mus musculus GN=Dusp11 PE=2 SV=1
ASAP2_MOUSE	Arf-GAP with SH3 domain, ANK repeat and PH domain-containing protein 2 OS=Mus musculus GN=Asap2 PE=1 SV=3
GATM_MOUSE	Glycine amidinotransferase, mitochondrial OS=Mus musculus GN=Gatm PE=1 SV=1
RL4_MOUSE	60S ribosomal protein L4 OS=Mus musculus GN=Rpl4 PE=1 SV=3
PO2F3_MOUSE	POU domain, class 2, transcription factor 3 OS=Mus musculus GN=Pou2f3 PE=2 SV=2
IQUB_MOUSE	
PDIA1_MOUSE	Protein disulfide-isomerase OS=Mus musculus GN=P4hb PE=1 SV=2
GGH_MOUSE	Gamma-glutamyl hydrolase OS=Mus musculus GN=Ggh PE=1 SV=2
PKHA7_MOUSE	Pleckstrin homology domain-containing family A member 7 OS=Mus musculus GN=Plekha7 PE=1 SV=2

IF4G2_MOUSE	Eukaryotic translation initiation factor 4 gamma 2 OS=Mus musculus GN=Eif4g2 PE=1 SV=2
EHMT1_MOUSE	Histone-lysine N-methyltransferase EHMT1 OS=Mus musculus GN=Ehmt1 PE=1 SV=2
DLGP4_MOUSE	
K0415_MOUSE	Protein KIAA0415 OS=Mus musculus GN=Kiaa0415 PE=2 SV=1
TRAP1_MOUSE	Heat shock protein 75 kDa, mitochondrial OS=Mus musculus GN=Trap1 PE=1 SV=1
HS90A_MOUSE	Heat shock protein HSP 90-alpha OS=Mus musculus GN=Hsp90aa1 PE=1 SV=4
GDIA_MOUSE	Rab GDP dissociation inhibitor alpha OS=Mus musculus GN=Gdi1 PE=1 SV=3
FBW10_MOUSE	F-box/WD repeat-containing protein 10 OS=Mus musculus GN=Fbxw10 PE=2 SV=1
SHRM3_MOUSE	Protein Shroom3 OS=Mus musculus GN=Shroom3 PE=1 SV=2
XPR1_MUSMC	
KAP0_MOUSE	

Mascot Score Histogram

Ions score is -10*Log(P), where P is the probability that the observed match is a random event.
Individual ions scores > 28 indicate identity or extensive homology (p<0.05).
Protein scores are derived from ions scores as a non-probabilistic basis for ranking protein hits.

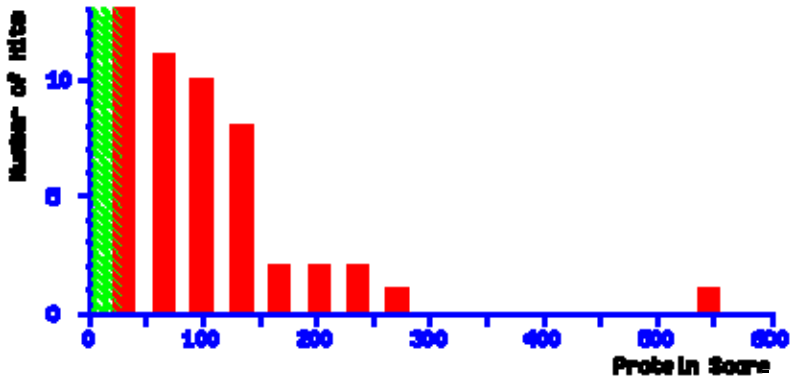

BAND 3 2h EXPERIMENTAL:

MS data file : Jena ZG band 7.tmp.tmp
Database : SwissProt 2012_04 (535698 sequences; 190107059 residues)
Taxonomy : Mus musculus (house mouse) (16528 sequences)
Timestamp : 8 May 2012 at 18:09:58 GMT
Protein hits :

LIPP_MOUSE	Pancreatic triacylglycerol lipase OS=Mus musculus GN=Pnlip PE=1 SV=1
K1C10_MOUSE	Keratin, type I cytoskeletal 10 OS=Mus musculus GN=Krt10 PE=1 SV=3
AMY1_MOUSE	Alpha-amylase 1 OS=Mus musculus GN=Amy1 PE=1 SV=2
VAT1_MOUSE	Synaptic vesicle membrane protein VAT-1 homolog OS=Mus musculus GN=Vat1 PE=1 SV=3
AMYP_MOUSE	Pancreatic alpha-amylase OS=Mus musculus GN=Amy2 PE=1 SV=2
K2C1_MOUSE	Keratin, type II cytoskeletal 1 OS=Mus musculus GN=Krt1 PE=1 SV=4
SERC_MOUSE	Phosphoserine aminotransferase OS=Mus musculus GN=Psat1 PE=1 SV=1
CEL_MOUSE	Bile salt-activated lipase OS=Mus musculus GN=Cel PE=1 SV=1
K1C14_MOUSE	Keratin, type I cytoskeletal 14 OS=Mus musculus GN=Krt14 PE=1 SV=2
CBPA2_MOUSE	Carboxypeptidase A2 OS=Mus musculus GN=Cpa2 PE=2 SV=1

CBPA1_MOUSE	Carboxypeptidase A1 OS=Mus musculus GN=Cpa1 PE=2 SV=1
K1C17_MOUSE	Keratin, type I cytoskeletal 17 OS=Mus musculus GN=Krt17 PE=1 SV=3
LIPR1_MOUSE	Pancreatic lipase-related protein 1 OS=Mus musculus GN=Pnliprp1 PE=2 SV=2
ATPB_MOUSE	ATP synthase subunit beta, mitochondrial OS=Mus musculus GN=Atp5b PE=1 SV=2
BCAT2_MOUSE	Branched-chain-amino-acid aminotransferase, mitochondrial OS=Mus musculus GN=Bcat2 PE=2 SV=2
K22E_MOUSE	Keratin, type II cytoskeletal 2 epidermal OS=Mus musculus GN=Krt2 PE=1 SV=1
K2C8_MOUSE	Keratin, type II cytoskeletal 8 OS=Mus musculus GN=Krt8 PE=1 SV=4
K1C13_MOUSE	Keratin, type I cytoskeletal 13 OS=Mus musculus GN=Krt13 PE=1 SV=2
ALDOB_MOUSE	Fructose-bisphosphate aldolase B OS=Mus musculus GN=Aldob PE=1 SV=3
PCBP1_MOUSE	Poly(rC)-binding protein 1 OS=Mus musculus GN=Pcbp1 PE=1 SV=1
K2C5_MOUSE	Keratin, type II cytoskeletal 5 OS=Mus musculus GN=Krt5 PE=1 SV=1
SPI2_MOUSE	Serpin I2 OS=Mus musculus GN=Serpini2 PE=1 SV=1
ACTB_MOUSE	Actin, cytoplasmic 1 OS=Mus musculus GN=Actb PE=1 SV=1
K1C15_MOUSE	Keratin, type I cytoskeletal 15 OS=Mus musculus GN=Krt15 PE=1 SV=2
CGL_MOUSE	Cystathionine gamma-lyase OS=Mus musculus GN=Cth PE=1 SV=1
K2C73_MOUSE	Keratin, type II cytoskeletal 73 OS=Mus musculus GN=Krt73 PE=1 SV=1
PCBP2_MOUSE	Poly(rC)-binding protein 2 OS=Mus musculus GN=Pcbp2 PE=1 SV=1
EF1A1_MOUSE	Elongation factor 1-alpha 1 OS=Mus musculus GN=Eef1a1 PE=1 SV=3
K2C1B_MOUSE	Keratin, type II cytoskeletal 1b OS=Mus musculus GN=Krt77 PE=1 SV=1
K1C42_MOUSE	Keratin, type I cytoskeletal 42 OS=Mus musculus GN=Krt42 PE=1 SV=1
AK1A1_MOUSE	Alcohol dehydrogenase [NADP(+)] OS=Mus musculus GN=Akr1a1 PE=1 SV=3
AATM_MOUSE	Aspartate aminotransferase, mitochondrial OS=Mus musculus GN=Got2 PE=1 SV=1
CLUS_MOUSE	Clusterin OS=Mus musculus GN=Clu PE=1 SV=1
K1C16_MOUSE	Keratin, type I cytoskeletal 16 OS=Mus musculus GN=Krt16 PE=1 SV=3
PSD7_MOUSE	26S proteasome non-ATPase regulatory subunit 7 OS=Mus musculus GN=Psmd7 PE=1 SV=2
ROAA_MOUSE	Heterogeneous nuclear ribonucleoprotein A/B OS=Mus musculus GN=Hnrnpab PE=1 SV=1
K2C79_MOUSE	Keratin, type II cytoskeletal 79 OS=Mus musculus GN=Krt79 PE=1 SV=2
K1C19_MOUSE	Keratin, type I cytoskeletal 19 OS=Mus musculus GN=Krt19 PE=1 SV=1
EIF3I_MOUSE	Eukaryotic translation initiation factor 3 subunit I OS=Mus musculus GN=Eif3i PE=1 SV=1
PCBP3_MOUSE	Poly(rC)-binding protein 3 OS=Mus musculus GN=Pcbp3 PE=2 SV=3
RL6_MOUSE	60S ribosomal protein L6 OS=Mus musculus GN=Rpl6 PE=1 SV=3
K2C6A_MOUSE	Keratin, type II cytoskeletal 6A OS=Mus musculus GN=Krt6a PE=2 SV=3
K2C4_MOUSE	Keratin, type II cytoskeletal 4 OS=Mus musculus GN=Krt4 PE=1 SV=2
KRT84_MOUSE	Keratin, type II cuticular Hb4 OS=Mus musculus GN=Krt84 PE=2 SV=2
K1H2_MOUSE	
GLRX3_MOUSE	Glutaredoxin-3 OS=Mus musculus GN=Glrx3 PE=1 SV=1
DJB11_MOUSE	DnaJ homolog subfamily B member 11 OS=Mus musculus GN=Dnajb11 PE=1 SV=1
CTRB1_MOUSE	Chymotrypsinogen B OS=Mus musculus GN=Ctrb1 PE=2 SV=1
PDIA1_MOUSE	Protein disulfide-isomerase OS=Mus musculus GN=P4hb PE=1 SV=2
FPPS_MOUSE	Farnesyl pyrophosphate synthase OS=Mus musculus GN=Fdps PE=2 SV=1
HNRPD_MOUSE	Heterogeneous nuclear ribonucleoprotein D0 OS=Mus musculus GN=Hnrnpd PE=1 SV=2
F16P1_MOUSE	Fructose-1,6-bisphosphatase 1 OS=Mus musculus GN=Fbp1 PE=2 SV=3

LIPR2_MOUSE	Pancreatic lipase-related protein 2 OS=Mus musculus GN=Pnliprp2 PE=2 SV=1
MTNA_MOUSE	Methylthioribose-1-phosphate isomerase OS=Mus musculus GN=Mri1 PE=2 SV=1
CATR_MOUSE	Cathepsin R OS=Mus musculus GN=Ctsr PE=2 SV=1
EIF3M_MOUSE	Eukaryotic translation initiation factor 3 subunit M OS=Mus musculus GN=Eif3m PE=2 SV=1
PURA_MOUSE	Transcriptional activator protein Pur-alpha OS=Mus musculus GN=Pura PE=1 SV=1
SPTB1_MOUSE	Spectrin beta chain, erythrocyte OS=Mus musculus GN=Sptb PE=1 SV=4
COT1_MOUSE	COUP transcription factor 1 OS=Mus musculus GN=Nr2f1 PE=2 SV=2
PO2F1_MOUSE	
PSD13_MOUSE	26S proteasome non-ATPase regulatory subunit 13 OS=Mus musculus GN=Psmd13 PE=1 SV=1
ACTBL_MOUSE	Beta-actin-like protein 2 OS=Mus musculus GN=Actbl2 PE=1 SV=1
ATN1_MOUSE	Atrophin-1 OS=Mus musculus GN=Atn1 PE=1 SV=1
PURB_MOUSE	Transcriptional activator protein Pur-beta OS=Mus musculus GN=Purb PE=1 SV=3
HYCCI_MOUSE	Hyccin OS=Mus musculus GN=Fam126a PE=1 SV=2
DNJC3_MOUSE	
MTHFS_MOUSE	5-formyltetrahydrofolate cyclo-ligase OS=Mus musculus GN=Mthfs PE=2 SV=2
DUS3_MOUSE	Dual specificity protein phosphatase 3 OS=Mus musculus GN=Dusp3 PE=1 SV=1
GNA13_MOUSE	Guanine nucleotide-binding protein subunit alpha-13 OS=Mus musculus GN=Gna13 PE=1 SV=1
GNAL_MOUSE	Guanine nucleotide-binding protein G(olf) subunit alpha OS=Mus musculus GN=Gnal PE=1 SV=1
GNAT1_MOUSE	Guanine nucleotide-binding protein G(t) subunit alpha-1 OS=Mus musculus GN=Gnat1 PE=1 SV=3
GNA12_MOUSE	Guanine nucleotide-binding protein subunit alpha-12 OS=Mus musculus GN=Gna12 PE=1 SV=3

Mascot Score Histogram

Ions score is -10*Log(P), where P is the probability that the observed match is a random event.
Individual ions scores > 28 indicate identity or extensive homology (p<0.05).
Protein scores are derived from ions scores as a non-probabilistic basis for ranking protein hits.

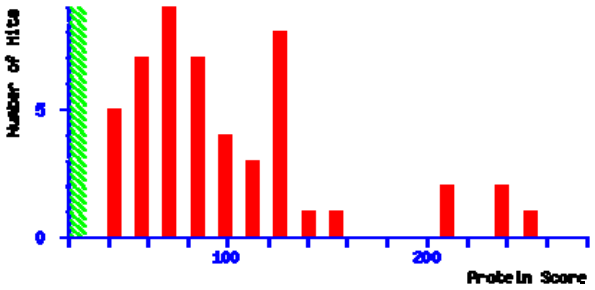

BAND 4 2h EXPERIMENTAL:

MS data file : Jena ZG band 8.tmp.tmp
Database : SwissProt 2012_04 (535698 sequences; 190107059 residues)
Taxonomy : Mus musculus (house mouse) (16528 sequences)
Timestamp : 8 May 2012 at 18:11:32 GMT
Protein hits :

K1C10_MOUSE	Keratin, type I cytoskeletal 10 OS=Mus musculus GN=Krt10 PE=1 SV=3

LIPP_MOUSE	Pancreatic triacylglycerol lipase OS=Mus musculus GN=Pnlip PE=1 SV=1
EF2_MOUSE	Elongation factor 2 OS=Mus musculus GN=Eef2 PE=1 SV=2
K2C1_MOUSE	Keratin, type II cytoskeletal 1 OS=Mus musculus GN=Krt1 PE=1 SV=4
CEL_MOUSE	Bile salt-activated lipase OS=Mus musculus GN=Cel PE=1 SV=1
SERC_MOUSE	Phosphoserine aminotransferase OS=Mus musculus GN=Psat1 PE=1 SV=1
K1C14_MOUSE	Keratin, type I cytoskeletal 14 OS=Mus musculus GN=Krt14 PE=1 SV=2
K1C17_MOUSE	Keratin, type I cytoskeletal 17 OS=Mus musculus GN=Krt17 PE=1 SV=3
ALBU_MOUSE	Serum albumin OS=Mus musculus GN=Alb PE=1 SV=3
AMY1_MOUSE	Alpha-amylase 1 OS=Mus musculus GN=Amy1 PE=1 SV=2
TALDO_MOUSE	Transaldolase OS=Mus musculus GN=Taldo1 PE=1 SV=2
K22E_MOUSE	Keratin, type II cytoskeletal 2 epidermal OS=Mus musculus GN=Krt2 PE=1 SV=1
CBPA1_MOUSE	Carboxypeptidase A1 OS=Mus musculus GN=Cpa1 PE=2 SV=1
AMYP_MOUSE	Pancreatic alpha-amylase OS=Mus musculus GN=Amy2 PE=1 SV=2
K1C13_MOUSE	Keratin, type I cytoskeletal 13 OS=Mus musculus GN=Krt13 PE=1 SV=2
ATPB_MOUSE	ATP synthase subunit beta, mitochondrial OS=Mus musculus GN=Atp5b PE=1 SV=2
K1C15_MOUSE	Keratin, type I cytoskeletal 15 OS=Mus musculus GN=Krt15 PE=1 SV=2
K1C42_MOUSE	Keratin, type I cytoskeletal 42 OS=Mus musculus GN=Krt42 PE=1 SV=1
ALDOB_MOUSE	Fructose-bisphosphate aldolase B OS=Mus musculus GN=Aldob PE=1 SV=3
LIPR1_MOUSE	Pancreatic lipase-related protein 1 OS=Mus musculus GN=Pnliprp1 PE=2 SV=2
K2C5_MOUSE	Keratin, type II cytoskeletal 5 OS=Mus musculus GN=Krt5 PE=1 SV=1
ERP44_MOUSE	Endoplasmic reticulum resident protein 44 OS=Mus musculus GN=Erp44 PE=1 SV=1
K2C71_MOUSE	Keratin, type II cytoskeletal 71 OS=Mus musculus GN=Krt71 PE=1 SV=1
K2C74_MOUSE	Keratin, type II cytoskeletal 74 OS=Mus musculus GN=Krt74 PE=2 SV=1
K2C1B_MOUSE	Keratin, type II cytoskeletal 1b OS=Mus musculus GN=Krt77 PE=1 SV=1
K1C16_MOUSE	Keratin, type I cytoskeletal 16 OS=Mus musculus GN=Krt16 PE=1 SV=3
ROAA_MOUSE	Heterogeneous nuclear ribonucleoprotein A/B OS=Mus musculus GN=Hnrnpab PE=1 SV=1
BCAT2_MOUSE	Branched-chain-amino-acid aminotransferase, mitochondrial OS=Mus musculus GN=Bcat2 PE=2 SV=2
VAT1_MOUSE	Synaptic vesicle membrane protein VAT-1 homolog OS=Mus musculus GN=Vat1 PE=1 SV=3
RL6_MOUSE	60S ribosomal protein L6 OS=Mus musculus GN=Rpl6 PE=1 SV=3
CLUS_MOUSE	Clusterin OS=Mus musculus GN=Clu PE=1 SV=1
K2C8_MOUSE	Keratin, type II cytoskeletal 8 OS=Mus musculus GN=Krt8 PE=1 SV=4
K2C79_MOUSE	Keratin, type II cytoskeletal 79 OS=Mus musculus GN=Krt79 PE=1 SV=2
K1C27_MOUSE	Keratin, type I cytoskeletal 27 OS=Mus musculus GN=Krt27 PE=1 SV=1
RSSA_MOUSE	40S ribosomal protein SA OS=Mus musculus GN=Rpsa PE=1 SV=4
AATM_MOUSE	Aspartate aminotransferase, mitochondrial OS=Mus musculus GN=Got2 PE=1 SV=1
CGL_MOUSE	Cystathionine gamma-lyase OS=Mus musculus GN=Cth PE=1 SV=1
SPI2_MOUSE	Serpin I2 OS=Mus musculus GN=Serpini2 PE=1 SV=1
EIF3M_MOUSE	Eukaryotic translation initiation factor 3 subunit M OS=Mus musculus GN=Eif3m PE=2 SV=1
DJB11_MOUSE	DnaJ homolog subfamily B member 11 OS=Mus musculus GN=Dnajb11 PE=1 SV=1
ACTB_MOUSE	Actin, cytoplasmic 1 OS=Mus musculus GN=Actb PE=1 SV=1
CBPA2_MOUSE	Carboxypeptidase A2 OS=Mus musculus GN=Cpa2 PE=2 SV=1
MTNA_MOUSE	Methylthioribose-1-phosphate isomerase OS=Mus musculus GN=Mri1 PE=2 SV=1

AK1A1_MOUSE	Alcohol dehydrogenase [NADP(+)] OS=Mus musculus GN=Akr1a1 PE=1 SV=3
EIF3I_MOUSE	Eukaryotic translation initiation factor 3 subunit I OS=Mus musculus GN=Eif3i PE=1 SV=1
MAT2B_MOUSE	Methionine adenosyltransferase 2 subunit beta OS=Mus musculus GN=Mat2b PE=2 SV=1
K1H2_MOUSE	Keratin, type I cuticular Ha2 OS=Mus musculus GN=Krt32 PE=2 SV=2
K1C24_MOUSE	
SRPR_MOUSE	Signal recognition particle receptor subunit alpha OS=Mus musculus GN=Srpr PE=1 SV=1
EF1A1_MOUSE	Elongation factor 1-alpha 1 OS=Mus musculus GN=Eef1a1 PE=1 SV=3
PURA_MOUSE	Transcriptional activator protein Pur-alpha OS=Mus musculus GN=Pura PE=1 SV=1
LIPR2_MOUSE	Pancreatic lipase-related protein 2 OS=Mus musculus GN=Pnliprp2 PE=2 SV=1
GMPPB_MOUSE	Mannose-1-phosphate guanyltransferase beta OS=Mus musculus GN=Gmppb PE=2 SV=1
FPPS_MOUSE	Farnesyl pyrophosphate synthase OS=Mus musculus GN=Fdps PE=2 SV=1
K2C6A_MOUSE	Keratin, type II cytoskeletal 6A OS=Mus musculus GN=Krt6a PE=2 SV=3
K2C4_MOUSE	Keratin, type II cytoskeletal 4 OS=Mus musculus GN=Krt4 PE=1 SV=2
K2C72_MOUSE	
K2C7_MOUSE	
RS27A_MOUSE	Ubiquitin-40S ribosomal protein S27a OS=Mus musculus GN=Rps27a PE=1 SV=2
UBC_MOUSE	Polyubiquitin-C OS=Mus musculus GN=Ubc PE=1 SV=2
EIF3H_MOUSE	Eukaryotic translation initiation factor 3 subunit H OS=Mus musculus GN=Eif3h PE=1 SV=1
PURB_MOUSE	Transcriptional activator protein Pur-beta OS=Mus musculus GN=Purb PE=1 SV=3
CTRB1_MOUSE	Chymotrypsinogen B OS=Mus musculus GN=Ctrb1 PE=2 SV=1
F16P1_MOUSE	Fructose-1,6-bisphosphatase 1 OS=Mus musculus GN=Fbp1 PE=2 SV=3
AKCL2_MOUSE	1,5-anhydro-D-fructose reductase OS=Mus musculus GN=Akr1e2 PE=1 SV=1
HNRPD_MOUSE	Heterogeneous nuclear ribonucleoprotein D0 OS=Mus musculus GN=Hnrnpd PE=1 SV=2
PDIA1_MOUSE	Protein disulfide-isomerase OS=Mus musculus GN=P4hb PE=1 SV=2
LRC8E_MOUSE	Leucine-rich repeat-containing protein 8E OS=Mus musculus GN=Lrrc8e PE=2 SV=2
SYNC_MOUSE	Asparagine--tRNA ligase, cytoplasmic OS=Mus musculus GN=Nars PE=1 SV=2
K1C20_MOUSE	
PSD7_MOUSE	26S proteasome non-ATPase regulatory subunit 7 OS=Mus musculus GN=Psmd7 PE=1 SV=2
DUS3_MOUSE	Dual specificity protein phosphatase 3 OS=Mus musculus GN=Dusp3 PE=1 SV=1
CATR_MOUSE	Cathepsin R OS=Mus musculus GN=Ctsr PE=2 SV=1
SPTB1_MOUSE	Spectrin beta chain, erythrocyte OS=Mus musculus GN=Sptb PE=1 SV=4
ASAP2_MOUSE	Arf-GAP with SH3 domain, ANK repeat and PH domain-containing protein 2 OS=Mus musculus GN=Asap2 PE=1 SV=3
PTPA_MOUSE	Serine/threonine-protein phosphatase 2A activator OS=Mus musculus GN=Ppp2r4 PE=1 SV=1
PO2F1_MOUSE	
NO66_MOUSE	
PRDX1_MOUSE	Peroxiredoxin-1 OS=Mus musculus GN=Prdx1 PE=1 SV=1
PRDX4_MOUSE	Peroxiredoxin-4 OS=Mus musculus GN=Prdx4 PE=1 SV=1
ATN1_MOUSE	Atrophin-1 OS=Mus musculus GN=Atn1 PE=1 SV=1
ABCA4_MOUSE	Retinal-specific ATP-binding cassette transporter OS=Mus musculus

	GN=Abca4 PE=2 SV=1
APOA4_MOUSE	Apolipoprotein A-IV OS=Mus musculus GN=Apoa4 PE=2 SV=3
SYHC_MOUSE	Histidine--tRNA ligase, cytoplasmic OS=Mus musculus GN=Hars PE=2 SV=2

Mascot Score Histogram

Ions score is -10*Log(P), where P is the probability that the observed match is a random event.
Individual ions scores > 28 indicate identity or extensive homology (p<0.05).
Protein scores are derived from ions scores as a non-probabilistic basis for ranking protein hits.

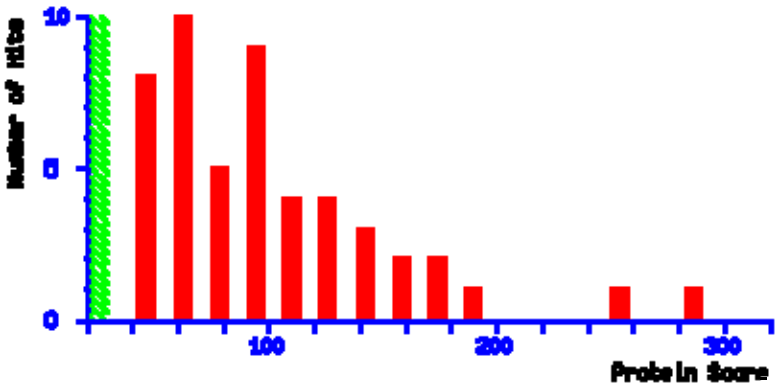

REFERENCES

1. Abu-Hamdah R, Cho W-J, Cho S-J, Jeremic A, Kelly M, Ilie AE, Jena BP. Regulation of the water channel aquaporin-1: isolation and reconstitution of the regulatory complex. *Cell Biology International* 28: 7-17, 2004.
2. Alverez de Toledo G, Fernandez-Chacon R, and Fernandez JM. Release of secretory products during transient vesicle fusion. *Nature*. 363:554-558, 1993.
3. American Heart Association. What your cholesterol levels mean. http://www.heart.org/HEARTORG/Conditions/Cholesterol/AboutCholesterol/What-Your-Cholesterol-Levels-Mean_UCM_305562_Article.jsp Retreived 1 December 2013.
4. Arispe, N, Doh, M, Simakova, O, Kurganov, B, De Maio, A. Hsc70 and Hsp70 interact with phosphatidylserine on the surface of PC12 cells resulting in a decrease of viability. *Federatin of European Biochemical Societies Journal.* 18:1636-1645, 2004.
5. Aufenanger J, Samman M, Quintel M, Fassbender K, Zimmer W, Bertsch T. Pancreatic phospholipase A2 activity in acute pancreatitis: a prognostic marker for early identification of patients at risk. *Clinical Chemistry and Laboratory Medicine* 40:293-297, 2002.
6. Bezrukov, SM, Rand,RP, Vodyanoy, I, Parsegian, VA. Lipid packing stress and polypeptide aggregation: alamethicin channel probed by proton titration of lipid charge. *Faraday Discuss.* 111, 1999.
7. Bhagat L, Singh VP, Song AM, van Acker GJ, Agrawal S, Steer ML, Saluja AK. Thermal stress-induced HSP70 mediates protection against intrapancreatic trypsinogen activation and acute pancreatitis in rats. *Gastroenterology* 122: 156-165, 2002.
8. Bragado S, San Roman JI, Gonzalez A, Garcia LJ, Lopez MA, Calvo JJ. Impairment of intracellular calcium homoeostasis in the exocrine pancreas after caerulein-induced acute

pancreatitis in the rat. *Clinical Science* 3: 365-369, 1996.

9. Brannon, PM. Adaption of the exocrine pancreas to diet. *Annual Reviews in Nutrition*. 10: 85-105, 1990.

10. Boron, W, Boulpaep, EL (Eds). Medical Physiology: A cellular and molecular approach. Updated 2E. Elsevier: 1009-1012, 2012.

11. Burke JE, Dennis EA. Phospholipase A2 structure/function, mechanism, and signaling. *Journal of Lipid Research* April Suppl: S237-S242, 2009.

12. Cabrera-Vera TM, Vanhauwe J, Thomas TO, Medkova M, Preininger A, Mazzoni MR, Ham HE. Insights into G protein structure, function, and regulation. *Endocrine Reviews* 24:765-781, 2003.

13. Chandler DE and Heuser JE. Exocytosis. *Journal of Cellular Bio*logy 86: 666-674, 1980.

14. Chen, X, Dolors Sans, M, Strahler, JR, Karnovsky, A, Ernst, SA, Michailidis, G, Andrews, PC, Williams, JA. Quantitative organellar proteomics analysis of rough endoplasmic reticulum from normal and acute pancreatitis rat pancreas. *Journal of Proteome Research*. 9:885-896, 2010.

15. Chen, Z-H, Lee, J-S, Shin, L, Cho, W-J, Jena, BP. Involvement of β-adrenergic receptor in synaptic vesicle swelling and implication in neurotransmitter release. *Journal of Cellular and Molecular Medicine* 15:572-576, 2011.

16. Chernomordik L. Non-bilayer lipids and biological fusion intermediates. *Chemistry and Physics of Lipids*. 81: 203-213, 1996.

17. Chiari H. Über die Selbstverdauung des menschlichen Pankreas. *Zeitschrift für Heilkunde.* 17: 69-96, 1896.

18. Cho S-J, Kelly M, Rognlien KT, Cho JA, Horber JKH, and Jena, BP. SNAREs in opposing bilayers interact in a circular array to form conducting pores. *Biophysical Journal* 83: 2522-2527, 2002.

19. Cho S–J, Sattar AK, Jeong EH, Satchi M, Cho J, Dash S, Mayes MS, Stromer MH, Jena BP. Aquaporin 1 regulates GTP-induced rapid gating of water in secretory vesicles. *Proceedings of the National Academy of Science USA* 99: 4720-4724, 2002.

20. Cho WJ, Jeremic A, and Jena BP. Direct interaction between SNAP-23 abd L-type Ca^{2+} channel. *Journal of Cellular and Molecular Medicine*. 9: 308-386, 2005.

21. Cho, W-J, Jeremic, A, Jin, H, Ren, G, Jena, BP. Neuronal fusion pore assembly requires membrane cholesterol. *Cell Biology International.* 31:1301-1308, 2007.

22. Coorssen JR, Blank PS, Tahara M, and Zimmerberg J. Biochemical and functional studies of cortical vesicle fusion: the SNARE complex and calcium sensitivity. *Journal of Cellular Biology*. 143: 1845-1857, 1998.

23. Cosen-Binker LI, Lam PP, Binker MG, Gaisano HY. Alcohol-induced protein kinase C alpha phosphorylation of Munc18c in carbachol stimulated acini causes basolateral exocytosis. *Gastroenterology.* 132: 1527-1545, 2007.

24. Cullis, PR, and DeKruijff, B. Lipid polymorphism and the func- tional role of lipids in biological membranes. *Biochimica et Biophysica Acta.* 559:399-420, 1979.

25. Dawra R, Sah RP, Dudeja V, Talukdar R, Garg P, Saluja AK. Intra-acinar trypsinogen activation mediates early stages of pancreatic injury but not inflammation in mice with acute pancreatitis. *Gastroenterology* 141: 2210-2217, 2011.

26. Degtyarev MY, Spiegel AM, Jones TLZ. Palmitoylation of a G protein alpha i subunit requires membrane localization not myristoylation. *Journal of Biological Chemistry* 269: 30898-30903, 1994.

27. Ding, S-P, Li, J-C, Chang, S. A mouse model of severe acute pancreatitis induced with caerulein and lipopolysaccharide. *World Journal of Gastroenterology*. 9(3): 584-589, 2003.

28. Dohlman HG, Caron MG, and Lefkowitz RJ. A family of receptors coupled to guanine nucleotide receptor proteins. *Biochemistry* 26:2657-2664, 1987.

29. Dumas, F, Tocanne, J, LeBlanc, G, Lebrun, MC. Consequences of hydrophobic mismatch between lipids and melibiose permease on melibiose transport. *Biochemistry*. 39: 4846–4854, 2000.

30. Fagenholz PJ, Fernandez-del Castillo C, Harris NS, Pelletier, AJ, Camargo, CA, Jr . Direct medical costs of acute pancreatitis hospitalizations in the United States. *Pancreas*. 35:302–7, 2007.

31. Fick TW. The role of calcium in acute pancreatitis. Surgery 152:S157-S163, 2012.

32. Foulis, A. Histological evidence of initiating factors in acute necrotizing pancreatitis in man. *Journal of Clinical Pathology*. 33: 1125-1131, 1980.

33. Fuller N, Rand RP. The influence of lysolipids on the on the spontaneous curvature and bending elasticity of phospholipid membranes. *Biophysical Journal* 81: 243-254, 2001.

34. Gilman AG. G-Proteins: transducers of receptor-generated signals. *Annual Reviews in Biochemistry*. 56: 615-649, 1987.

35. Gorelick FS, Matovcik LM. Lysosomal enzymes and pancreatitis. *Gastroenterology* 109: 620-625, 1995.

36. Gruner, SM. Intrinsic curvature hypothesis for biomembrane lipid composition: a role for nonbilayer lipids. *Proceedings of the National Academy of Science U.S.A.* 82:3665–3669, 1985.

37. Haeggström JZ, Funk CD. Lipoxygenase and Leukotriene Pathways: Biochemistry,

Biology, and Roles in Disease. *Chemical Reviews* 111(10): 5866-98, 2011.

38. Halangk, W and Lerch, MM. Early events in acute pancreatitis. *Gastroenterology Clinics of North America*. 33(4): 717-731, 2004.

39. Hanukoglu, I. Steroidogenic enzymes: structure, function, and role in regulation of steroid hormone biosynthesis. *Journal of Steroid Biochemestry and Molecular Biology*. 43 (8): 779–804, 1992.

40. Helin H, Mero M, Markkula H, Helin M. Pancreatic acinar ultrastructure in human acute pancreatitis. *Arch Pathology and Anatomical Histology*. 387: 259-270, 1980.

41. Higashijima T, Wakamatsu K, Takemitsu M, Fujino M, Nakajima T, and Miyazawa T. Conformational change of mastoparan from wasp venom on binding with phospholipid membrane. *Federation of European Biochemical Societies Letters*. 152: 227-230, 1983.

42. Higashijima T, Uzu S, Nakajima T, Ross E. Mastoparan, a peptide toxin from wasp venom, mimics receptors by activating GTP-binding regulatory proteins (G proteins). *Journal of Biological Chemistry* 263: 6491– 6494, 1988.

43. Hirano T, Saluja A, Ramarao P, Lerch M, Saluja M, Steer M. Apical secretion of lysosomal enzymes in rabbit pancreas occurs via a secretagogue regulated pathway and is increased after pancreatic duct obstruction. Journal of Clinical *Investigation*. 87: 865-869, 1991.

44. Hofbauer, B, Salvia, A, Lerch, M, Bhagat, L, Bhatia, M, Lee, H, Frossard, J, Alder, G, Steer, M. Intra-acinar cell activation of trypsinogen during caerulein-induced pancreatitis in rats. *American Journal of Physiology Gastrointestinal and Liver Physiology*. 275(38): G352-G362, 1998.

45. Jena BP, Padfield PJ, Ingebritsen TS, and Jamieson JD. Protein tyrosine phosphatase stimulates Ca^{2+}-dependant amylase secretion from pancreatic ancini. *Journal of Biological Chemistry*. 266: 17744-17746, 1991.

46. Jena BP, Schneider SW, Geibel JP, Webster P, Oberleithner H, Sritharan KC. G_i regulation of secretory vesicle swelling examined by atomic force microscopy. *Proceedings of the National Academy of Science U.S.A*. 94: 13317-13322, 1997.

47. Jeremic A, Cho WJ, BP. Membrane fusion: what may transpire at the atomic level. *Journal of Biological Physics and Chemistry*. 4: 139-142, 2004.

48. Jeremic A, Kelly M, Cho JA, Cho S-J, Horber JKH, and Jena, BP. Calcium drives fusion of SNARE-apposed bilayers. *Cell Biology International* 28: 19-31, 2004b.

49. Jeremic A, Cho WJ, Jena BP. Involvement of water channels in synaptic vesicle swelling. *Experimental Biology and Medicine*. 230: 674-80, 2005.

50. Jeremic A, Cho WJ, Jena BP. Cholesterol is critical to the integrity of neuronal prosome/fusion pore. *Ultramicroscopy*. 106(8-9): 674-677, 2006.

51. Katz M, Carangelo R, Miller LJ, Gorelick F. Effect of ethanol on cholecystokinin-stimulated zymogen conversion in pancreatic acinar cells. *American Journal of Physiology*. 270: G171-G175, 1996.

52. Kelly M, Cho WJ, Jeremic A, Abu-Hamdah R, Jena BP. Vesicle swelling regulates content expulsion during secretion. *Cell Biology International.* 28: 709-716, 2004a.

53. Kelly M, Cho W-J, Jeremic A, Abu-Hamdah R, Jena BP. Vesicle swelling regulates content expulsion during secretion. *Cell Biology International.* 28: 709-716, 2004b.

54. Knepper MA. The aquaporin family of molecular water channels. *Proceedings of the National Academy of Science*. 91: 6255-6258, 1994.

55. Knepper MA and Inoue T. Regulation of Aquaporin-2 water channel trafficking by vasopressin. *Current Opinions in Cell Biology*. 9: 560-564, 1997.

56. Ko SBH, Mizuno M, Yatabe Y, Yoshikawa T, Ishiguro H, Yamamoto A, Azuma S, Naruse S, Yamao K, Muallem S, Goto H. Aquaporin 1 water channel is overexpressed in the plasma membrane of pancreatic ducts in patients with autoimmune pancreatitis. *Journal of Medical Investigation* 56: 318-321, 2009.

57. Konings AW, Ruifrok AC. Role of membrane lipids and membrane fluidity in thermosensitivity and thermotolerance of mammalian cells. *Radiation Research Society* 102(1):86-98, 1985.

58. Konrad RJ, Young RA, Record RD, Smith RM, Butkerait P, Manning D, Jarett L, and Wolf BA. The heterotrimeric G protein Gi is localized to the insulin secretory granules of beta cells and is involved in insulin exocytosis. *Journal of Biological Chemistry.* 270:12869-12876,1995.

59. Kukor Z, Mayerle J, Kruger B, Tóth M, Steed P, Halangk W, Lerch M, Sahin-Tóth M. Presence of cathepsin B in the human pancreatic secretory pathway and its role in trypsinogen activation during hereditary pancreatitis. *Journal of Biological Chemistry*. 277: 21389-21396, 2002.

60. Laemmli UK. Cleavage of structural proteins during the assembly of the head of bacteriophage T4. *Nature*. 227:680–685, 1970.

61. Lam, AD, Tryoen-Toth, P, Tsai, B, Vatile, N, and Stuenkel, EL. SNARE-catalyzed fusion events are regulated by syntaxin1A-lipid interactions. *Molecular Biology of the Cell.* 19, 485–497, 2008.

62. Lee J-S, Cho WJ, Shin L, and Jena BP. Involvement of cholesterol in synaptic vesicle swelling. *Experimental Biology and Medicine*. 235: 470-477, 2010.

63. Lu HAJ, Sun TX, Matsuzaki T, Yi XH, Eswara J, Bouley R, McKee M, Brown D. Heat shock protein 70 interacts with aquaporins-2 and regulates its traffiking. *Journal of Biological Chemistry.* 282: 28721-28732, 2007.

64. Lundbaek, J. A. 2008. Lipid bilayer-mediated regulation of ion channel function by amphiphilic drugs. *Journal of General Physiology*. 131: 421–429.

65. Magana-Gomez, J, Lopez-Cervantes, G, Calderon de la Barca, A. Caerulein induced pancreatitis in rats: Histological and genetic expression changes from acute phase to recouperation. *World Journal of Gastroenterology*. 12(25): 3999-4003, 2006.

66. Matyash, V, Liebisch, G, Kurzchalia, TV, Shevchenko, A, and Schwudke, D. Lipid extraction by methyl-tert-butyl ether for high-throughput lipidomics. *Journal of Lipid Research.* 49(5):1137-46, 2008.

67. McMahon HT and Gallop JL. Membrane curvature and mechanisms of dynamic cell membrane remodeling. *Nature*.

68. Meimaridou E, Gooljar SB, Ramnarace N, Anthonypillai L, Clark AJ, Chapple JP. The cutosolic chaperone Hsc70 promotes traffic to the cell surface of intracellular retained melanocortin-4 receptor mutants. *Molecular Endocrinology.* 25: 1650-1660, 2011.

69. Morales J, Fishburn CS, Wilson PT, Bourne HR. Plasma membrane localization of G alpha z requires two signals. *Molecular Biology of the Cell* 10: 1-14, 1998.

70. Mouritsen, OG, and Bloom, M.. Mattress model of lipidprotein interactions in membranes. *Biophysical Journal*. 46: 141–153, 1984.

71. Mumby SM, Kleuss C, Gilman AG. Receptor regulation of G-protein palmitoylation. *Proceedings of the National Academy of Science U.S.A.* 91: 2800-2804, 1994.

72. National Institute of Health. High cholesterol levels. National Health Service. Retreived 11 2011. http://www.nhs.uk/conditions/cholesterol/Pages/Introduction.aspx.

73. National Pancreas Foundation. Fact sheet: pancreatic disease. Accessed from http://pancreasfoundation.org/Docs/patient_info/PancreaticDisease.pdf. Retreived 1 December 2013.

74. Nevalainen, T, Eskola, J, Aho, A, Havia, V, Lovgren, T, Nanto, V. Immunoreactive phospholipase A2 in serum in acute pancreatitis and pancreatic cancer. *Clinical Chemistry*. 31(7): 1116-1120, 1985.

75. Neurath H, Walsh KA. Role of proteolytic enzymes in biological regulation. *Proceedings of the National Academy of Science U.S.A.* 73: 3825-3832, 1976.

76. NIDDK. Pancreatitis. National digestive disease information clearinghouse: National Institute of Health. 0: 1-6, 2012.

77. Nyholm, T, Ozdirekcan, S, Killian, J. How protein transmembrane segments sense the lipid environment. *Biochemistry*. 46: 1457–1465, 2007.

78. Ohta E, Itoh T, Nimoto T, Kumagai J, Ko SBH, Ishibashi K, Ohno M, Uchida K, Ohta A, Sohara E, Uchida S, Sasaki S, Rai T. Pancreas-specific aquaporin 12 null mice showed increased susceptibility to caerulein-induced acute pancreatitis. *American Journal of Cellular Physiology.* 297: C1368-1378, 2009.

79. Pandol, SJ. *The exocrine pancreas*. Morgan & Claypool Life Sciences; San Rafael, CA, 2010

80. Pandol SJ, Saluja AK, Imrie CW, and Banks PA. Acute Pancreatitis: Bench to Bedside. *Gastroenterology.* 132:1127-1151, 2007.

81. Pandol SJ, Periskic S, Gukovsky I, Zaninovic V, Jung Y, Zong Y, Solomon TE, Gukovskaya AS, Tsukamoto H. Ethanol diet increases the sensitivity of rats to pancreatitis induced by cholecystokinin octapeptide. *Gastroenterology.* 117: 706-716 1999.

82. Peery AE, Dellon ES, Lund J *et al.* Burden of gastrointestinal diseases in the United States: 2012 Update. *Gastroenterology*. 2012;143:1179–87, 2012.

83. Perozo, E., Kloda, A., Cortes, D., Martinack, B. Physical principles underlying the transduction of bilayer deformation forces during mechanosensitive channel gating. *Nature Structural and Molecular Biology*. 9: 696–703, 2002.

84. Piiper A, Plusczyk T, Eckhardt L, Schulz I. Effects of cholecystokinin, cholecystokinin JMV-180 and GTP analogs on enzyme secretion from permeabilized acini and choloride conductance in isolated zymogen granules of the rat pancreas. *Federatin of European Biochemical Societies*. 197: 391-398, 1991.

85. Ravnskov, U. Is atherosclerosis caused by high cholesterol? *Quarterly Journal of Medicine*. 95:397-403, 2002.

86. Rubin RP, Thompson RH, Laychock SG. Characterization of phospholipase A2 and acyltransferase activities in purified zymogen granule membranes. *Biochemistry and Biophysical Acta.* 1045: 245-251, 1990.

87. Rubin RP, Withiam-Leitch M, Laychock SG. Modulation of phospholipase A2 activity in zymogen granule membrane by GTPγS; evidence for GTP-binding protein regulation. *Biochemical and Biophysical Research Community*. 177: 22-26, 1991.

88. Saito, I, Hashimoto, S, Salvia, A, Steer, M, Meldolesi, J. Intracellular transport of pancreatic zymogens during caerulein supramaximal stimulation. *American Journal of Physiology*. 253(4 Pt 1): G517-G526, 1987.

89. Saluja A, Saito I, Saluja M, Houlihan MJ, Powers RE, Meldolesi J, Steer ML. In-vivo rat pancreatic acinar cell function during supramaximal stimulation with caerulein. *American Journal of Physiology.* 249: G702-710, 1985.

90. Saluja A, Hashimoto S, Saluja M, Powers RE, Meldolesi J, Steer ML. Subcellular

redistribution of lysosomal enzymes during caerulein-induced pancreatitis. *American Journal of Physiology*. 253: G508-516, 1987.

91. Saluja M, Saluja A, Lerch MM, Steer ML. A plasma esterase which is expressed during supramaximal stimulation causes in vitro subcellular redistribution of lysosomal enzymes in rat exocrine pancreas. *Journal of Clinical Investigation.* 87: 1280-1285, 1991.

92. Saluja AK, Donovan EA, Yamanaka K, Yamaguchi Y, Hofbauer B, Steer ML. Caerulein-induced in vitro activation of trypsinogen in rat pancreatic acini is mediated by cathepsin B. *Gastroenterology*. 113: 304-310, 1997a.

93. Saluja AK, Lu L, Yamaguchi Y, Hofbauer B, Runzi M, Dawra R, Bhatia M, Steer ML. A cholecystokinin releasing factor mediates ethanol-induced stimulation of rat pancreatic secretion. *Journal of Clinical Investigation.* 99: 506-512, 1997b.

94. Saluja AK, Bhagat L, Lee HS, Bhatia M, Frossard J-L, Steer ML. Secretagogue-induced digestive enzyme activation and cell injury in rat pancreatic acini. *American Journal of Physiology*. 276: G835-842, 1999.

95. Schwiebert EM, Kizer N, Gruenert DC, and Stanton BA. GTP-binding proteins inhibit cAMP activation of chloride channels in cystic fibrosis airway epithelial cells. *Proceedings of the National. Academy of Science*. 89: 10623-10627, 1992.

96. Serhan CN, Petasis NA. Resolvins and Protectins in Inflammation Resolution. *Chemistry Reviews.* 111(10): 5922-43, 2011.

97. Simons, K, and Ehehalt, R. Cholesterol, lipid rafts, and disease. *Journal of Clinical Investigation*. 110: 597-603, 2002.

98. Smith WL, Urade Y, Jakobsson P-J. Enzymes of the Cyclooxygenase Pathways of Prostanoid Biosynthesis. *Chemistry Reviews.* 111(10): 5821-65, 2011.

99. Shin, L, Cho, W-J, Cook, J, Stemmler, T, Jena, BP. Membrane Lipids Influence Protein

Complex Assembly-Disassembly. *Journal of the American Chemistry Society.* 132:5596-5597, 2010.

100. Shin, L, Wang, S, Lee, J-S, Flack, A, Mao, G, Jena, BP. Lysophosphatidylcholine inhibits membrane-associated SNARE complex disassembly. *Journal of Cellular and Molecular Medicine.* 16(8): 1701-1708, 2011.

101. Tong, J, Briggs, M, McIntosh, T. Water permeability of the AQP-4 channel depends on bilayer composition, thickness, and elasticity. *Biophysical Journal*. 103: 1899-1908, 2012.

102. Tong, J, Canty, J, Briggs, M., McIntosh, J. The water permeability of lens aquaporin-0 depends on its lipid bilayer environment. *Experimental Eye Research.* 113: 32-40, 2013.

103. Tooze J, Hollinshead M, Hensel G, Kern H, Hoflack B. Regulated secretion of mature cathepsin B from rat exocrine pancreatic cells. *European Journal of Cell Biology*. 56: 187-200, 1991.

104. Umenishi F, Yoshihara S, Narikiyo T, Schrier RW. Modulation of hypertonicity-induced aquaporins-1 by sodium chloride, urea, betaine, and heat shock in maurine renal medullary cells. *Journal of American Society of Nephrology.* 16: 600-607, 2005.

105. VanAcker, G, Salvia, A, Bhagat, L, Sing, V, Song, A, Steer, M. Cathepsin B inhibition prevents trypsinogen activation and reduces pancreatitis severity. *American Journal of Physiology: Gastrointestinal & Liver Physiology*. 283: G794-G800, 2002.

106. VanAcker, G, Weiss, E, Steer, M, Perides, G. Cause-effect relationshiops between zymogen activation and other early events in secreatagogue-induced acute pancreatitis. *American Journal of Physiology: Gastrointestinal & Liver Physiology*. 292: G1738-1746, 2007.

107. Van Meer, G, Voelker, DR, Feigenson, GW. Membrane lipids: where they are and how

they behave. *Nature Reviews in Molecular and Cellular Biology*. *9*, 112–124, 2008.

108. Vitale N, Mukai H, Rouot B, Thierse´ D, Aunis D, Bader MF. Exocytosis in chromaffin cells. Possible involvement of the heterotrimeric GTP-binding protein G(o). *Journal of Biological Chemistry*. 268: 14715–14723, 1993.

109. Waterford SD, Kolodecik TR, Thrower EC, Gorelick FS. Vacuolar ATPase regulates zymogen activation in pancreatic acini. *Journal of Biological Chemistry*. 280: 5430-5434, 2005.

110. Weingarten R, Ransnas L, Mueller H, Sklar L, Bokoch G. Mastoparan interacts with the carboxyl terminus of the alpha subunit of Gi. *Journal of Biological Chemistry*. 265: 11044 –11049, 1990.

111. Wise A, Grassie MA, Parenti M, Lee M, Rees S, Milligan G. A cysteine-3 to serine mutation of the G-protein Gi1 alpha abrogates functional activation by the alpha 2A-adrenoceptor but not interactions with the beta gamma complex. *Biochemistry*. 36: 10620-10629, 1997.

112. Yadav, D, and Lowenfels, A. The epidemiology of pancreatitis and pancreatic cancer. *Gerontology*. 144(6): 1252-1261, 2013.

113. Young JC, Barral JM, Hartl FU. More than folding: localized functions of cytosolic chaperones. *Trends in Biochemical Science.* 28: 541-547, 2003.

114. Yuan, C, O'Connell, R, Jacob, R, Mason, R, Treistman, S. Regulation of the gating of BKCa channel by lipid bilayer thickness. *Journal of Biological Chemistry*. 282: 7276–7286, 2007.

115. Zhelev, DV. Material property characteristics for lipid bilayers containing lysolipid. *Biophysical Journal.* 75:321–330, 1998.

116. Zhu, Y-Z, Cao, M-M, Wang, W-B, Ren, H, Zhao, Pl, Qi, Z-T. Association of heat-shock

protein 70 with lipid rafts is required for Japanese encephalitis virus infection in Huh7 cells. *Journal of General Virology*. 93:61-71, 2012.

ABSTRACT

ALTERED MORPHOLOGY AND COMPOSITION OF ZYMOGEN GRANULES IN ACUTE PANCREATITIS

by

AMANDA FLACK

August 2014

Advisor: Dr. Bhanu Jena

Major: Physiology

Degree: Doctor of Philosophy

In healthy physiology, pancreatic digestive enzymes secreted following a meal are stored as inactive zymogens within membrane-bound secretory vesicles called Zymogen Granules (ZG), and activated extracellularly. In acute pancreatitis however, the digestive enzymes are prematurely activated within the cell, resulting in autodigestion of the tissue. Pancreatitis is gastrointestinal disorder in which there are over 200,000 hospitalizations per year with a 5% mortality rate. It has been demonstrated that in acute pancreatitis the digestive enzymes are blocked from being secreted and are activated within the cell leading to acinar cell and surrounding pancreatic tissue death. Little is known about the specific mechanism and the proteins and lipids that might participate in this process. Here it is reported that in acute pancreatitis, there are specific changes to both the proteome and lipidome of the ZG, contributing to altered ZG morphology and function. Using EM and AFM it is demonstrated that there is an increase in ZG size as early as 2h following induction of acute pancreatitis. LC-MS-based lipid and protein profiling and immunochemistry, collectively demonstrate altered ZG volume and activity regulating proteins and lipids, in acute pancreatitis.

AUTOBIOGRAPHICAL STATEMENT

AMANDA FLACK

EDUCATION

2014 PhD in Physiology, Wayne State University School of Medicine, Detroit, MI
2007 BS in Psychology, Wayne State University, Detroit, MI

EXPERIENCE

Graduate Research Assistant – Wayne State University School of Medicine, Department of Physiology. Mentor: Bhanu P. Jena, PhD. 11/09 – present.

Research Assistant – Wayne State University School of Medicine Department of Physiology. Mentor: Patrick Mueller, PhD. 05/07 – 08/09.

Undergraduate Research Assistant – Wayne State University, Department of Psychology, Mentor: George S. Borszcz, PhD. 05/06 – 12/08.

PEER REVIEWED PUBLICATIONS

In Preparation:

1. **Flack A**, Chen X, Taatjes DJ, Maddipati KR, Skallos P, Wang S, Lewis KT, Kulkarni SP, Rajagopal A, Mao G, Manke CW, Potoff JJ, Jena BP. Altered Morphology and Composition of Zymogen Granules in Acute Pancreatitis: Implication of the G-protein Coupled Receptor 98 in Granule Volume Regulation. *In preparation for Submission to Cell*.

Submitted:

1. Lewis, KT, Bhatnagar, N, Wang, S, Nico, L, **Flack, A**, Stemmler, TL, Mao, G, Manke, CW, Potoff, JJ, and Jena, BP. Low pH-Induced changes in membrane associated protein complexes: Implication in neurotransmitter release. Submitted to JACS

Published:

1. Hou X, Lewis KT, Wu Q, Wang S, **Flack A**, Mao G, Taatjes DJ, Sun F, Jena BP. Proteome of the porosome complex in human airway epithelia: interaction with the cystic fibrosis transmembrane conductance regulator (CFTR). J Proteomics, 16(96): 82-91, 2014.

2. Lee JS, Hou X, Bishop N, Wang S, **Flack A**, Cho WJ, Chen X, Mao G, Taatjes DJ, Sun F, Zhang K, and Jena BP. Aquaporin-assisted and ER-mediated mitochondrial fission: a hypothesis. Micron, 47:50-8, 2013.

3. Shin L, Wang S, Lee JS, **Flack A**, Mao G, and Jena BP. Lysophosphatidylcholine inhibits membrane-associated SNARE complex disassembly. J Cell Mol Med. Aug;16(8):1701-8, 2012.